Theory and Application of Nonlinear Wave Propagation Phenomena in Combined Reaction/Separation Processes

Dissertation

zur Erlangung des akademischen Grades

Doktoringenieurin/Doktoringenieur
(Dr.-Ing.)

von Dipl.-Ing. Stefan Grüner

geb. am 23. Februar 1974 in Backnang

genehmigt durch die Fakultät für Elektrotechnik und Informationstechnik der Otto-von-Guericke-Universität Magdeburg

Gutachter: Prof. Dr.-Ing. Achim Kienle
Prof. Dr.-Ing. Wolfgang Marquardt

Promotionskolloquium am 10. Mai 2007

Contents

Symbols

In working out the nomenclature for the thesis at hand the following aspects were taken into account. To enhance readability for application oriented people care was taken to use familiar notation in the application specific parts. Application independent notion is used in the theoretically oriented part to point out the common mathematical foundation of all considered processes.

As a consequence most symbols have a unique meaning. However there are some exceptions to this rule hence the following list gives more than one meaning for some symbols. In any cases the correct meaning follows from the context the symbol is used in or is explicitly mentioned in the text.

Since the aspects to be covered are independent of specific physical units and as symbols may have different units in some situation all symbols are given without units. Parameters given in the text are in consistent units unless otherwise stated.

Latin Letters

Symbol	Meaning
a	(Langmuir) isotherm parameter
A	component label
A	flow rate ratio
b	(Langmuir) isotherm parameter
B	component label
B	mass transfer coefficient
c	molar concentration
C	component label

D	component label
E	component label
E	axial dispersion coefficient
f	flow rate
g	binaphthol system isotherm parameter
	product purity for TMB(R) processes
h	binaphthol system isotherm parameter
	holdup in prototype equation
q	molar load of solid
I	identity matrix of suitable dimensions
j	mass transfer rate
J	molar flow rate
K	reaction equilibrium constant
K_{kin}	reaction rate constant
l	column length
L	projection matrix to the left null space of matrix
m	flow rate ratio in zones of a TMB(R) processes
M	capacity matrix
n	molar holdup
N	flow rate matrix
N_c	number of components in distillation processes
N_{grid}	number of grid points in spatially discretized equations
N_r	number of reactions
N_s	number of adsorbable solutes in chromatographic processes
N_v	number of independent components
r	reaction rate
	right eigenvectors of Jacobian of equilibrium function
	rarefaction or expansive wave
R	monomer of the binaphthol system
RR	monodimer of monomer R
RS	heterodimer of R and S

s	right eigenvectors of flux matrix $(M)^{-1}(N)$
	shock or constant pattern wave
S	monomer of the binaphthol system
SS	monodimer of monomer S
t	dimensionless time
v	velocity
w	wave propagation speed
x	mole fraction liquid phase
y	mole fraction vapor phase
z	dimensionless spatial coordinate

Greek Letters

Symbol	Meaning
α	relative volatility
ϵ	molar hold-up ratio
	column void fraction
ϕ	composition in phase (')
Φ	reaction invariant composition in phase (')
Γ	expansive wave
ι	mass transfer rate (prototype equation)
I	reaction invariant mass transfer rate (prototype equation)
λ	eigenvalue of Jacobian of equilibrium function
Λ	jump ratio for shock waves
μ	volumetric flow rate ratio
ν	mole number
	volume ratio
	stoichiometric matrix
π_f	flow rate ratio
π_h	holdups ratio

ϱ	reaction rate
ρ	reaction equilibrium
σ	eigenvalue of flux matrix $(M)^{-1}(N)$
Σ	shock wave
ω	length along wave in hodograph space
Ω	wave, independent of wave type
ξ	composition in phase (")
Ξ	reaction invariant composition in phase (")
ζ	parameter along expansive wave

Subscripts

Symbol	Meaning
+	value at positions ahead of a shock
-	value at positions behind a shock
R	reference component(s)
T	component(s) to be transformed
in	denotes quantities entering the process

Superscripts

Superscripts given in braces, e.g. $^{(k)}$ indicate the k is the index of the wave family, see Sec. 2.2 for details.

Symbol	Meaning
'	phase containing the processes yield
"	other phase
$*$	point of jump in initial conditions

Kurzfassung

Die Anforderungen an die Effizienz der in der Chemischen Industrie verwendeten Prozesse steigt ständig. Gleichzeitig haben die Methoden zur Auslegung der einzelnen Prozessstufen und deren Verbindung zu hochintegrierten Prozessen ihre Grenzen erreicht. Um diese Begrenzungen zu überwinden konzentriert sich die aktuelle Forschung auf kombinierte Prozesse, d.h. Prozesse bei denen in einer einzelnen Prozessstufe mehrere Prozesse kombiniert werden.

Die vorliegende Arbeit befasst sich mit kombinierten Reaktions-/Stofftrennprozessen am Beispiel der Reaktivdestillation und der reaktiven Chromatographie. Zur Gewinnung und Ausnutzung eines umfassenden Prozessverständnisses wird eine Theorie zur Beschreibung des statischen und dynamischen Verhaltens dieser Prozesse entwickelt. Diese Theorie basiert auf einer Transformation in einen äquivalenten Stofftrennprozess unter der Annahme von simultanem Phasen- und Reaktionsgleichgewicht und ermöglicht so einen Analyse im Rahmen der Theorie der nichtlinearen Wellenausbreitung. In einer anschließenden Diskussion sekundärer Effekte wie z.B. endlicher Reaktions- und Stoffaustauschraten zeigt sich dann, dass die theoretischen Ergebnisse auch auf Prozesse die hinreichend nahe dem simultanen Phasen- und Reaktionsgeichgewicht betrieben werden angewendet werden knnen.

Die Analyse einfacher Beispielprozesse mit der entwickelten Theorie deckt Analogien zwischen Stofftrenn- und entsprechenden kombinierten Reaktions-/Stofftrennprozessen sowie Destillation und Chromatographie auf. Die entwickelte Theorie ist bei der anschließenden Analyse komplexer Multireaktionsprozesse ein wertvolles Hilfsmittel da sie ein globales Abbild der Systemdynamik liefert.

Das so gewonnene umfassende Prozessverständnis wird schließlich bei der Entwicklung neuer Konzepte zur Prozessführung genutzt. Diese Konzepte umfassen z.B. eine konstruktive Methode zum Beobachterentwurf, ein modellbasiertes Regelungskonzepte für chromatographische Prozesse bis hin zur nichtlinearen und modelprädiktiven Regelung von Destillationskolonnen.

Abstract

In the chemical industry the demands regarding process efficiency are permanently increasing. At the same time methods to design indiviual process stages and interconnect them to higly integrated process are reaching their preformance limit. To overcome these limitations the focus of current research has turned to combined processes, i.e. processes that combine the tasks of different process stages into a single process stage.

The thesis at hand concentrates on combined reaction/separation processes, namely reactive distillation and reactive chromatography. In order to fully understand and exploit these processes a theory describing their stationary and dynamic behavior is developed. This theory is based on a transformation to equivalent separation processes in the limit of simultaneous phase and reaction equilibrium and enables an analysis in the framework of nonlinear wave propagation theory. A subsequent discussion of secondary effects such as e.g. finite reaction rates and finite mass transfer rates then shows that the theoretical results may be extended to processes that are sufficiently close to simultaneous phase and reaction equilibrium.

The developed theory is used to analyse processes ranging from simple model systems to highly complex multi reaction systems. In the analysis of simple model systems analogies between separtion processes and corresponding combined reaction/separation processes as well as distillation and chromatographic processes are revealed. In the analysis of the complex multi reaction systems the developed theory is a valuable tool since it gives a global picture of the system dynamics.

Finaly new concepts for process control are developed based on the comprehensive insight to the process dynamics provided by the developed theory. These concepts comprise constructive methods to observer design, a model based control concept for chromatographic processes as well as nonlinear and model predictive control of distillation columns.

Chapter 1

Introduction

Background It is common practice for chemical engineers to design processes by decomposing the overall process into several basic operations. Subsequently the basic operations are assigned to suitable equipment. This leads to plants that perform the overall process step by step in a sequence of process stages. The individual processes stages are well understood by now and thus a sophisticated individual design of the stages is engineering standard just as operating each of them at an optimal operating point.

While this design procedure ensures optimal operation of each basic operation taken for itself the overall process might still be far from its overall optimum. E.g. due to repeated heating, cooling and then re-heating of educts and intermediates energy is wasted. To overcome such drawbacks of the traditional basic operation oriented design approach modern processes are highly integrated. E.g. the energy withdrawn from the process by cooling at some process stage is re-introduced at some other process stage for heating. In developing such highly integrated process the complete process may be operated at an overall optimal operating point. However the overall process remains limited by the operating limits of each basic operation, e.g. reactions will never proceed beyond reaction equilibrium in a traditional reactor while e.g separations will never proceed beyond azeotropes in a distillation column operated at steady stated.

These limitations may be overcome by extending the concept of process integration to include processes which combine several basic operations such that they take place simultaneously in the very same process stage. One class of such combined process that received much attention over the last decade is the combination of reaction and separa-

tion. Apart from heat integration aspects of combined reaction/separation process they have the potential to overcome the limitations of the basic operations of reaction and separation. This becomes obvious by considering a simple experiment: In a traditional reactor a reversible degradation reaction takes places yielding two products. This reaction will proceed until reaction equilibrium is reached and thus conversion will stop at some point. In a combined reaction/separation process one of the products might be continuously removed from the reactor and thus the reaction will proceed until total conversion is achieved, i.e. the reaction equilibrium is shifted in a favorable way. However such favorable behavior of combined reaction/separation processes is not always observed and thus a theory of such combined reaction/separation processes is needed. Such a theory should cover both steady state as well as dynamic behavior of the processes.
Recently a theory for steady state analysis of reactive distillation processes has been introduced by Doherty and co-workers.
The thesis at hand shows that this theory is generally applicable to combined reaction/separation processes and develops an elegant way to extend it to the dynamics of combined reaction/separation processes. This leads to a comprehensive theory of combined reaction/separation processes. The present work is not only about the theory itself but also about using the theory e.g. in the development of automatic control concepts for combined reaction/separation processes.

Outline The present work is split into two main chapters. The first part, chapter 2, is concerned with the underlying mathematical theory of nonlinear wave propagation in combined reaction/separation process while the second part, chapter 3, illustrates the use of the developed theory in process analysis and process control.
In section 2.1 the mathematical modeling of combined reaction/separation processes is discussed for reactive distillation and chromatographic reactors eventually yielding the very same model structure. Section 2.2 is dedicated to a review of the known theory of nonlinear wave propagation on basis of the common model structure for ordinary separation processes. Here some emphasis is put on aspects that are of little importance for ordinary separation process but will come important in the analysis of combined reaction/separation processes. Since the common model structure for combined processes does not directly fit in the framework of nonlinear wave propagation theory the subse-

quent section 2.3 develops a transformation of combined reaction/separation processes to equivalent separation processes. Section 2.4 concludes the theoretical part of the thesis at hand by considering the influence of secondary effects that were neglected in the development of the theory.

The second, application oriented part, chapter 3, starts by discussing some illustrative examples in section 3.1. These examples range from simple nonreactive monovariant systems to highly complex multireaction systems. The discussion does not aim at covering all aspects of the systems. Rather focus is on showing how to use the developed theory in the analysis of the systems. Section 3.2 presents new concepts for processes control arising from a nonlinear wave propagation based point of view. The resulting control concepts range from a simple PI-controller based design for chromatographic processes to nonlinear model predictive control of distillation columns.

Chapter 2

Nonlinear Wave Propagation in Reaction/Separation Processes

This chapter develops the mathematical theory of nonlinear wave propagation in combined reaction/separation processes with focus on reactive distillation and chromatographic reactors.

The theory is based on mathematical models of the considered processes that are rather simple but nevertheless describe the underlying physics in sufficient detail. The analysis reveals that both, the equations of reactive distillation as well as those of chromatographic reactors can be cast to what will be called the prototype equation of combined reaction/separation processes in this work.

On the basis of these model equations it is then shown that, in the limit of phase and reaction equilibrium, they represent 1st order homogeneous quasilinear partial differential equations. Due to the combination of phase and reaction equilibrium those equations are highly nonlinear and a profound knowledge of the theory of hyperbolic systems is necessary in order to properly analyze their dynamics. This knowledge is provided together with some instructive examples. Afterward some of the assumptions necessary for the analytical treatment and their relaxations are discussed.

2.1 Mathematical Modeling

The subsequent analysis are based on a rather simple model of a process having two continuous phases with a single spatial coordinate. The process is governed by counter current flow, mass transfer across the phase boundary and reaction in either one or both phases.

This schematic is applicable to reactive distillation processes as well as chromatographic reactors. However in the past both processes have been considered independently and their common mathematical structure has been hardly exploited. Therefore in the following two sections the modeling of both processes is described separately and then a common model structure is worked out. This model structure forms the basis for the theoretical analysis of the process dynamics.

2.1.1 Reactive Distillation Processes

As noted before the models to be considered have two continuous phases. Such models are strictly valid for sections of packed columns only. However this type of model is also capable of describing staged columns if they have a sufficiently large number of trays [36]. In the following the part of a distillation column either between feed tray and condenser or reboiler and feed tray will be refered to as column section, i.e. the feed tray, reboiler and condeser are not considered as part of a column section. The column section, as depicted in Fig. 2.1, has a liquid phase denoted by (') and a vapor phase denoted by (''). Assuming

- constant molar flow rates,
- constant molar holdups,
- negligible axial dispersion,
- constant pressure and
- thermal equilibrium

the dynamic model of the column section is obtained from the material balances of the $N_c - 1$ linearly independent species in both phases. In dimensionless form they read

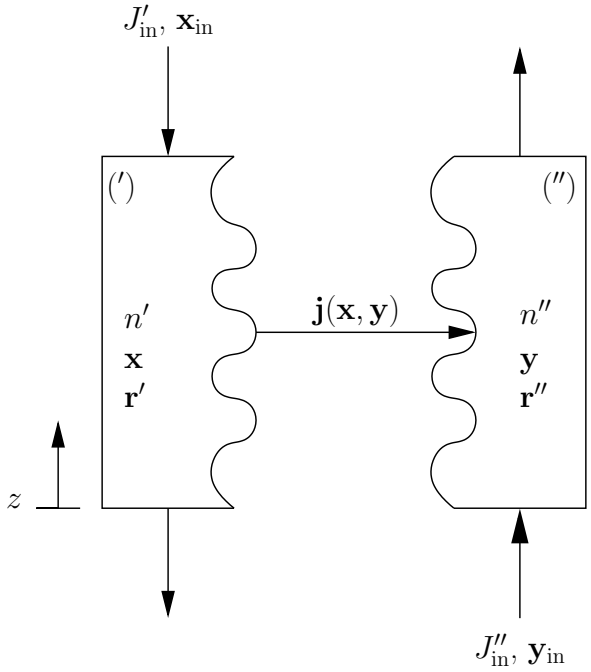

Figure 2.1: Schematic of a distillation column section.

according to [26],[36]

$$\frac{\partial x_i}{\partial t} - \frac{\partial x_i}{\partial z} = -j_i(\boldsymbol{x}, \boldsymbol{y}) + \sum_{k=1}^{N'_r} \nu'_{ik} r'_k(\boldsymbol{x}) \tag{2.1}$$

for the liquid phase and

$$\epsilon \frac{\partial y_i}{\partial t} + \frac{1}{A} \frac{\partial y_i}{\partial z} = j_i(\boldsymbol{x}, \boldsymbol{y}) + \sum_{k=1}^{N''_r} \nu''_{ik} r''_k(\boldsymbol{y}) \tag{2.2}$$

for the vapor phase together with the boundary conditions

$$x_i(z = 1, t) = x_{i,\text{in}}(t), \tag{2.3}$$

$$y_i(z = 0, t) = y_{i,\text{in}}(t), \tag{2.4}$$

and the initial conditions

$$x_i(z, t = 0) = x_{i,0}(z), \tag{2.5}$$

$$y_i(z, t = 0) = y_{i,0}(z), \tag{2.6}$$

$i = 1(1)N_c - 1, \quad z \in [0, 1]$.

Here z and t represent the dimensionless spatial and time coordinate and are defined by

$$z := \frac{\overline{z}}{l}, \qquad t := \frac{\overline{t} J'_{\text{in}}}{l n'} \tag{2.7}$$

where the overlined variables denote the dimensional equivalents. The ratio of the molar holdups and the molar convective flow rates are defined as

$$\epsilon := \frac{n''}{n'}, \qquad A := \frac{J'_{\text{in}}}{J''_{\text{in}}} \tag{2.8}$$

respectively.

Assuming phase equilibrium this set of equations can be further simplified since now the composition of the vapor phase is a function of the fluid phase composition and hence

$$y_i = y_i(\boldsymbol{x}), \qquad i = 1(1)N_c. \tag{2.9}$$

As a consequence the mass transfer rates $j_i(\boldsymbol{x}, \boldsymbol{y})$ are indeterminate and can be eliminated by summing up Eqs. 2.1 and 2.2. This results in the pseudo homogeneous model

$$\frac{\partial}{\partial t}\left(\epsilon y_i(\boldsymbol{x}) + x_i\right) + \frac{\partial}{\partial z}\left(\frac{1}{A} y_i(\boldsymbol{x}) - x_i\right) = \sum_{k=1}^{N'_r} \nu'_{ik} r'_k(\boldsymbol{x}) + \sum_{k=1}^{N''_r} \nu''_{ik} r''_k(\boldsymbol{y}(\boldsymbol{x})). \tag{2.10}$$

The dynamics of the pseudo homogeneous model Eq. 2.10 for the nonreactive case, i.e. with right hand side identically zero, are well understood [62], [50], [51]. Their application to distillation processes are discussed in detail in e.g. [26], [23], [36] on the basis of the theory of homogeneous hyperbolic systems e.g. [19], [50], [51]. In the reactive case Eq. 2.10 is inhomogeneous and thus this theory is no longer directly applicable nor is an equivalent mathematical theory for inhomogeneous hyperbolic systems available. The existing theory based on characteristics fails to enable an explicit construction of solutions for the reactive case.

2.1.2 Chromatographic Reactors

In contrast to distillation columns where the spatially distributed modeling strictly applies only for the special case of packed columns chromatographic reactors are by nature spatially distributed. The reactor is decomposed into a fluid phase and an adsorbens phase denoted by ($'$) and ($''$) respectively as shown on in Fig. 2.2. A moving solid phase is assumed as denoted by v'' in Fig. 2.2. In practical applications this movement of the solid is critical [47] and thus avoided. Instead the simulated moving bed technology is used to approximate a continuous movement of the solid phase. The classical fixed bed is included in the setup by setting the solid velocity identically zero, i.e $v'' \equiv 0$. Assuming

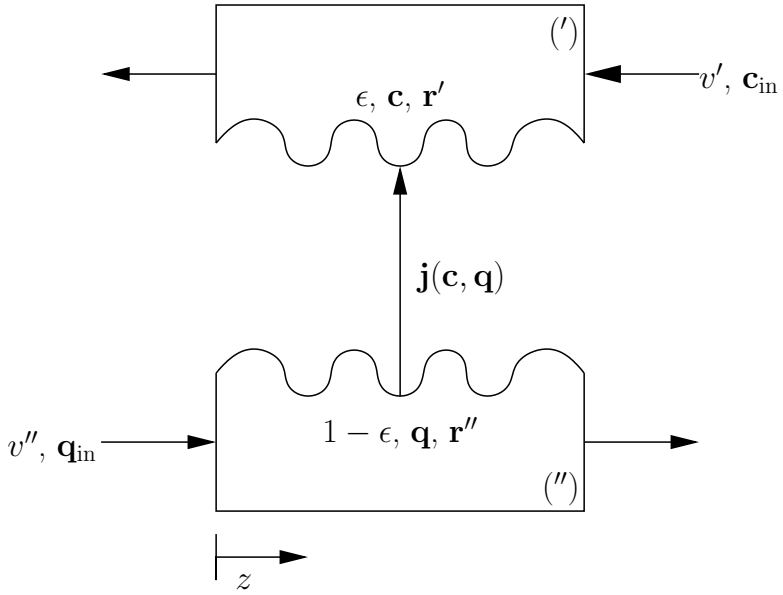

Figure 2.2: Schematic of a chromatographic reactor.

- constant fluid velocity v' and adsorbens velocity v'',
- isothermal operation and
- negligible axial dispersion

the dynamic equations for the moving bed adsorber are obtained from material balances of the N_s adsorbable solutes in the fluid and the adsorbed phase. Using dimensionless spatial and time coordinates they read according to e.g. [63]

$$\frac{\partial c_i}{\partial t} - \frac{\partial c_i}{\partial z} = -\tilde{j}_i(\boldsymbol{c}, \boldsymbol{q}) + \sum_{k=1}^{N_r'} \nu'_{i,k} \tilde{r}'_k(\boldsymbol{c}) \tag{2.11}$$

for the fluid phase and

$$\nu \frac{\partial q_i}{\partial t} + \mu \frac{\partial q_i}{\partial z} = \tilde{j}_i(\boldsymbol{c}, \boldsymbol{q}) + \sum_{k=1}^{N_r''} \nu''_{i,k} \tilde{r}''_k(\boldsymbol{q}) \tag{2.12}$$

for the adsorbed phase together with the boundary conditions

$$c_i(z = 1, t) = c_{i,\text{in}}(t), \tag{2.13}$$

$$q_i(z = 0, t) = q_{i,\text{in}}(t), \tag{2.14}$$

and the initial conditions

$$c_i(z, t = 0) = c_{i,0}(z), \tag{2.15}$$

$$q_i(z, t = 0) = q_{i,0}(z), \tag{2.16}$$

$i = 1(1)N_s, \quad z \in [0, 1]$.

The tilde over the reaction rate and the mass transfer terms indicates that they now represent volumetric quantities. Again z and t denote the dimensionless spatial and time coordinate and are now defined as

$$z := \frac{\overline{z}}{l}, \qquad t := \frac{\overline{t} v'}{l} \tag{2.17}$$

where the overlined variables denote the dimensional equivalents. Note that in typical models for chromatographic process the spatial coordinate does not point in the direction chosen here but in the opposite direction. This choice is made in order to get the same spatial orientation as in the distillation processes. The volume ratio and the volumetric flow rate ratio are defined as

$$\nu := \frac{1 - \epsilon}{\epsilon}, \qquad \mu := \frac{1 - \epsilon}{\epsilon} \frac{v''}{v'} \tag{2.18}$$

respectively. As before Eqs. 2.11 and 2.12 can be further simplified upon assuming phase equilibrium, i.e. assuming that

$$q_i = q_i(\boldsymbol{c}), \qquad i = 1(1)N_s \tag{2.19}$$

and just as before the mass transfer rates $\tilde{j}_i(\boldsymbol{c}, \boldsymbol{q})$ become indeterminate. The $\tilde{j}_i(\boldsymbol{c}, \boldsymbol{q})$ are eliminated by summing up Eqs. 2.11 and 2.12 and yield the pseudo homogeneous model

$$\frac{\partial}{\partial t} \left(\nu q_i(\boldsymbol{c}) + c_i \right) + \frac{\partial}{\partial z} \left(\mu q_i(\boldsymbol{c}) - c_i \right) = \sum_{k=1}^{N_r'} \nu_{ik}' \tilde{r}_k'(\boldsymbol{c}) + \sum_{k=1}^{N_r''} \nu_{ik}'' \tilde{r}_k''(\boldsymbol{q}(\boldsymbol{c})). \tag{2.20}$$

The dynamic behavior of Eq. 2.20 for nonreactive systems, i.e. with the right hand side identically zero has been intensively investigated and a comprehensive mathematical theory was introduced by [50, 51] with detailed application to fixed and moving bed chromatography. [20] independently obtained equivalent results on basis of physical insight. This approach was recently reviewed in a series of articles [19], [21], [18].

Note that Eq. 2.20 is completely analogous to Eq. 2.10 and again the reaction terms make the equations inhomogeneous and thus the before mentioned theory is inapplicable.

2.1.3 Mathematical Prototype Equation

As noted in the two previous sections the models presented for both processes are quite similar. This similarity is now used to derive a common mathematical prototype equation for both Eq. 2.10 and Eq. 2.20 and forms the basis for the unified mathematical analysis of both classes of processes.

Since the mathematical similarity of both processes is rather evident it is somewhat astonishing that it was hardly exploited in the past. However some first efforts in this direction can be found in e.g. [23] and [45].

The first step towards a unified treatment of reactive distillation and chromatographic reactors is the derivation of a prototype equation capable of describing both classes of processes. Before this equation is given the relevant common characteristics of both processes as well as their differences shall be quickly reviewed.

Both processes are characterized by two phases ($'$) and ($''$) that are flowing in counter current along a common spatial coordinate z as shown in Fig. 2.3. The phases exchange matter across their phase boundary as denoted by the mass transfer term $\boldsymbol{\iota}(\boldsymbol{\phi}, \boldsymbol{\xi})$. Here $\boldsymbol{\phi}$ denotes the composition in the ($'$) phase and $\boldsymbol{\xi}$ in the ($''$) phase. In either phase chemical reactions $\boldsymbol{r}'$ and $\boldsymbol{r}''$ may take place. One of the two phases can be considered as the phase that contains the yield of the process and is denoted by ($'$). In both processes this role is taken by the liquid phase. A function $\boldsymbol{\xi}(\boldsymbol{\phi})$ of the composition in phase ($'$) is used to express the equilibrium composition in phase ($''$). The orientation of the spatial coordinate is in the direction of flow in phase ($''$) as shown in Fig. 2.3.

Based on these conventions the prototype equations can be given as

$$\frac{\partial \phi_i}{\partial t} - \frac{\partial \phi_i}{\partial z} = -\iota_i(\boldsymbol{\phi}, \boldsymbol{\xi}) + \sum_{k=1}^{N'_r} \nu'_{i,k} \varrho'_k(\boldsymbol{\phi}) \tag{2.21}$$

for phase ($'$) and

$$\pi_h \frac{\partial \xi_i}{\partial t} + \pi_f \frac{\partial \xi_i}{\partial z} = \iota_i(\boldsymbol{\phi}, \boldsymbol{\xi}) + \sum_{k=1}^{N''_r} \nu''_{i,k} \varrho''_k(\boldsymbol{\xi}) \tag{2.22}$$

for phase ($''$) together with the boundary conditions

$$\phi_i(z = 1, t) = \phi_{i,\mathrm{in}}(t), \tag{2.23}$$

$$\xi_i(z = 0, t) = \xi_{i,\mathrm{in}}(t), \tag{2.24}$$

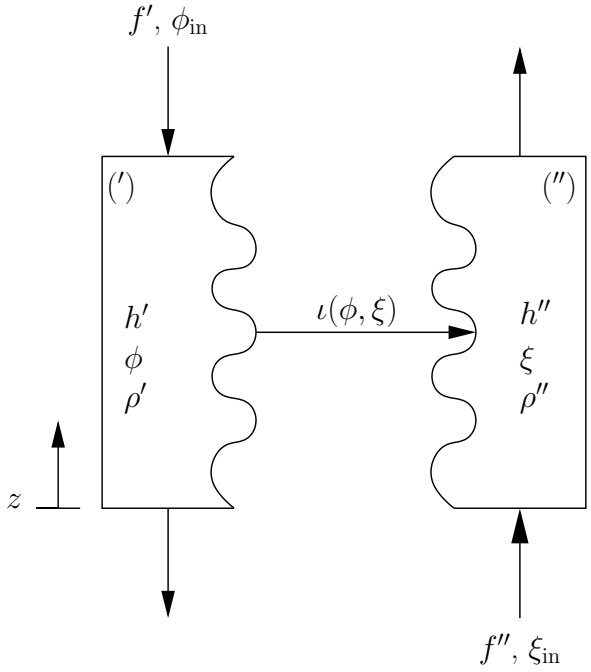

Figure 2.3: Schematic of the prototype process.

and the initial conditions

$$\phi_i(z, t = 0) = \phi_{i,0}(z), \tag{2.25}$$

$$\xi_i(z, t = 0) = \xi_{i,0}(z), \tag{2.26}$$

$i = 1(1)N_v, \quad z \in [0, 1]$. $\pi_h = h''/h'$ denotes the ratio of the holdups of both phases and $\pi_f = f''/f'$ the ratio of the flow rates. The correspondence between these abstract variables and their equivalents in Eqs. 2.1, 2.2 and Eqs. 2.11, 2.12 is given in table 2.1. Assuming phase equilibrium further simplification of Eqs. 2.21 and 2.22 is possible and yields

$$\frac{\partial}{\partial t}\left(\pi_h \xi_i(\boldsymbol{\phi}) + \phi_i\right) + \frac{\partial}{\partial z}\left(\pi_f \xi_i(\boldsymbol{\phi}) - \phi_i\right) = \sum_{k=1}^{N_r} \nu_{ik} \varrho_k(\boldsymbol{\phi}). \tag{2.27}$$

In Eq. 2.27 the stoichiometric matrices $\boldsymbol{\nu}'$ and $\boldsymbol{\nu}''$ have been combined to

$$\boldsymbol{\nu} = [\boldsymbol{\nu}', \boldsymbol{\nu}''] \tag{2.28}$$

and the reaction rates $\boldsymbol{\varrho}'$ and $\boldsymbol{\varrho}''$ have been combined to

$$\boldsymbol{\varrho}(\boldsymbol{\phi}) = \begin{bmatrix} \boldsymbol{\varrho}'(\boldsymbol{\phi}) \\ \boldsymbol{\varrho}''(\boldsymbol{\xi}(\boldsymbol{\phi})) \end{bmatrix} \tag{2.29}$$

with

$$N_r = N_r' + N_r'' \tag{2.30}$$

	prototype	distillation	adsorber
composition in ($'$)	ϕ_i	x_i	c_i
composition in ($''$)	ξ_i	y_i	q_i
holdup ratio	$\pi_h = \frac{h''}{h'}$	$\epsilon = \frac{n''}{n'}$	$\nu = \frac{1-\epsilon}{\epsilon}$
flow rate ratio	$\pi_f = \frac{f''}{f'}$	$\frac{1}{A} = \frac{J''_{\text{in}}}{J'_{\text{in}}}$	$\mu = \frac{1-\epsilon}{\epsilon}\frac{v''}{v'}$
mass transfer rate	ι_i	j_i	$\tilde{j}_i$
reaction rate	ϱ_k	r_k	$\tilde{r}_k$
number of independent components	N_v	$N_c - 1$	N_s

Table 2.1: Correspondence between the variables of the prototype equations and the process models.

as the total number of reactions. Obviously Eq. 2.27 is again inhomogeneous due to the reaction terms appearing on the right hand side. An other way of writing Eq. 2.27 that will be handy in the following is

$$\frac{\partial \phi_i}{\partial t} + \pi_h \frac{\partial \xi_i(\boldsymbol{\phi})}{\partial t} - \frac{\partial \phi_i}{\partial z} + \pi_f \frac{\partial \xi_i(\boldsymbol{\phi})}{\partial z} = \sum_{k=1}^{N_r} \nu_{ik} \varrho_k(\boldsymbol{\phi}). \tag{2.31}$$

As has been shown by deducing the prototype equation distillation process and chromatographic processes are internally completely analogous. This leads to the question why a detailed common treatment of both classes of processes has not been established in the field of chemical engineering. A possible answer lies in the typical boundary systems that are needed for the processes.

Distillation columns usually comprise a reboiler and a condenser. Considering e.g. the column end equipped with the condenser one finds that the vapor is (partially) condensed and mixes with the holdup of the condenser from which in turn the liquid entering the column is this taken. Hence the composition of the liquid entering the column is strongly related to the composition of the leaving vapor flow. Similar considerations apply for the reboiler. Further more the flow rates in a column section are not independent. At steady state the reflux form the condenser cannot exceed the vapor flow that is coming up the

column while the boilup from the reboiler cannot exceed the liquid flow coming down the column. Hence there are natural limits to the flow rate ratios A in distillation column sections.

For adsorbers the boundary systems do not affect the achievable product compositions as much as it is the case for distillation processes but it is the need for regeneration of the solid phase that imposes limitations on the entering compositions. For a typical fixed bed process one would require an empty fixed bed before and after the injection of a pulse. I.e. $\boldsymbol{c}_0(z) = \boldsymbol{q}_0(z) = \mathbf{0}$ and $\boldsymbol{c}(z,T) = \boldsymbol{q}(z,T) = \mathbf{0}$. Considering the flow rate ratios μ in counter current chromatography there are no such stringent limitations as in distillation processes. At least from a theoretical point of view arbitrary flow rate ratios are possible. In simulated moving bed processes constraints are imposed as the liquid flow rate cannot increase in the section following the extract or the raffinate port while it cannot decrease in the section following the feed or the solvent port.

In summary the dynamics of both classes of processes are of the same nature but due to the differences imposed by boundary systems and typical modes of operation each class of processes was designed and analyzed separately in the past.

The following theoretical development aims at being independent of those differences and thus allows to point out and exploit similarities in both processes. This will become most explicit in the sections dealing with applications of the developed theory.

2.2 Nonlinear Wave Propagation Theory

This short review of nonlinear wave propagation theory is mainly based on the presentation in [26] and [36] and establishes the results given there in the notation used in this thesis. For a detailed understanding of the theory the reader is referred to [26] and [36] which includes an in depth discussion on the application to nonreactive distillation. A more general discussion can be found in [62], [70], [50], [51] and [32], while [20] and the series of articles [19], [21], [18] focuses on application to chromatography.

Elementary Wave Types and Combined Waves

The starting point for nonlinear wave propagation theory is the nonreactive version of Eq. 2.27, i.e

$$\frac{\partial}{\partial t}\left(\pi_h \boldsymbol{\xi}(\boldsymbol{\phi}) + \boldsymbol{\phi}\right) + \frac{\partial}{\partial z}\left(\pi_f \boldsymbol{\xi}(\boldsymbol{\phi}) - \boldsymbol{\phi}\right) = \mathbf{0} \tag{2.32}$$

but now over the infinite spatial domain

$$-\infty < z < \infty$$

and with piecewise constant initial conditions, i.e.

$$\boldsymbol{\phi}(z, t=0) = \begin{cases} \boldsymbol{\xi}^{-1}(\boldsymbol{\xi}_{in}) & -\infty < z < z^* \\ \boldsymbol{\phi}_{\text{in}} & z^* < z < \infty \end{cases} \tag{2.33}$$

as shown in Fig. 2.4. for some z^* inside the spatial domain. By explicitly performing the

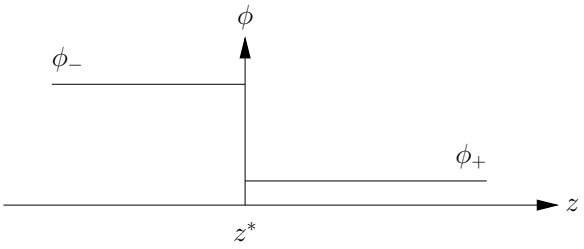

Figure 2.4: Piecewise constant initial conditions.

differentiations Eq. 2.32 can be transformed into the standard form of nonlinear wave propagation theory:

$$\frac{\partial \boldsymbol{\phi}}{\partial t} + \boldsymbol{M}^{-1}\boldsymbol{N}(\boldsymbol{\phi})\frac{\partial \boldsymbol{\phi}}{\partial z} = \mathbf{0} \tag{2.34}$$

with

$$\boldsymbol{M}(\boldsymbol{\phi}) = \pi_h \frac{\partial \boldsymbol{\xi}}{\partial \boldsymbol{\phi}} + \boldsymbol{I}, \quad \boldsymbol{N}(\boldsymbol{\phi}) = \pi_f \frac{\partial \boldsymbol{\xi}}{\partial \boldsymbol{\phi}} - \boldsymbol{I} \tag{2.35}$$

and $\boldsymbol{I}$ denotes an identity matrix of suitable dimensions.

The system Eq. 2.34 is hyperbolic if the matrix $\boldsymbol{M}^{-1}\boldsymbol{N}(\boldsymbol{\phi})$ has real eigenvalues and a complete set of linearly independent eigenvectors exists. If all eigenvalues are different the system is called strictly hyperbolic and otherwise it is called weakly hyperbolic. If there are multiple eigenvalues and there is no complete set of linearly independent eigenvectors the system is parabolic degenerate and if there are complex eigenvalues it is elliptic.

Note that the eigenvalues σ_k of the matrix $\boldsymbol{M}^{-1}\boldsymbol{N}(\boldsymbol{\phi})$ directly follow from the eigenvalues λ_k of the jacobian $\frac{\partial \boldsymbol{\xi}}{\partial \boldsymbol{\phi}}$ of the equilibrium function $\boldsymbol{\xi}(\boldsymbol{\phi})$ as $\sigma_k = \frac{\pi_f \lambda_k - 1}{1 + \pi_h \lambda_k}$. Further the eigenvectors $\boldsymbol{s}_k$ of the matrix $\boldsymbol{M}^{-1}\boldsymbol{N}(\boldsymbol{\phi})$ are identical to the eigenvectors $\boldsymbol{r}_k$ of the jacobian $\frac{\partial \boldsymbol{\xi}}{\partial \boldsymbol{\phi}}$ of the equilibrium function $\boldsymbol{\xi}(\boldsymbol{\phi})$. The straight forward computations to show these properties can be found in the appendix of [26].

The system Eq. 2.34 is genuinely nonlinear if

$$\nabla \sigma_k \boldsymbol{s}_k \neq 0 \Leftrightarrow \nabla \lambda_k \boldsymbol{r}_k \neq 0 \quad \forall k. \tag{2.36}$$

Expansive Waves Expansive waves are smoothly differentiable solutions to Eq. 2.34 of the type

$$\boldsymbol{\phi}(z,t) = \boldsymbol{\phi}(\zeta = z/t) \tag{2.37}$$

as schematically shown in Fig. 2.5.

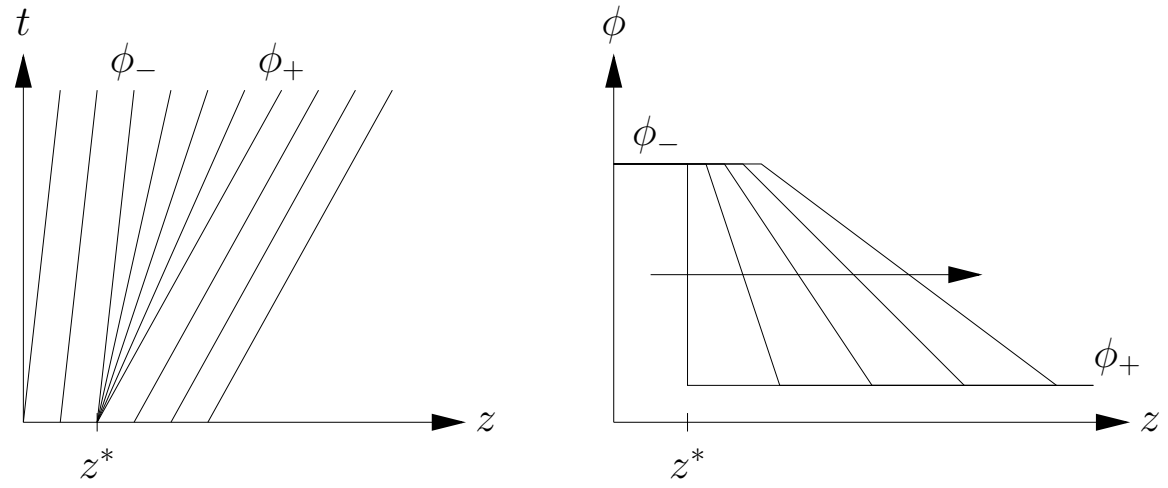

Figure 2.5: Expansive wave centered at z^*. Left: Spectrum of the characteristics between $\boldsymbol{\phi}_-$ and $\boldsymbol{\phi}_+$. Right: Spatial profiles at equidistant time intervals

They can be represented as time invariant curves $\Gamma^{(k)}$ in the space of the compositions $\boldsymbol{\phi}$ according to

$$\Gamma^{(k)}: \quad \frac{d\boldsymbol{\phi}}{d\zeta} = \boldsymbol{s}_k(\boldsymbol{\phi}(\zeta)), \quad \boldsymbol{\phi}(\zeta = 0) = \boldsymbol{\phi}_-, \quad \zeta > 0, \tag{2.38}$$

$$\zeta = \left.\frac{dz}{dt}\right|_{\Gamma^{(k)}} = \sigma_k(\boldsymbol{\phi}(\zeta)) = \frac{\pi_f \lambda_k - 1}{1 + \pi_h \lambda_k}. \tag{2.39}$$

While Eq. 2.38 defines the path of $\Gamma^{(k)}$ in the composition space, also termed as hodograph space Eq. 2.39 defines the concentration dependent propagation speed. Note that,

according to Eq. 2.39 all species at a specific location ζ^* propagate with the same speed but the speed varies with ζ.

Shock Waves In contrast to the expansive waves introduced in the previous paragraph shock waves are discontinuous solutions to the system Eq. 2.34 of the form:

$$\boldsymbol{\phi}(z,t) = \begin{cases} \boldsymbol{\phi}_- & z < wt \\ \boldsymbol{\phi}_+ & z > wt \end{cases} \tag{2.40}$$

as shown in Fig. 2.6

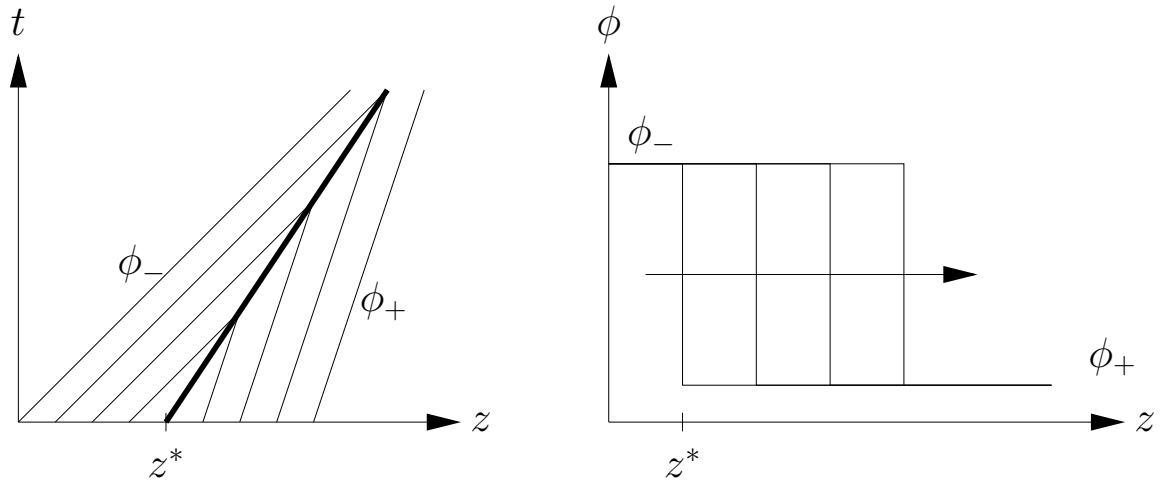

Figure 2.6: Shock wave from initial conditions Eq. 2.33. Left: Spectrum of the characteristics between $\boldsymbol{\phi}_-$ and $\boldsymbol{\phi}_+$, the shock is shown in bold. Right: Spatial profiles at equidistant time intervals

Again these solutions can be defined as time invariant curves, now labeled $\Sigma^{(k)}$ in the hodograph space.

$$\Sigma^{(k)}: \qquad \frac{\Delta\xi_1}{\Delta\phi_1} = \frac{\Delta\xi_2}{\Delta\phi_2} = \cdots = \frac{\Delta\xi_{N_v}}{\Delta\phi_{N_v}}, \tag{2.41}$$

$$w^{(k)} = \frac{\pi_f \Lambda_k - 1}{1 + \pi_h \Lambda_k}, \quad \text{with } \Lambda_k = \frac{\Delta\xi_i}{\Delta\phi_i}. \tag{2.42}$$

Here $\Delta\boldsymbol{\phi}$ is used as short form for $\boldsymbol{\phi}_+ - \boldsymbol{\phi}_-$ and similarly $\Delta\boldsymbol{\xi} = \boldsymbol{\xi}_+ - \boldsymbol{\xi}_-$. As before the first equation Eq. 2.41 defines the path of $\Sigma^{(k)}$ and the second equation Eq. 2.42 the propagation speed of the shock wave. In contrast to expansive waves along a shock wave all compositions along $\Sigma^{(k)}$ travel at the same speed $w^{(k)}$.

Combined Waves and Failure of Genuine Nonlinearity The wave type is determined by the so called entropy conditions. For a shock they require that

$$\sigma_{k-1}(\boldsymbol{\phi}_-) < \quad w^{(k)} \quad < \sigma_k(\boldsymbol{\phi}_-) \text{ and} \tag{2.43}$$

$$\sigma_k(\boldsymbol{\phi}_+) < \quad w^{(k)} \quad < \sigma_{k+1}(\boldsymbol{\phi}_+) \tag{2.44}$$

holds. These inequalities state that exactly N_v+1 characteristics of the N_v characteristics starting from $\boldsymbol{\phi}_-$ and the N_v characteristics starting from $\boldsymbol{\phi}_+$ enter the shock. The characteristics belonging to $\sigma_j,\ j = k+1(1)N_v$ enter the shock from $\boldsymbol{\phi}_-$ but not $\boldsymbol{\phi}_+$ and those belonging to $\sigma_j,\ j = 1(1)k-1$ enter from $\boldsymbol{\phi}_+$ but not $\boldsymbol{\phi}_-$. It is only the characteristics belonging to σ_k that enter from both, $\boldsymbol{\phi}_+$ and $\boldsymbol{\phi}_-$. This can only happen if

$$\sigma_k(\boldsymbol{\phi}_+) < w^{(k)} < \sigma_k(\boldsymbol{\phi}_-) \tag{2.45}$$

i.e. if the upper boundary composition $\boldsymbol{\phi}_+$ travels slower than the lower boundary composition $\boldsymbol{\phi}_-$. Hence the shock speed is between those two propagation speeds. For an expansive wave the opposite holds, i.e.

$$\sigma_k(\boldsymbol{\phi}_+) > \sigma_k(\boldsymbol{\phi}(\zeta)) > \sigma_k(\boldsymbol{\phi}_-). \tag{2.46}$$

Assuming genuine nonlinearity the wave type along either a $\Gamma^{(k)}$ or a $\Sigma^{(k)}$ does not change. However if some $\Gamma^{(k)}$ or $\Sigma^{(k)}$ crosses a line where genuine nonlinearity fails (in the remainder **f**ailure **o**f **g**enuine **non**linearity will be abbreviated by **fognol**) things may change. For a $\Gamma^{(k)}$ the effects are obvious (see Fig. 2.7): it changes to a $\Sigma^{(k)}$ at the point where **fognol** occurs i.e. where

$$\nabla\sigma_k \boldsymbol{s}_k = 0. \tag{2.47}$$

For a $\Sigma^{(k)}$ things are a bit more complicated. Simply crossing the line of **fognol** is not a sufficient condition but only a necessary condition for $\Sigma^{(k)}$ becoming a combined wave. A sufficient condition is the violation of Eq. 2.45 at some $\boldsymbol{\phi}$. At the $\boldsymbol{\phi}$ that violates Eq. 2.45 the $\Sigma^{(k)}$ changes to a $\Gamma^{(k)}$ and it is again a combined wave (see Fig. 2.8). A more precise definition of the point $\boldsymbol{\phi}_{\Sigma\to\Gamma}$ is

$$\boldsymbol{\phi}_{\Sigma\to\Gamma}:\ \Lambda_k(\boldsymbol{\phi}_-, \boldsymbol{\phi}_{\Sigma\to\Gamma}) = \lambda_k(\boldsymbol{\phi}_{\Sigma\to\Gamma}), \quad \boldsymbol{\phi}_{\Sigma\to\Gamma} \in \Sigma^{(k)} \text{ starting at } \boldsymbol{\phi}_-. \tag{2.48}$$

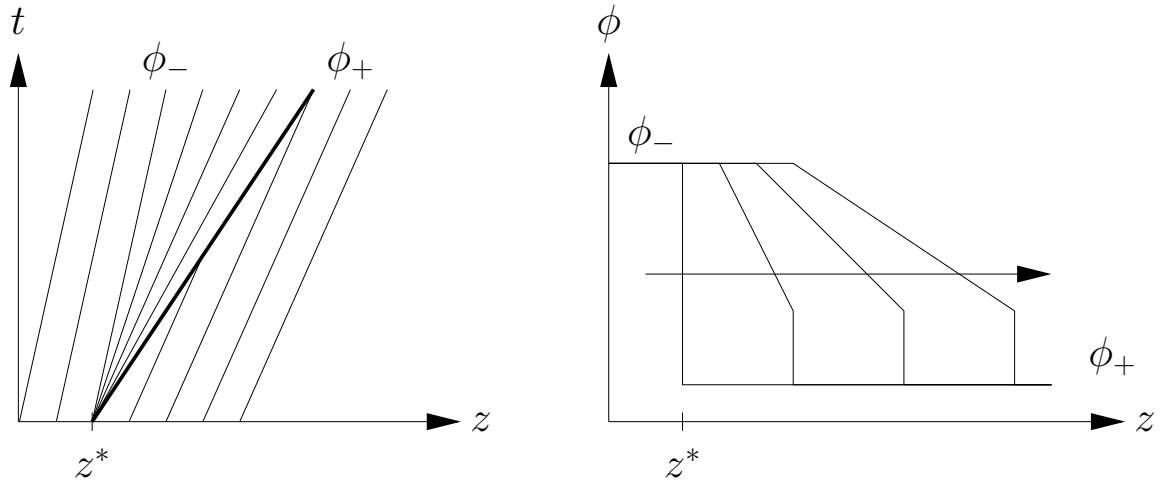

Figure 2.7: Combined wave from initial conditions Eq. 2.33: expansive wave preceded by a shock wave. Left: Spectrum of the characteristics between $\boldsymbol{\phi}_-$ and $\boldsymbol{\phi}_+$, the shock is shown in bold. Right: Spatial profiles at equidistant time intervals

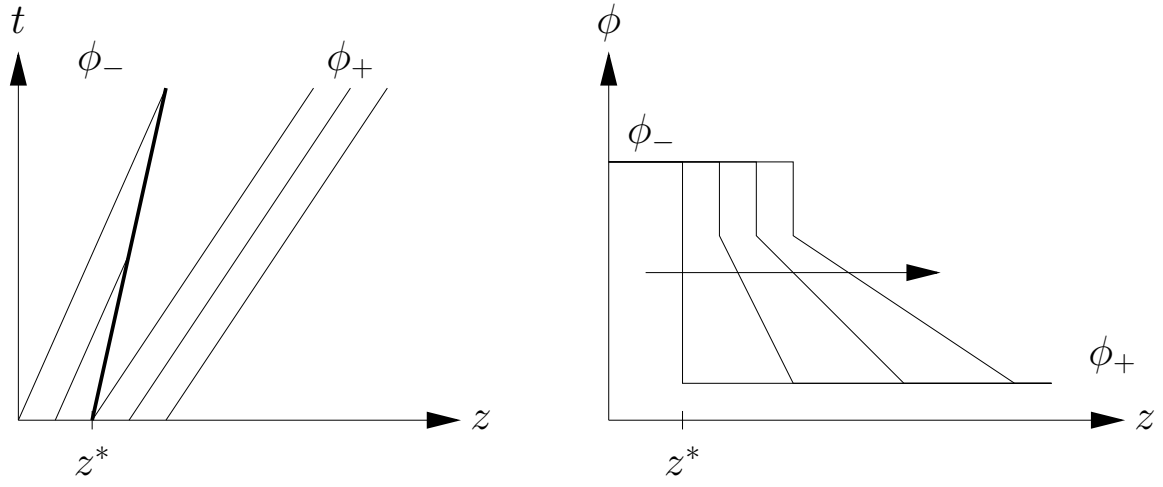

Figure 2.8: Combined wave from initial conditions Eq. 2.33: shock wave preceded by an expansive wave. Left: Spectrum of the characteristics between $\boldsymbol{\phi}_-$ and $\boldsymbol{\phi}_+$, the shock is shown in bold. Right: Spatial profiles at equidistant time intervals

In general even more complicated combined waves, involving several $\Sigma^{(k)}$ and $\Gamma^{(k)}$ sub waves are possible. Based on these considerations **fognol** lines are a good, but not sufficient, indicator for combined waves.
In order to be independent of the wave type or the fact that combined wave may be present a wave of family (k) will be denoted by $\Omega^{(k)}$ in the following no matter if it is a shock, an expansive or a combined wave.

General Wave Solution

Under the assumption of both, genuine nonlinearity and strict hyperbolicity the system Eq. 2.34 with initial conditions Eq. 2.33 has a unique solution for arbitrary entry compositions $\boldsymbol{\xi}^{-1}(\boldsymbol{\xi}_{in})$ and $\boldsymbol{\phi}_{in}$ with at most $N_v + 1$ spatially constant states

$$\boldsymbol{\phi}^{(k)}, \quad k = 1(1)N_v + 1 \qquad with\ \boldsymbol{\phi}^{(1)} = \boldsymbol{\phi}_{\text{in}}\ and\ \boldsymbol{\phi}^{(N_v+1)} = \boldsymbol{\xi}^{-1}(\boldsymbol{\xi}_{\text{in}}) \tag{2.49}$$

that are separated by at most N_v waves that are either expansive or shock waves. Since the waves have different propagation speeds an asymptotic pattern will eventually evolve. This happens as the waves line up in such a way that their individual propagation speed increases from wave to wave in the direction of the spatial coordinate. Once this pattern is reached the waves cannot overtake each other. Starting form initial conditions as in Eq. 2.33 the asymptotic pattern will emerge immediately. This self ordering ability implies an ordering of the waves speeds in Eq. 2.39 according to

$$\sigma_1 < \sigma_2 < \cdots < \sigma_{N_v}\ or\ \lambda_1 < \lambda_2 < \cdots < \lambda_{N_v}. \tag{2.50}$$

If the assumption of genuine nonlinearity is omitted only a slight modification of the above statement is necessary: The constant states are separated by at most N_v waves that are either expansive, shock or combined waves.
In general the solution of the system Eq. 2.34 with initial conditions Eq. 2.33 is the wave pattern

$$\boldsymbol{\phi}^{(1)} \xrightarrow{\Omega^{(1)}} \boldsymbol{\phi}^{(2)} \xrightarrow{\Omega^{(2)}} \boldsymbol{\phi}^{(3)} \cdots \boldsymbol{\phi}^{(N_v)} \xrightarrow{\Omega^{(N_v)}} \boldsymbol{\phi}^{(N_v+1)}. \tag{2.51}$$

If a wave $\Omega^{(k)}$ is not present Eq. 2.51 still holds by setting $\boldsymbol{\phi}^{(k)} = \boldsymbol{\phi}^{(k+1)}$.

Umbilic Points and Degenerated Systems

The system Eq. 2.34 is called degenerated if it is not strictly hyperbolic. For degenerated systems the construction of the wave pattern may become far more complicated than explained in the previous paragraphs. As the general case [53, 24] is clearly beyond the scope of the thesis at hand, the following remarks concentrate on the effects of isolated points of weak hyperbolicity, i.e. points where eigenvalues coincide. For systems with $N_v = 2$ such points are also called umbilic points.

Even though such degenerated points are isolated points just a single umbilic point affects the global structure of the $\Sigma^{(k)}$ and $\Gamma^{(k)}$ i.e. the topology of the hodograph space.

Associated with this change of topology there are two new phenomena that can arise for weakly hyperbolic systems: over compressive shock waves and transitional waves [22].

The term over compressive shock waves describes the phenomenon of two neighboring shock waves that travel at the same speed. This situation arises when the shock conditions Eq. 2.43 and Eq. 2.44 are violated in such a way that not only the characteristics belonging to σ_k but also those belonging to σ_{k+1} enter the shock from both, $\boldsymbol{\phi}_-$ and $\boldsymbol{\phi}_+$.

In the non strictly hyperbolic case the wave solution may consist of more than N_v waves $\Omega^{(k)}$ due to the presence of transitional waves. A transitional wave is always embedded in between an $\Omega^{(k)}$ and $\Omega^{(k+1)}$. Transitional expansive waves occur when a $(k+1)$-expansive wave is preceded by a (k)-expansive wave. This situation comes up when a (k)-expansive waves is followed by $(k+1)$-expansive wave that passes through a point where eigenvalues coincide. By passing through that point the wave becomes a (k)-expansive wave again and the final state is reached by a $(k+1)$ expansive wave. For transitional shock waves the situation is similar. A (k) shock hits the degenerated point or boundary of such an area and continues as the transitional wave which is then followed by a $(k+1)$ shock wave. The propagation speed of the transitional wave must be greater than that of the (k) shock.

Note that this is the case for watershed points in Langmuir systems. (In Langmuir systems one axis is intersected by slow waves only and the other is intersected by fast waves up to some point and from there on by slow waves. This point is the watershed point. Further details on watershed points in Langmuir systems can by found in [21].) However in Langmuir systems their effects are not evident as the watershed points only occur on

pure component axis.

The Pathgrid

In the previous section focus was on the theoretical basis of nonlinear wave propagation. This section deals with some more practical issues namely the construction of wave patterns. Two special cases, monovariant and bivariant systems, are treated in detail since they can be addressed by nice and clear graphical procedures. The general multivariant case is only briefly considered since a comparable graphical procedure is not possible. A further reason is the fact that typical chemical engineering application can be rendered as mono- or bivariant systems.

Monovariant Systems Monovariant systems are scalar equations of the same type as Eq. 2.34 i.e.

$$\frac{\partial \phi}{\partial t} + M^{-1} N(\phi) \frac{\partial \phi}{\partial z} = 0. \tag{2.52}$$

In the scalar case the eigenvalue is $\lambda = \frac{d\xi}{d\phi}$ and the eigenvector $r = 1$. The conditions for genuine nonlinearity Eq. 2.36 reduce to $\frac{d^2\xi}{d\phi^2} \neq 0$ which can be interpreted as a convexity condition. Since there is only a single trivial eigenvector the construction of the wave solution can be made in an $\xi(\phi)$ over ϕ graph. Construction of the wave pattern is now quite simple: The construction starts from ϕ_-. There are two cases to discriminate.

a) $\xi(\phi)$ is convex when looking toward ϕ_+: The solution starts with a Σ. If the shock cord, i.e. the line connecting ϕ_- and ϕ_+ intersects the graph, the solution is a combined wave. The point where the shock cord starting from ϕ_- becomes tangent to $\xi(\phi)$ for the first time is the point $\phi_{\Sigma\to\Gamma}$ and from there on the construction is as for case b).

b) $\xi(\phi)$ is concave when looking toward ϕ_+: The solution starts with a Γ. If, moving along the $\xi(\phi)$ graph, an inflection point is passed before ϕ_+ is reached the wave type changes to a Σ and the construction is as for case a) from there on.

A typical combined wave construction is depicted in Fig. 2.9. The solution consists of a shock from ϕ_- to $\phi_{\Sigma\to\Gamma}$ and an expansive wave from there to the end point ϕ_+.

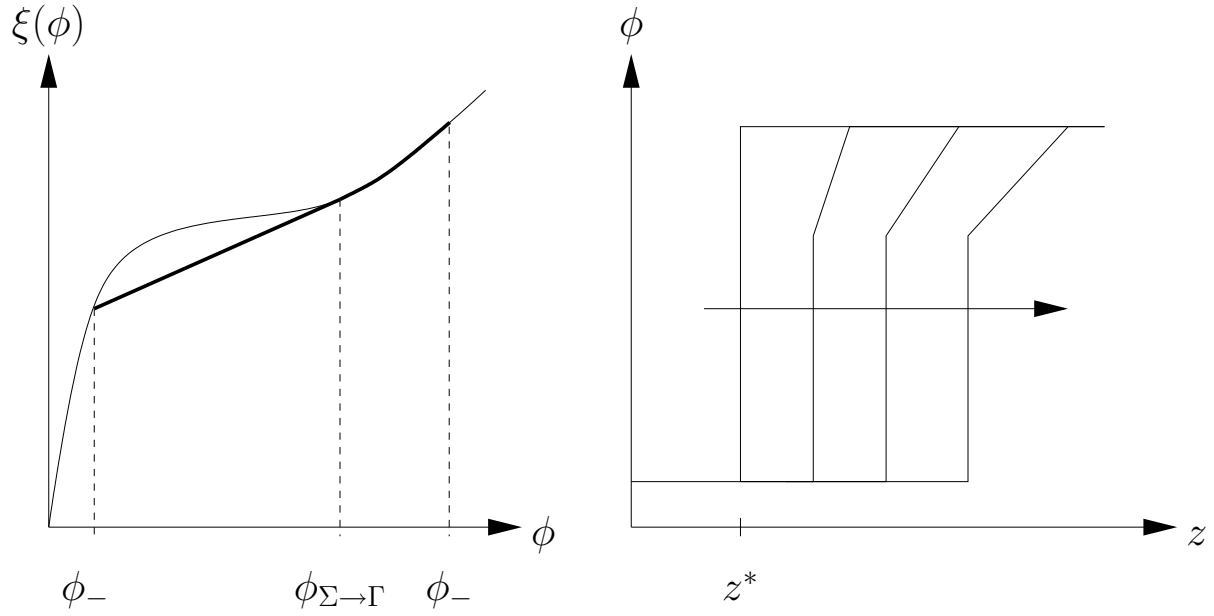

Figure 2.9: Left: construction of the wave solution for a combined wave. Right: corresponding spatial profiles.

Bivariant Systems For bivariant systems there are two eigenvalues λ_1 and λ_2 together with the corresponding eigenvectors $\boldsymbol{r}_1$ and $\boldsymbol{r}_2$. The solution is now constructed in the ϕ_2-ϕ_1 space as follows. Starting from $\boldsymbol{\phi}_-$ first a wave of family (1), i.e. a slow wave is taken. This wave is followed by a wave of the fast (2) family to the endpoint $\boldsymbol{\phi}_+$. The decision regarding the wave type depends on the direction the path is followed. In direction of increasing λ_k it is an expansive wave and in the other it is a shock wave until either the wave family is switched or the conditions for a combined wave are fulfilled. In contrast to the monovariant case no graphical shortcut is available and the more complex conditions Eq. 2.47 or Eq. 2.48 have to be applied. Which direction has to be taken cannot be stated a priori and hence a procedure similar to a shooting method has to be applied: Assume ω_1 and ω_2 are lengths along $\Omega^{(1)}$ and $\Omega^{(2)}$ respectively. Assume further that they take positive values if the $\Omega^{(k)}$ is followed at first in direction of increasing λ_k. Now follow $\Omega^{(1)}$ up to some ω_1, switch there to $\Omega^{(2)}$ and follow it up to some ω_2 to $\boldsymbol{\phi}(\omega_1, \omega_2)$. Then the distance from $\boldsymbol{\phi}(\omega_1, \omega_2)$ to $\boldsymbol{\phi}_+$ is computed and ω_1^s and ω_2^s are adjusted suitably. Note that this is an iterative procedure that eventually leads to the solution. However there are cases where no solution exists especially if the distance between $\boldsymbol{\phi}_-$ and $\boldsymbol{\phi}_+$ is large. A typical situation is shown in Fig. 2.10. In this sketch a differentiation between $\Gamma^{(k)}$ and

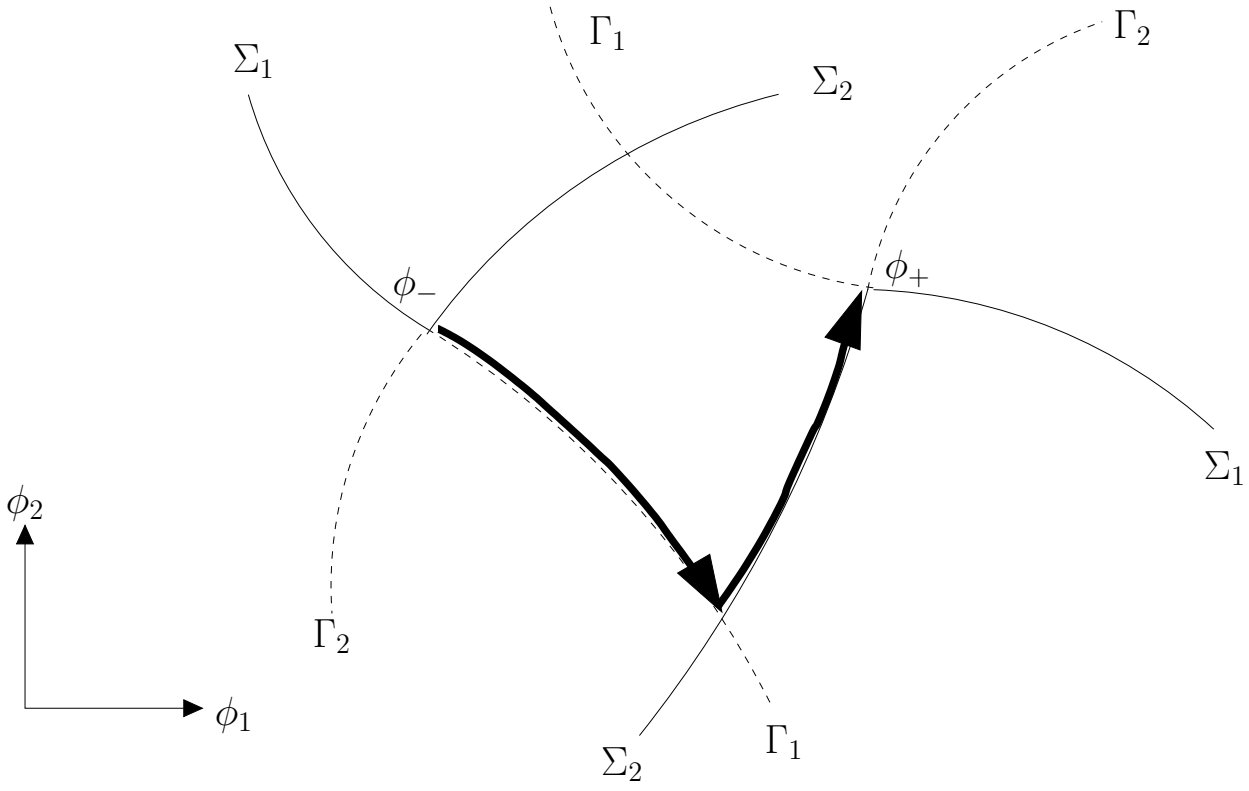

Figure 2.10: Construction of the wave solution in the ϕ_2-ϕ_1 space. Due to the curvature of the $\Gamma^{(k)}$s they are different from the $\Sigma^{(k)}$s. Note the different line styles for the $\Gamma^{(k)}$s and the $\Sigma^{(k)}$s.

$\Sigma^{(k)}$ has been made and hence the exact solution is shown. This procedure is difficult to apply since the $\Sigma^{(k)}$ depend on the starting point and thus they cannot be drawn a priori. The $\Gamma^{(k)}$ do not depend on their starting point but for every point a set of 2 $\Gamma^{(k)}$ exists. This allows an a priori construction of a whole grid of $\Gamma^{(k)}$s called the pathgrid. Due to the fact that the $\Sigma^{(k)}$ starting at some $\boldsymbol{\phi}$ is tangent to the $\Gamma^{(k)}$ at that point and typically the $\Sigma^{(k)}$ do not differ much from the $\Gamma^{(k)}$ the pathgrid can be used as a graphical short cut method to construct the solution.

Multivariant Systems Since for multivariant systems a graphical construction is not applicable the iterative procedure sketched in the previous paragraph has to be applied rigorously. However now with a whole set of $\Omega^{(k)}$, $k = 1(1)N_v$ and hence there are $k = 1(1)N_v$ ω_k to be determined.

2.3 Equilibrium Model for Combined Reaction and Phase Equilibrium

In this section a transformation of Eq. 2.31 to an equivalent homogeneous set of equations will be presented. This transformation establishes an elegant way to analyze combined reaction/separation processes in the framework of the theory of hyperbolic 1st order homogeneous quasilinear partial differential equations. The transformation is based on the assumption of simultaneous phase and reaction equilibrium. Since Eq. 2.31 represents an open system upon assuming reaction equilibrium the N_r reaction rates ϱ_k in Eq. 2.31 become indefinite and thus have to be eliminated. This elimination can be achieved by summing up suitable linear combinations of the individual equations Eq. 2.31.

In order to make this procedure clear, it's application to a simple example system with a single reactions of type $A + C \rightleftharpoons 2B$ in the ($'$) phase is shown. The system equations are

$$\frac{\partial \phi_A}{\partial t} + \pi_h \frac{\partial \xi_A}{\partial t} - \frac{\partial \phi_A}{\partial z} + \pi_f \frac{\partial \xi_A}{\partial z} = -\varrho, \tag{2.53}$$

$$\frac{\partial \phi_B}{\partial t} + \pi_h \frac{\partial \xi_B}{\partial t} - \frac{\partial \phi_B}{\partial z} + \pi_f \frac{\partial \xi_B}{\partial z} = 2\varrho, \tag{2.54}$$

$$\frac{\partial \phi_C}{\partial t} + \pi_h \frac{\partial \xi_C}{\partial t} - \frac{\partial \phi_C}{\partial z} + \pi_f \frac{\partial \xi_C}{\partial z} = -\varrho, \tag{2.55}$$

i.e. $\nu_A = -1,\ \nu_B = +2,\ \nu_C = -1$. One component is chosen as so called reference component ϕ_R. Here $\phi_R = \phi_B$ shall be chosen. The corresponding equation Eq. 2.54 is divided by the stoichiometric coefficient ν_B and before subtracting it from all other equations it is multiplied with the stoichiometric coefficient of those equations, i.e. ν_A and ν_C, one at a time. This yields

$$\begin{aligned} &\frac{\partial}{\partial t}\left(\phi_A + \frac{1}{2}\phi_B\right) + \pi_h \frac{\partial}{\partial t}\left(\xi_A + \frac{1}{2}\xi_B\right) \\ &\qquad -\frac{\partial}{\partial z}\left(\phi_A + \frac{1}{2}\phi_B\right) + \pi_f \frac{\partial}{\partial z}\left(\xi_A + \frac{1}{2}\xi_B\right) = 0, \end{aligned} \tag{2.56}$$

$$\begin{aligned} &\frac{\partial}{\partial t}\left(\phi_C + \frac{1}{2}\phi_B\right) + \pi_h \frac{\partial}{\partial t}\left(\xi_C + \frac{1}{2}\xi_B\right) \\ &\qquad -\frac{\partial}{\partial z}\left(\phi_C + \frac{1}{2}\phi_B\right) + \pi_f \frac{\partial}{\partial z}\left(\xi_C + \frac{1}{2}\xi_B\right) = 0. \end{aligned} \tag{2.57}$$

The quantities in the brackets can now be taken as new variables which will be referred to as transformed variables or transformed compositions. In terms of these transformed

variables Eqs. 2.56 and 2.57 can be rewritten as

$$\frac{\partial \Phi_A}{\partial t} + \pi_h \frac{\partial \Xi_A}{\partial t} - \frac{\partial \Phi_A}{\partial z} + \pi_f \frac{\partial \Xi_A}{\partial z} = 0, \tag{2.58}$$

$$\frac{\partial \Phi_C}{\partial t} + \pi_h \frac{\partial \Xi_C}{\partial t} - \frac{\partial \Phi_C}{\partial z} + \pi_f \frac{\partial \Xi_C}{\partial z} = 0. \tag{2.59}$$

Note that the indices of the transformed variables are the same as those of the component equation they were obtained from. In Eqs. 2.58 and 2.59 Ξ_i is written for the new combined phase and reaction equilibrium function which must be expressed in terms of the Φ_i. Since the ξ_i are only given as functions of the ϕ_i the inverse transformation, i.e. expressions for the ϕ_i as functions of the Φ_i are needed. These expressions can be obtained by solving the complete transformation equations

$$\Phi_A = \phi_A + \frac{1}{2}\phi_B, \tag{2.60}$$

$$\boldsymbol{\Phi}(\boldsymbol{\phi}): \quad \Phi_C = \phi_C + \frac{1}{2}\phi_B, \tag{2.61}$$

$$0 = \rho(\phi_A, \phi_B, \phi_C) \tag{2.62}$$

for the ϕ_i. Note, $\rho(\phi_A, \phi_B, \phi_C)$ describes the reaction equilibrium.

In multi-reaction systems this procedure is somewhat more complicated but the following formal approach is easily applicable. The stoichiometric matrix $\boldsymbol{\nu}$ has N_v rows and N_r columns with typically $N_v \geq N_r$, i.e. there are more components than reactions. Now the components are ordered in such a way that the last N_r equations represent the reference components. The stoichiometric matrix $\boldsymbol{\nu}$ is then partitioned as

$$\boldsymbol{\nu} = \begin{bmatrix} \boldsymbol{\nu}_T \\ \boldsymbol{\nu}_R \end{bmatrix} \tag{2.63}$$

where the matrix $\boldsymbol{\nu}_R$ of dimension $N_r \times N_r$ comprises the stoichiometric coefficients of the reference components and the matrix $\boldsymbol{\nu}_T$ of dimension $N_v - N_r \times N_r$ those of all other components. This choice of the reference components is not arbitrary. It has to be made in such a way that the resulting square matrix $\boldsymbol{\nu}_R$ has full rank i.e. $\mathrm{rank}(\boldsymbol{\nu}_R) = N_r$. Now the transformed variables can be obtained as

$$\boldsymbol{\Phi} = \left[\boldsymbol{I}_{N_v - N_r}, \quad -\boldsymbol{\nu}_T \left(\boldsymbol{\nu}_R\right)^{-1}\right] \boldsymbol{\phi} = \boldsymbol{L}\boldsymbol{\phi}, \tag{2.64}$$

$$\mathbf{0} = \boldsymbol{\rho}(\boldsymbol{\phi}). \tag{2.65}$$

The transformation matrix is called $\boldsymbol{L}$ since it projects $\boldsymbol{\phi}$ onto the left null-space of the stoichiometric matrix $\boldsymbol{\nu}$. The idea of utilizing the left null-space to analyze pure reaction systems was introduced by [49] in the area of metabolic control-theory, while at the same time [5] used a similar transformation method to investigate simultaneous phase and reaction equilibria for systems with single reaction which was later extended to multireaction systems [68], [69].

The combined phase and reaction equilibrium function is obtained by expressing the $\boldsymbol{\phi}$ in

$$\boldsymbol{\Xi} = \left[\boldsymbol{I}_{N_v - N_r}, \quad -\boldsymbol{\nu}_T \left(\boldsymbol{\nu}_R\right)^{-1}\right] \boldsymbol{\xi}(\boldsymbol{\phi}). \tag{2.66}$$

with the $\boldsymbol{\phi}(\boldsymbol{\Phi})$ according to Eqs. 2.64 and 2.65. In most cases an explicit calculation of the combined phase and reaction equilibrium function will not be possible due to the strong nonlinearities in the reaction equilibrium Eq. 2.65. As shown in appendix A an implicit definition of the combined phase and reaction equilibrium function $\boldsymbol{\Xi}(\boldsymbol{\Phi})$ is sufficient. Formally the transformed equation Eq. 2.31 now reads

$$\frac{\partial \Phi_i}{\partial t} + \pi_h \frac{\partial \Xi_i(\boldsymbol{\Phi})}{\partial t} - \frac{\partial \Phi_i}{\partial z} + \pi_f \frac{\partial \Xi_i(\boldsymbol{\Phi})}{\partial z} = 0 \tag{2.67}$$

and after some basic rearrangements and explicit differentiation of $\Xi_i(\boldsymbol{\Phi})$ one finds that Eq. 2.27 can be transformed into

$$\frac{\partial \boldsymbol{\Phi}}{\partial t} + \boldsymbol{M}^{-1}\boldsymbol{N}(\boldsymbol{\Phi}) \frac{\partial \boldsymbol{\Phi}}{\partial z} = \boldsymbol{0} \tag{2.68}$$

with

$$\boldsymbol{M}(\boldsymbol{\Phi}) = \pi_h \frac{\partial \boldsymbol{\Xi}}{\partial \boldsymbol{\Phi}} + \boldsymbol{I}, \quad \boldsymbol{N}(\boldsymbol{\Phi}) = \pi_f \frac{\partial \boldsymbol{\Xi}}{\partial \boldsymbol{\Phi}} - \boldsymbol{I} \tag{2.69}$$

where $\boldsymbol{I}$ denotes an identity matrix of suitable dimensions.

This is completely analogous to Eq. 2.34 and hence the complete theory presented in the previous section on nonlinear wave propagation can be applied.

2.4 Secondary Effects and Equilibrium Theory

In the equilibrium theory presented so far no secondary effects such as e.g. finite mass transfer rates and reaction rates or axial dispersion have been considered. In real systems these phenomena are always present and hence the question arises whether they do affect the results of equilibrium theory and if so, what are the consequences.

In the following section the influence of axial dispersion and in a subsequent section the influence of finite mass transfer and finite reaction rates is discussed.

2.4.1 Axial Dispersion

In order to include the effect of axial dispersion the model Eq. 2.31 may be extended by second order terms in the spatial coordinate [40, 25, 59] yielding

$$\frac{\partial \phi_i}{\partial t} + \pi_h \frac{\partial \xi_i(\boldsymbol{\phi})}{\partial t} - \frac{\partial \phi_i}{\partial z} + \pi_f \frac{\partial \xi_i(\boldsymbol{\phi})}{\partial z} - E' \frac{\partial^2 \phi_i}{\partial z^2} - E'' \pi_f \frac{\partial^2 \xi_i(\boldsymbol{\phi})}{\partial z^2} = \sum_{k=1}^{N_r} \nu_{ik} \varrho_k(\boldsymbol{\phi}). \tag{2.70}$$

Applying the developed transformation to Eq. 2.70, i.e. multiplying from left with the transformation matrix $\boldsymbol{L}$ gives the known transformed homogeneous equations

$$\frac{\partial \Phi_i}{\partial t} + \pi_h \frac{\partial \Xi_i(\boldsymbol{\Phi})}{\partial t} - \frac{\partial \Phi_i}{\partial z} + \pi_f \frac{\partial \Xi_i(\boldsymbol{\Phi})}{\partial z} - E' \frac{\partial^2 \Phi_i}{\partial z^2} - E'' \pi_f \frac{\partial^2 \Xi_i(\boldsymbol{\Phi})}{\partial z^2} = 0 \tag{2.71}$$

but now with second order spatial derivatives. While here only a brief summary of the results is given a detailed analysis of the effects of second order terms and the consequences in conjunction with nonlinear wave propagation can be found in [40], [36] and [26]. Focus of the analysis is on shock waves. Upon introducing the wave coordinate $\zeta = z - wt$ in equation Eq. 2.71 and integration from $-\infty$ to some ζ the effects of second order terms can be studied with the equation

$$\frac{1}{\pi_f - \pi_h w} \left(E'' \pi_f \frac{\partial \boldsymbol{\Xi}}{\partial \boldsymbol{\Phi}} + E' \boldsymbol{I} \right) \frac{d\boldsymbol{\Phi}}{d\zeta} = \boldsymbol{\Xi}(\boldsymbol{\Phi}) - \boldsymbol{\Xi}(\boldsymbol{\Phi}_-) - \frac{1+w}{\pi_f - \pi_h w} (\boldsymbol{\Phi} - \boldsymbol{\Phi}_-). \tag{2.72}$$

As the right hand side of equation Eq. 2.72 is independent of the dispersion coefficients E' and E'' the analysis is concerned with the properties of the matrix expression in the brackets on the left hand side which is called the dispersion matrix.

The main results of the analysis are as follows. To every shock wave solution of Eq. 2.67 exists a corresponding constant pattern wave with finite slope as solution of Eq. 2.71 provided Eq. 2.67 is strictly hyperbolic and $\boldsymbol{\Phi}_-$ and $\boldsymbol{\Phi}_+$ are sufficiently close to each other. For weakly hyperbolic systems Eq. 2.27 or $\boldsymbol{\Phi}_+$ far away from $\boldsymbol{\Phi}_-$ a strict mathematical proof is yet unknown but simulations studies indicate that the given results still apply. In any case the propagation speed of shock waves remains the same.

A further source of dispersion is the discretization of the partial differential equations Eq. 2.27 for their numerical solution by the method of lines [30]. In the numerical treatment,

especially that of chromatographic processes, this fact is often exploited in the following way. Instead of simulating a discretized version of the dispersive system Eq. 2.70 and thereby introducing additional, unwanted numerical dispersion, the system Eq. 2.27 is discretized and the number of discretization points is chosen such that the numerical dispersion matches the real dispersion due to the second order terms in Eq. 2.70. The correlation between the number of discretization points N_{grid} and dispersion coefficient E in physical units is [59]

$$N_{\text{grid}} = \frac{fl}{2E}. \tag{2.73}$$

As a consequence the number of discretization points has to be adjusted even during the simulation if the flow rates are varied in order to accurately render the dispersive effect of the second order term. Further details can be found in e.g. [59].

In the simulation studies that follow the partial differential equations, i.e either Eq. 2.10 or Eq. 2.20, have been discretized. The discretization is made by applying the finite volume method yielding simulation equations of the equilibrium cell model type. A consequence of the thereby introduced numerical dispersion is that shock waves do not become discontinuities but constant pattern waves, i.e. solutions to Eq. 2.10 or Eq. 2.20 with finite slope that do not change shape as they travel along the spatial coordinate. However, as the number of cells per unit length tends to infinity the constant pattern waves approach discontinuities.

In summary all analytical results and beyond their reach numerical investigations show that the structure of the wave solution is correctly predicted by equilibrium theory. But instead of discontinuities constant pattern waves with finite slope are observed.

2.4.2 Influence of Finite Rates

The fundamental assumption of the equilibrium theory presented is simultaneous phase and reaction equilibrium. Upon considering real systems it becomes obvious that the assumption of phase equilibrium as well as reaction equilibrium shall better be relaxed to the assumption of being close to phase equilibrium and close to reaction equilibrium. This in turn implies that there are finite mass transfer rates and finite reaction rates and hence the applicability of equilibrium theory needs some further justification. In the following first, the effects of finite mass transfer rates and finite reaction rates will be discussed

separately and finally their interaction. Note that the simulation based investigations are a case study and validity of the results for arbitrary systems may fail.

Finite Mass Transfer Rates

The mathematical treatment of finite mass transfer rates is similar to that of axial dispersion and is again focused on stationary solutions in a coordinate system that is moving with constant velocity w, i.e. solutions that solely depend on $\zeta = z - wt$. In the following the assumption of reaction equilibrium shall be valid.

Starting from Eq. 2.21 and Eq. 2.22 both equations can be added and the reaction terms can be eliminated by multiplying from left with $\boldsymbol{L}$. In contrast to Eq. 2.27 and Eq. 2.67 the $\boldsymbol{\Xi}$ are not substituted by $\boldsymbol{\Xi}(\boldsymbol{\Phi})$. Recall that $\boldsymbol{\Phi}$ is the reaction invariant composition in the (') and $\boldsymbol{\Xi}$ in the (") phase. After changing independent variables to the moving coordinate system and integration from $-\infty$ to some z inside the spatial domain the following relation between $\boldsymbol{\Xi}$ and $\boldsymbol{\Phi}$ is found:

$$\boldsymbol{\Xi} = \boldsymbol{\Xi}(\boldsymbol{\Phi}_-) + \frac{1+w}{\pi_f - \pi_h w}\left(\boldsymbol{\Phi}_- - \boldsymbol{\Phi}\right). \tag{2.74}$$

This relationship is linear and, by construction is valid in the presence of finite mass transfer rates. Upon substitution into the transformed material balances of the ($'$)-phase in the moving coordinate system one obtains

$$(1+w)\frac{d\boldsymbol{\Phi}}{d\zeta} = \mathbf{I}\left(\boldsymbol{\Phi}, \boldsymbol{\Xi}(\boldsymbol{\Phi}_-) + \frac{1+w}{\pi_f - \pi_h w}\left(\boldsymbol{\Phi}_- - \boldsymbol{\Phi}\right)\right). \tag{2.75}$$

In general the mass transfer terms are of the type

$$\boldsymbol{\iota}(\boldsymbol{\phi}, \boldsymbol{\xi}) = \pi_f \boldsymbol{B}(\boldsymbol{\phi}, \boldsymbol{\xi})(\boldsymbol{\xi}(\boldsymbol{\phi}) - \boldsymbol{\xi}) \tag{2.76}$$

with a full rank matrix $\boldsymbol{B}$ with non zero off-diagonal elements. For the commonly used case of a diagonal matrix $\boldsymbol{B}$ with equal diagonal elements it is shown in [26] that a constant pattern wave exists if a shock exists for the equivalent equilibrium model. Matrices $\boldsymbol{B}$ with a different structure may result in different behaviors for the finite mass transfer rate model and the equilibrium model as discussed in [26] for the nonreactive case. Hence in the following the commonly used case of a diagonal matrix $\boldsymbol{B}$ with equal diagonal elements is used.

	component A	component C
$\mathbf{\Phi}_-$	0.6	0.3
$\mathbf{\Phi}_+$	0.0	0.8789...
$\mathbf{\Xi}_-$	0.8064...	0.1798...
$\mathbf{\Xi}_+$	0.0	0.9561...

Table 2.2: Compositions used in the following simulation studies in transformed variables. Starting point was $\mathbf{\Phi}_-$ and $\mathbf{\Phi}_+$ was found as the point where one of the Σ intersects $\Phi_A \equiv 0$.

The transformed mass transfer terms are obtained by straight forward computation as

$$\mathbf{I}(\mathbf{\Phi}, \mathbf{\Xi}) = \pi_f B \left(\mathbf{\Xi}(\mathbf{\Phi}) - \mathbf{\Xi}\right). \tag{2.77}$$

and the transformed Eq. 2.75 reads after some rearrangements

$$\frac{1+w}{\pi_f}\left(\frac{1}{B}\right)\frac{d\mathbf{\Phi}}{d\zeta} = \mathbf{\Xi}(\mathbf{\Phi}) - \mathbf{\Xi}(\mathbf{\Phi}_-) - \frac{1+w}{\pi_f - \pi_h w}\left(\mathbf{\Phi} - \mathbf{\Phi}_-\right). \tag{2.78}$$

This equation is structurally completely equivalent to Eq. 2.72 which proves that both effects result in a similar modification of the wave solutions.

In order to complement the above theoretical consideration numerical simulations were performed. These simulations are based on discretized versions of equations Eq. 2.21 and 2.22. The mixture consists of three components A, B and C. The phase equilibrium is of the type $\xi_i = (a_i\xi_i)/(1 + \sum_{k=1}^{N_v} b_i\xi_i)$ with $a_A > a_B > a_C$ as well as $b_A > b_B > b_C$ and the mass transfer rate is $\iota_i = B(\xi_i(\boldsymbol{\phi}) - \xi_i)$ i.e. the same constant mass transfer coefficient for all components. A single reaction of the type $2B \rightleftharpoons A + C$ occurs in the ($'$) phase. The boundary conditions were chosen such that inside the spatial domain $0 < z < 1$ a single wave exists for the combined phase and reaction equilibrium while for phase equilibrium and no reaction two waves, one with higher and one with lower propagation speed exist. The flow rate ratio π_f was then chosen such that for the combined phase and reaction equilibrium $w \approx 0$ holds and therefore for the case of phase equilibrium and no reaction one wave has positive while the other wave has negative propagation speed. this is illustrated in Fig. 2.11. The numerical values used in the following are given in table 2.3 and as transformed values in table 2.2.

The stationary profiles for varied mass transfer coefficient are shown in Fig. 2.12. In the

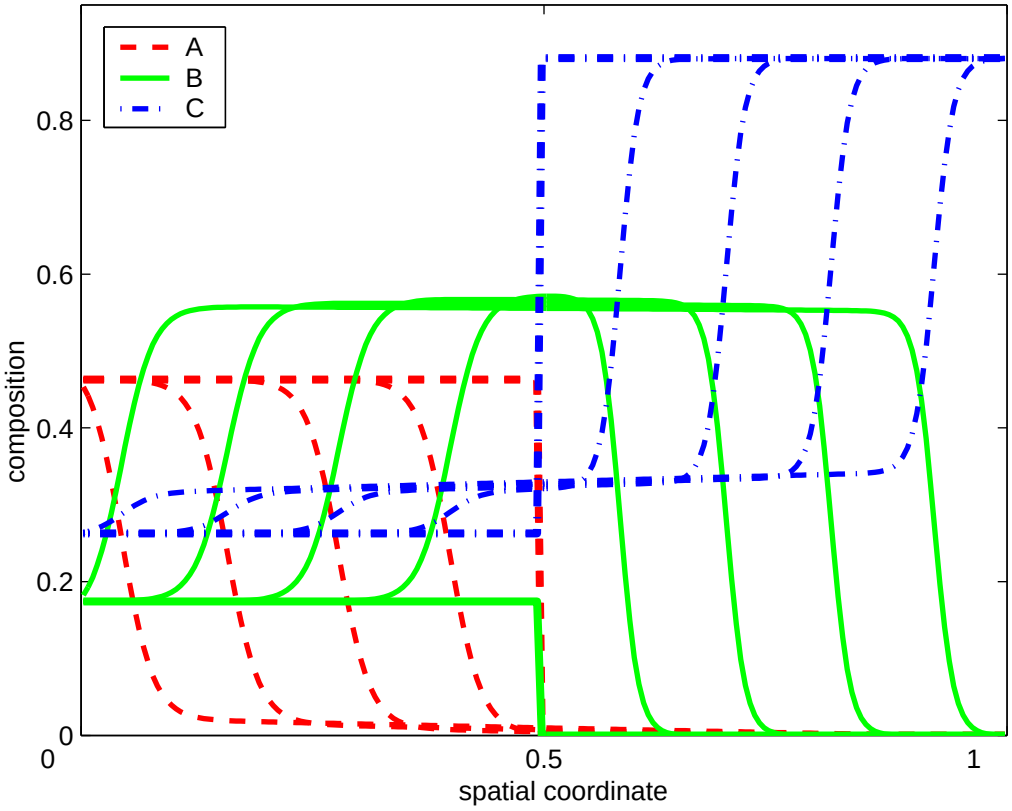

Figure 2.11: Boundary conditions as in table 2.3. Initial conditions render a jump from the left to the right boundary condition at $z = 0.5$. In this simulation a low reaction rate constant was chosen and hence the initial condition is resolved into two shocks with opposite propagation speed.

	component A	component B	component C
ϕ_-	0.5164...	0.1672...	0.2164...
ϕ_+	0.0	0.0	0.8789...
ξ_-	0.7262...	0.1567...	0.1014...
ξ_+	0.0	0.0	0.1561...

Table 2.3: Compositions used in the following simulation studies computed from the values given in table 2.2.

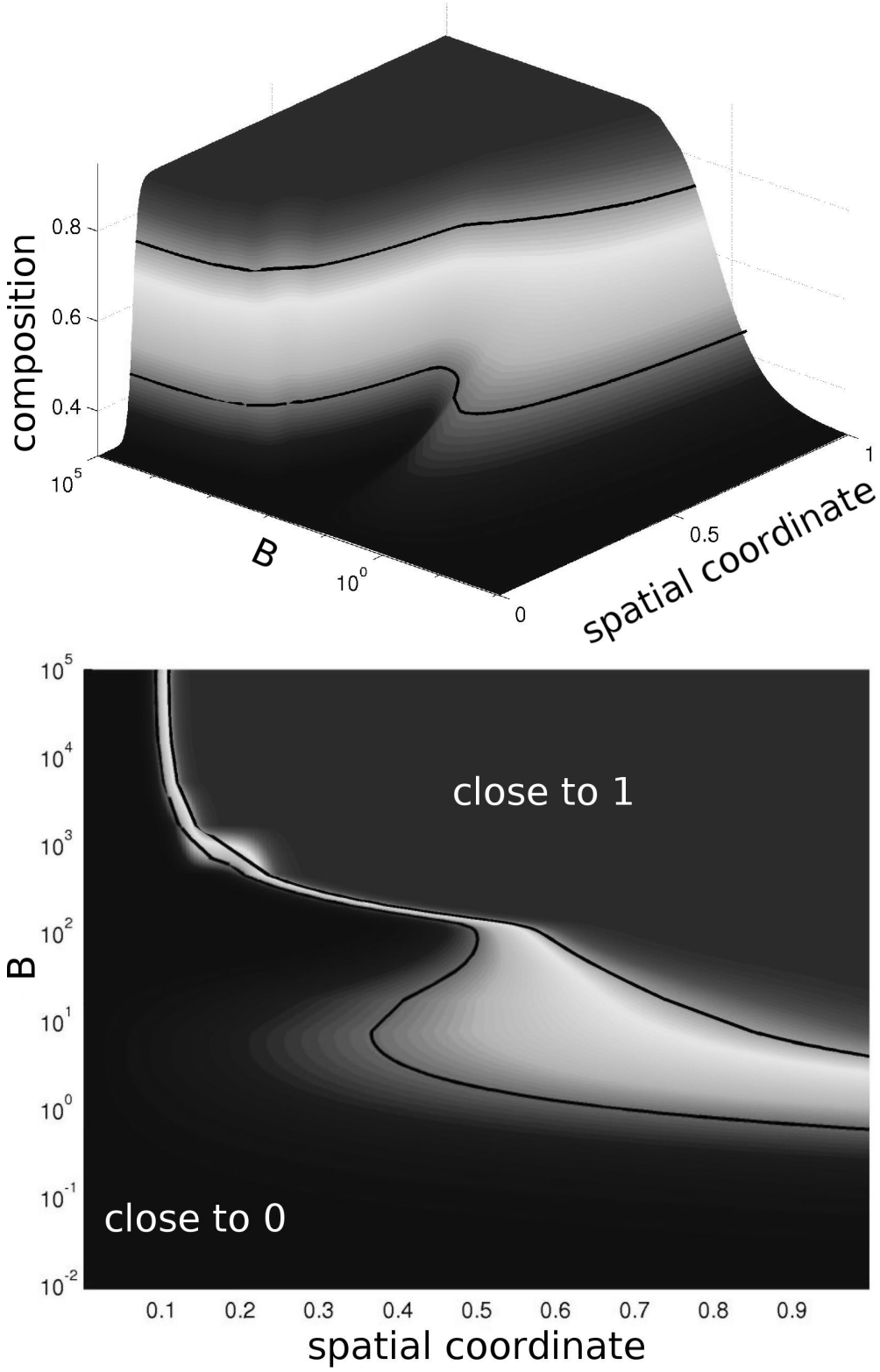

Figure 2.12: Influence of finite mass transfer rates on the stationary profiles in a counter current combined reaction separation process. Solid lines indicate the locus of the wave centers for an equivalent separation process. Top: composition profiles over the spatial domain as the mass transfer coefficient B is varied. Bottom: top view of the same graph.

top figure the spatial coordinate is shown from the front corner to the rear right corner and B is decreasing to the rear left corner. The concentration in transformed variables $\mathbf{\Phi}$ is shown as height and is color coded. The solid black lines indicate the center of the waves for the phase equilibrium only case and are defined as $(\mathbf{\Phi}_+ + \mathbf{\Phi}_-)/2$ for each wave. If the combined phase and reaction equilibrium and thus the developed equilibrium theory is valid they must behave as a common entity. At the bottom the same graph is shown as a top view.

As can be seen for very high values of B there is a single sharp wave located close to the left boundary, i.e. w is slightly negative. As B is decreased the wave continuously spreads. At first the wave centers remain very close together and the wave is pushed to the center of the spatial domain until about at $B = 10^2$. From there on the wave spreads considerably and for $B < 5$ the wave has spread over the complete spatial domain. This is most evident in the top view where it is easily seen that the two wave centers quickly move away from each other as B drops below $B \approx 5$. Since this simulation studies were performed in normalized space and time coordinates it can be concluded that the system is dominated by the effects according to the equilibrium theory at least down to a normalized mass transfer coefficient of $B = 10^2$ while below this value the effects due to the finite mass transfer rate become dominant.

Finite Reaction Rates

While the assumption of phase equilibrium is commonly adopted in the modeling of both, separation processes as well as combined reaction and separation processes, see e.g. [65, 39, 66], the assumption of reaction equilibrium may seem very restrictive. Hence in the following the effects of finite reaction rates on the predictions of the proposed combined phase and reaction equilibrium theory are discussed.

Instead of a theoretical treatment on basis of the equations Eq. 2.21 and Eq. 2.22 a simulation based approach is applied. This is justified by a strict mathematical proof, given in [9], that shows that the solutions of equations Eq. 2.31 gradually converge to the solutions of Eq. 2.67 as the reaction rate constant goes to infinity and thus reaction equilibrium is approached.

The simulation setup is identical to that of the previous section but now the mass transfer

coefficient B is kept constant at a very high fixed value to ensure phase equilibrium over the entire spatial domain. The stationary profiles for varying reaction rate constants K_{kin} are shown in Fig. 2.13. Considering figure Fig. 2.13 it is obvious that while reducing reaction rate constants at first the two wave centers remain a common entity but are pushed to the center of the spatial domain and are slightly spread. A similar behavior was previously found due to the finite mass transfer rates. Close to $K_{kin} \approx 1$ there is a rather quick change in the qualitative behavior of the profiles. Both waves move away from each other and get pushed against the system boundary. A more detailed analysis by further numerical simulations verifies that the two waves now behave as individual entities that behave according to the phase equilibrium only. These results clearly show that the proposed combined phase and reaction equilibrium theory is still applicable for finite reaction rates down to a reaction rate constant of $K_{kin} \approx 1$.

Interaction between Mass Transfer and Reaction Rates

As discussed in the preceding sections finite mass transfer or reaction rates have a considerable impact on the profile shape. In order to assess whether the combined phase and reaction equilibrium determines the profiles the distance between the wave centers of the corresponding separation process i.e. phase equilibrium was used. In Fig. 2.14 the color codes the distance of the two wave centers, while the mass transfer rate constant varies from bottom to top the reaction rate constant is increased from left to right. Small distances indicate the regime dominated by the combined phase and reaction equilibrium while the phase equilibrium is dominant in regions with distances close to 1. As noted in the considerations of the individual rates a critical reaction rate constant $K_{kin} \approx 1$ can be identified due to the quick increase in the distance of the wave centers around that value for simultaneous phase equilibrium, i.e. high values of the mass transfer rate constant B. On the other hand for high values of the reaction rate constant K_{kin}, i.e. reaction equilibrium, clearly a value of $B \approx 10^2$ marks the transition from a sharp wave to a wide spread wave. These estimates for the limits in the rate constants are rather optimistic. Stricter estimates for the rate constants are obtained by requiring the wave centers to have a distance of less than e.g. 10% of the spatial domain. This leads to $K_{kin} > 10$ and $B > 10^3$ as lower boundaries for the applicability of the combined phase and reaction

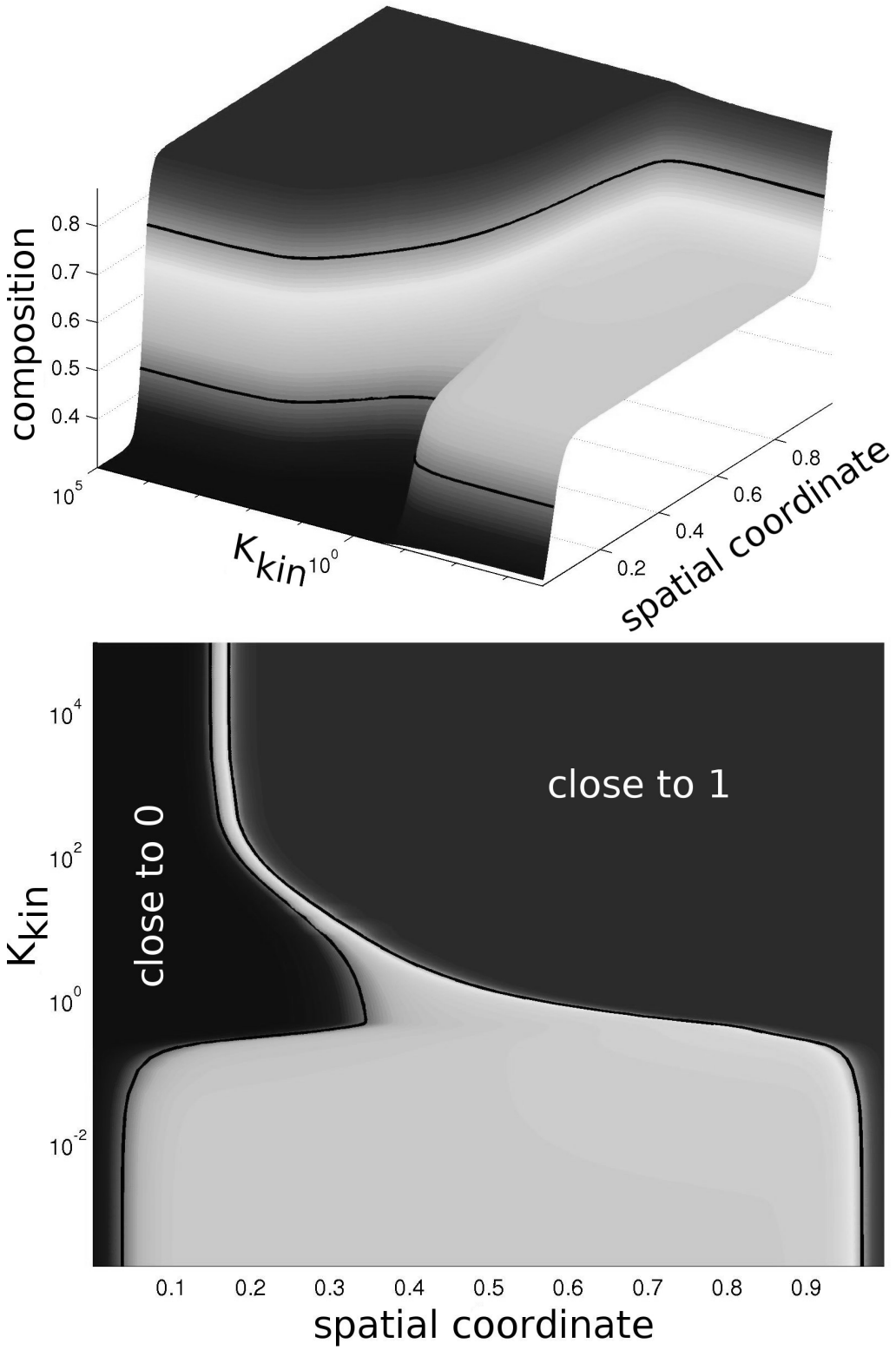

Figure 2.13: Influence of finite reaction rates on the stationary profiles in a counter current combined reaction separation process. Solid lines indicate the locus of the wave centers for an equivalent separation process. Top: composition profiles over the spatial domain as the reaction rate constant K_{kin} is varied. Bottom: top view of the same graph.

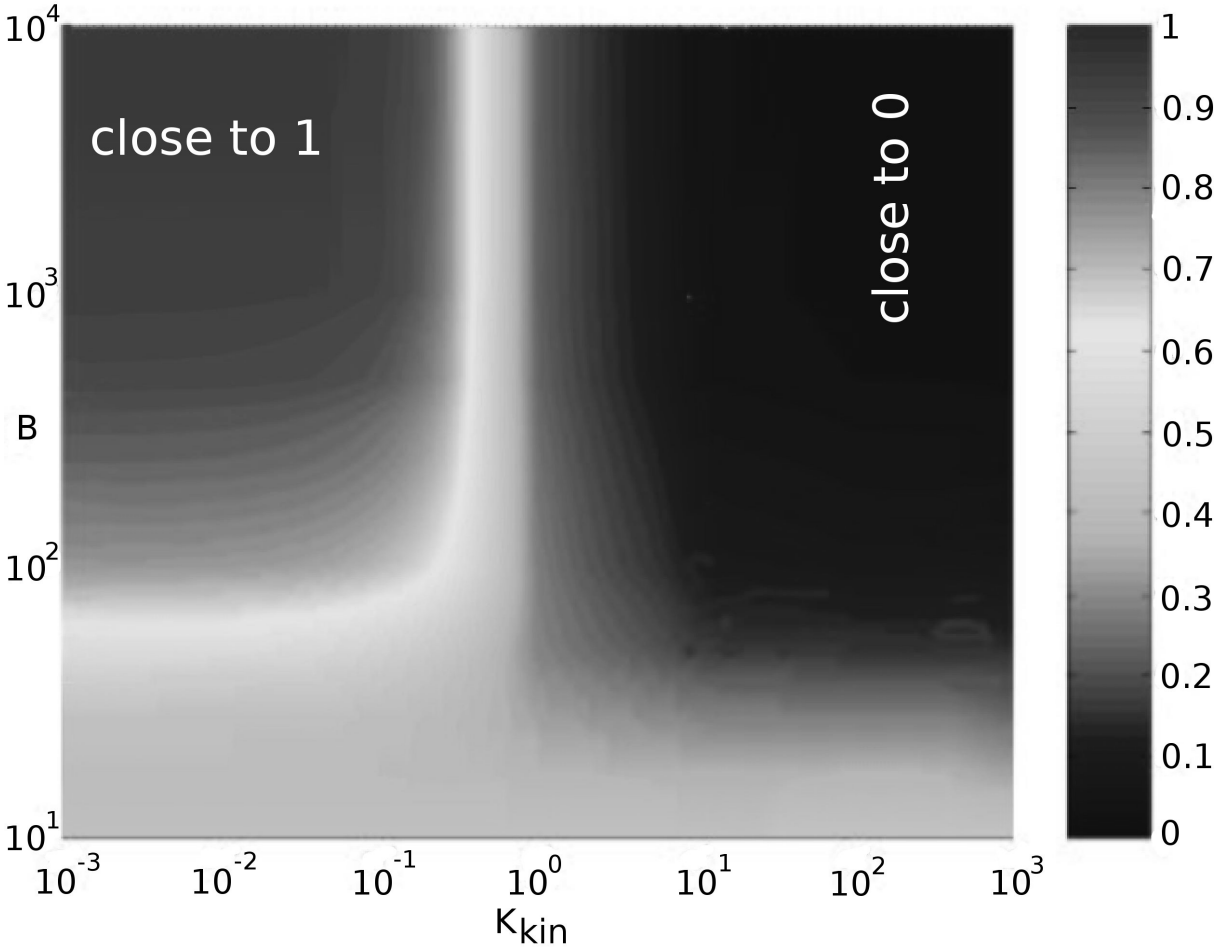

Figure 2.14: Cross influences of finite reaction and mass transfer rates in a counter current combined reaction separation process. The color codes the distance of the wave centers for the corresponding phase equilibrium only process.

equilibrium theory. Note that Fig. 2.14 also shows that there are hardly any interactions between the finite mass transfer rate and reaction rate.
Not that the above discussion is based on the specific reaction and phase equilibrium. The influence of the reaction and phase equilibrium on the results has not been investigated so far and hence they may not be transferable to other reaction and phase equilibria.

2.5 Summary

In this chapter, at first, the model equations for the two processes considered in the work at hand, i.e. reactive distillation columns and chromatographic reactors were derived. In order to allow for a detailed theoretical treatment the equations were then simplified and put into dimensionless form. Based on these simplified model equations a common prototype equation was deduced. In a short discussion it was then pointed out, that it is only due to different boundary conditions, imposed by external equipment needed to operate the processes, that both processes have been investigated individually in the past. To overcome this situation the subsequent development of the mathematical theory of combined reaction/separation processes was independent of any specific boundary conditions.
On basis of the prototype equation the known theory of nonlinear wave propagation was reviewed. Most of the previous work on nonlinear wave propagation in chemical engineering, especially in chromatography, concentrated on simple systems with linear or Langmuir type isotherms and hence the basic aspects of nonlinear wave propagation theory were sufficient to handle these systems. Here some emphasis was put on the more complicated aspects of nonlinear wave propagation theory since they become omnipresent for even simple combined reaction/separation processes.
Following this presentation of the known theory the development of the theory for combined reaction/separation processes was given. This extension to the theory of nonlinear wave propagation can be put in an elegant formalism and is thus easy to understand.
Finally the assumptions necessary to allow for a mathematical treatment of the system equations were investigated. Where feasible this was done theoretically and beyond that numerical investigations were used to give insight. These investigations eventually gave confidence that the results of the developed theory are not only valid for the idealized

model equations but also carry over to a wide range of real systems operated close to combined phase and reaction equilibrium.

Chapter 3

Applications

In the preceding chapter a mathematical theory of nonlinear wave propagation in combined reaction/separation processes was developed. Along with the mathematical theory some graphical methods to apply the theory to practical applications were introduced. In this chapter the use of the developed theory and graphical methods in conjunction with realistic applications is presented in some detail. The theory is first applied to illustrative examples and is then used to solve problems concerning process control. Note, since focus is on the use of the developed theroy and graphical methods the actual controller design is, in most cases, only sketched.

3.1 Illustrations for Reactive and Non-Reactive Systems

The developed transformation of reactive systems to equivalent non-reactive systems in the limit of combined phase and reaction equilibrium is now illustrated starting with some rather simple example systems while towards the end highly complex multireaction systems are considered. The main intention of these illustrations, especially of the simple example systems, is threefold. The basic intention is to show exemplarily how to apply the theory and what can be deduced from the theory. Further these illustrative examples show that reactive systems can behave similar to corresponding non-reactive systems. But at the same time the reactive systems show some additional features that cannot be found in the non-reactive counter parts. Finally some striking similarities between distillation

and chromatographic processes are uncovered.

3.1.1 Monovariant Systems

As a very first starting example two monovariant systems are considered. The first is the familiar distillation of a binary mixture while the second is the reactive distillation of an ideal ternary mixture with a single reaction in the fluid phase. Both examples represent monovariant systems in the framework of equilibrium theory since in distillation processes there are only $N_c - 1$ independent mole fractions and in the mentioned reactive system the reaction equilibrium imposes an additional constraint. As pointed out before monovariant systems are preferably analyzed in $y(x)$ diagrams.

Binary Distillation

Since ideal and moderately nonideal mixtures are characterized by convex equilibrium functions $y(x)$ the solution consists of a single constant pattern wave. This constant pattern wave is either balanced, i.e. the propagation speed according to Eq. 2.42 is zero, and the wave is standing in the middle of the column section or it is not and thus pushed against the boundary where it is stopped due to repelling effects of this boundary and the propagation speed becomes zero. In Fig. 3.1 a) such a situation in a rectifying section of a distillation column is shown. As can be seen in the $y - x$-graph in the left part of Fig. 3.1 a) there is one constant pattern wave from x_- to $x_+ = 1$. The profiles shown on the right half of Fig. 3.1 a) are snapshots at equidistant time intervals and show the propagation of the constant pattern wave in direction of the arrow. Note that according to Eq. 2.42 this constant pattern wave is balanced if and only if $\pi_f \Lambda - 1 = 0$. Remember that π_f is defined as the ratio of the vapor flow rate coming up the column section to the liquid flow rate going down the section. In a rectifying section the liquid flow is a fraction of the condensed vapor and consequently $\pi_f \geq 1$. Asking now for the Λ values that allow a balanced wave one easily finds that $\Lambda \leq 1$ has to be fulfilled. In other words this means that the slope of the shock cord from x_- to x_+ must not exceed 1 for being able to balance the wave.

A more complex situation is shown in Fig. 3.1 b). Here the equilibrium function $y(x)$ has an inflection point and thus becomes concave. In the depicted situation this property

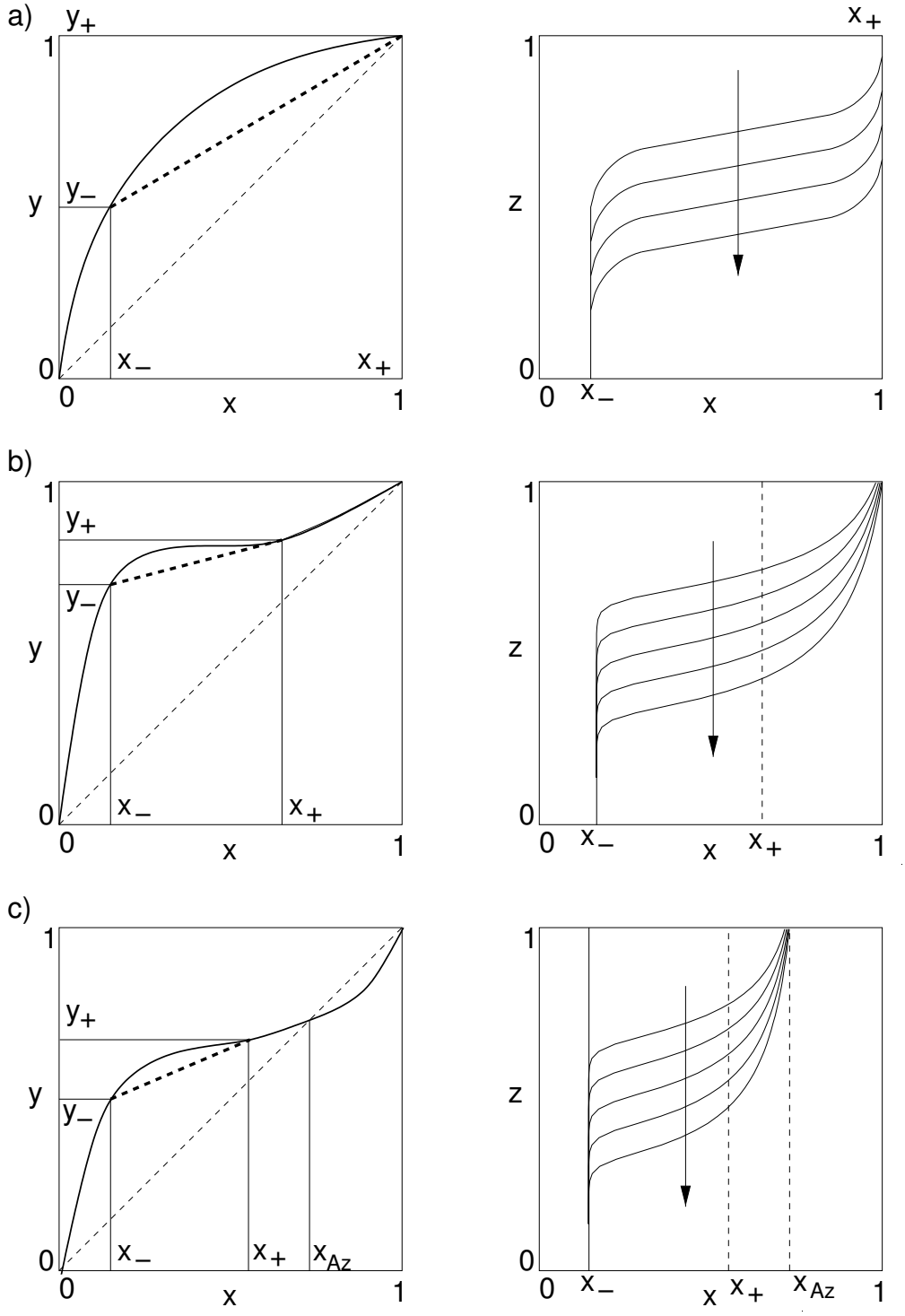

Figure 3.1: Typical wave solution in a binary rectifying section of a distillation column a) ideal mixture, b) nonideal zeotropic mixture with inflection point, c) nonideal azeotropic mixture with minimum azeotrope.

of the equilibrium function is sufficiently strong developed to allow for a combined wave. The shock cord becomes tangent at $x = x_+$ and from there on up to $x = 1$ an expansive wave emerges. In order to obtain the desired product of composition $x = 1$ in such a column the propagation speed has to be adjusted such that $\pi_f \lambda(x = 1) - 1 = 0$. As a consequence the shock wave from x_- to x_+ has a negative propagation speed and is pushed to the lower boundary of the column section.

For highly nonideal mixtures, as shown in Fig. 3.1 c), azeotropic compositions occur. The construction of the wave solution starts again at x_- with a shock wave up to x_+ and from there on it is an expansive wave ending at the azeotropic composition x_{Az}. Regarding the propagation speed the arguments given for Fig. 3.1 b) are valid but $x = 1$ has to be replaced with $x = x_{Az}$. Taking a closer look at the hypothetic wave solution beyond the azeotropic composition for suitable boundary conditionsone finds that the solution still exist up to the second possible product composition $x = 1$. Considering the flow rate ratio π_f needed to balance this composition it is directly seen from the $y(x)$ graph that $\pi_f < 1$ is required to fulfill $\pi_f \lambda(x = 1) - 1 = 0$. At steady state this is not possible in a rectifying section since it would require more liquid to flow down the column than vapor is coming up which is not possible and thus this product composition is not feasible.

Reactive Distillation

After considering nonreactive systems in the previous this section is concerned with the analysis of a very simple reactive distillation example. The phase equilibrium of the ideal mixture is described by constant relative volatilities and in the fluid phase a simple reaction of type $2A \rightleftharpoons B + C$ is occurring. The finite rate model of such a section can be given as

$$\frac{\partial x_1}{\partial t} - \frac{\partial x_1}{\partial z} = -j_1(\boldsymbol{x}, \boldsymbol{y}) - 2r(\boldsymbol{x}) \tag{3.1}$$

$$\frac{\partial x_2}{\partial t} - \frac{\partial x_2}{\partial z} = -j_2(\boldsymbol{x}, \boldsymbol{y}) + r(\boldsymbol{x}) \tag{3.2}$$

for the liquid phase and

$$\epsilon \frac{\partial y_1}{\partial t} + \frac{1}{A} \frac{\partial y_1}{\partial z} = j_1(\boldsymbol{x}, \boldsymbol{y}) \tag{3.3}$$

$$\epsilon \frac{\partial y_2}{\partial t} + \frac{1}{A} \frac{\partial y_2}{\partial z} = j_2(\boldsymbol{x}, \boldsymbol{y}) \tag{3.4}$$

for the vapor phase. With component A having index '1', B index '2' and C index '3'. Hence the stoichiometric matrix is $\nu = [-2 \;\; 1]^T$. Choosing A with index '1' as reference component the transformation matrix is

$$\boldsymbol{L} = [\frac{1}{2} \;\; 1] \tag{3.5}$$

and the transformed composition variables read

$$X = L\,[x_1 \;\; x_2]^T = \frac{x_1}{2} + x_2, \tag{3.6}$$

$$Y = L\,[y_1 \;\; y_2]^T = \frac{y_1}{2} + y_2. \tag{3.7}$$

Introducing the assumption of phase equilibrium the model equations become

$$\frac{\partial X}{\partial t} + \frac{\frac{1}{A}\frac{\partial Y}{\partial X} - 1}{\epsilon\frac{\partial Y}{\partial X} + 1}\frac{\partial X}{\partial z} = 0 \tag{3.8}$$

and the system is again monovariant. Due to the ordering of the equations the transformed composition variables X and Y have the following properties. $X = 1$ corresponds to pure product B, $X = 0$ to pure product C and $X = 0.5$ to pure reactant A. Feeding pure reactant to the distillation column thus means $X_{feed} = 0.5$ and the desired products for complete separation and thus full conversion of the educt A are $X_{prod} = 0$ and $X_{prod} = 1$ which is in perfect analogy to nonreactive distillation of a binary mixture with equimolar feed.

The key in the further analysis is the combined equilibrium function which is derived now. Starting from the phase equilibrium relation

$$y_i = \frac{\alpha_i x_i}{1 + \sum_{k=1}^{2}(\alpha_k - 1)x_k}, \quad i = 1, 2 \tag{3.9}$$

and the reaction equilibrium

$$K = \frac{x_2 x_3}{x_1^2} = \frac{x_2(1 - x_1 - x_2)}{x_1^2} \tag{3.10}$$

the transformed equilibrium function is obtained by solving

$$X = \frac{x_1}{2} + x_2 \tag{3.11}$$

$$K = \frac{x_2(1 - x_1 - x_2)}{x_1^2} \tag{3.12}$$

for $x_1(X)$ and $x_2(X)$ yielding

$$x_1 = \frac{3}{2}X - \frac{K}{4} - \frac{\sqrt{(K+2)^2 - (8+12K)X + 4X^2}}{4} - \frac{1}{2} \tag{3.13}$$

$$x_2 = -X + \frac{K}{2} - \frac{\sqrt{(K+2)^2 - (8+12K)X + 4X^2}}{4} + 1 \tag{3.14}$$

and upon substituting the results in

$$Y = y_1(x_1, x_2) + \frac{y_2(x_1, x_2)}{2} \tag{3.15}$$

one obtains an explicit expression for

$$Y = Y(X). \tag{3.16}$$

In Fig. 3.2 three different cases for this reactive system are considered. The left column shows the equilibrium functions while the right column shows profiles along the spatial coordinate of the reactive distillation column. In Fig. 3.2 a) the educt is intermediate boiling while it is light boiling in Fig. 3.2 b) and heavy boiling in Fig. 3.2 c). The first case corresponds to an ideal binary nonreactive system while the second and third case to a system with a minimum and a maximum azeotrope respectively. These points are called reactive azeotropes as they are characterized by compensation of reaction and distillation [6]. As pointed out before in the discussion of nonreactive systems an azeotrope cannot be crossed at steady state. Since this limitation might be over come by combining reactive and nonreactive sections in a single column the statement refers to fully reactive distillation columns only. To further illustrate the different situations a single feed fully reactive distillation column is considered with pure educt as feed, i.e $X_{feed} = 0.5$. The emerging wave patterns are shown in the right column of Fig. 3.2 while Fig. 3.3 shows the same profiles in physical coordinates. In the first case with A as intermediate boiling component both products can be obtained pure and thus full conversion can be achieved. In the case with A as light boiling component a ternary mixture is obtained at the top while pure product C can be obtained at the bottom. For the third case with A as heavy boiling component pure product B can be obtained at the top while at the bottom only a ternary mixture can be obtained. Note that in the second and third case the equilibrium function has an inflection point and since it does not coincide with the azeotropic point combined waves occur. A more detailed analysis of the situation shows that the shock cords from

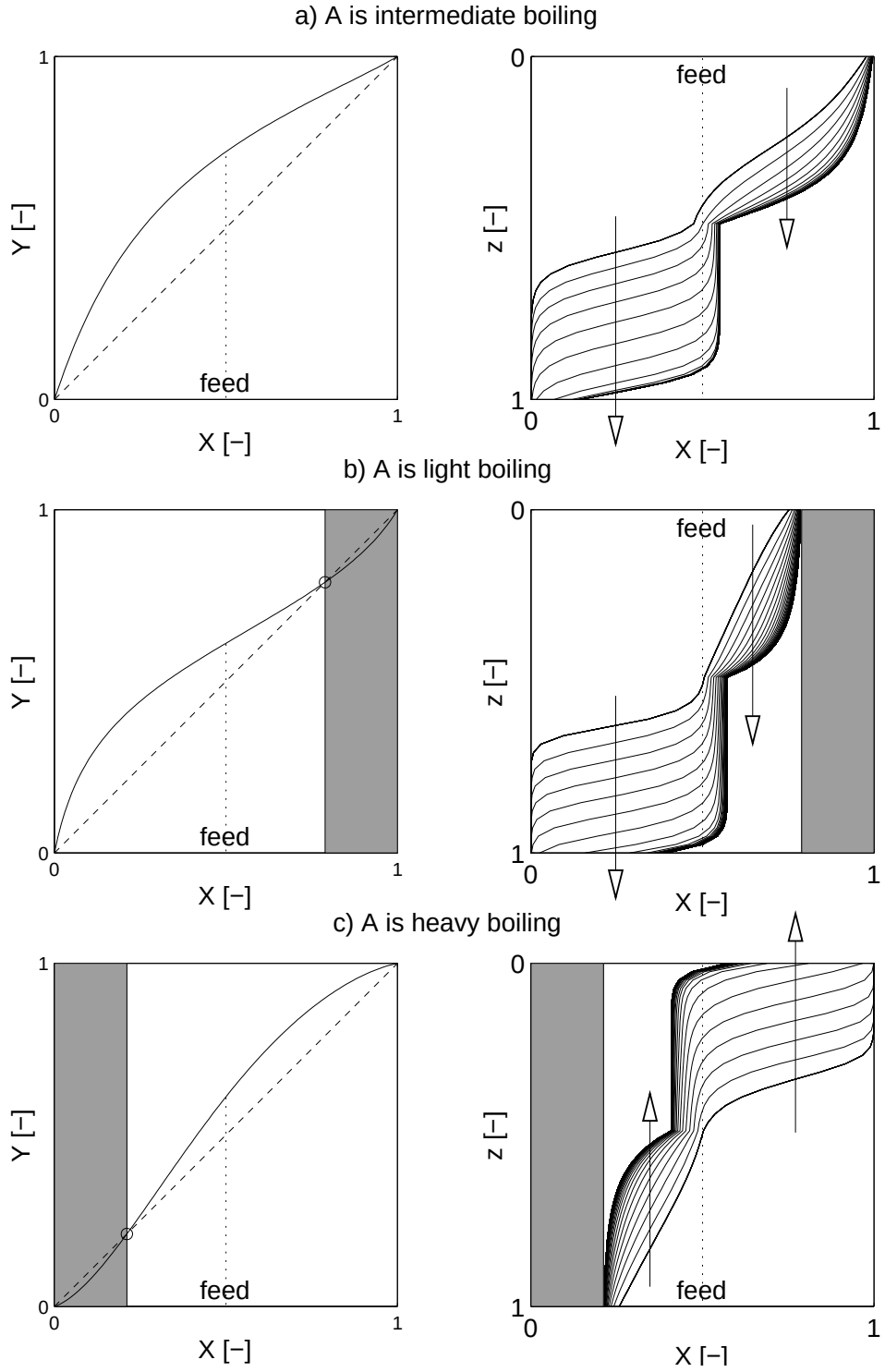

Figure 3.2: Left column: combined phase and reaction equilibrium function $Y(X)$ for constant relative volatilities and a chemical reaction $2A \rightleftharpoons B + C$ in the liquid phase. Right column: typical profiles in a reactive distillation column. a) educt is intermediate boiling, b) educt is light boiling, c) educt is heavy boiling.

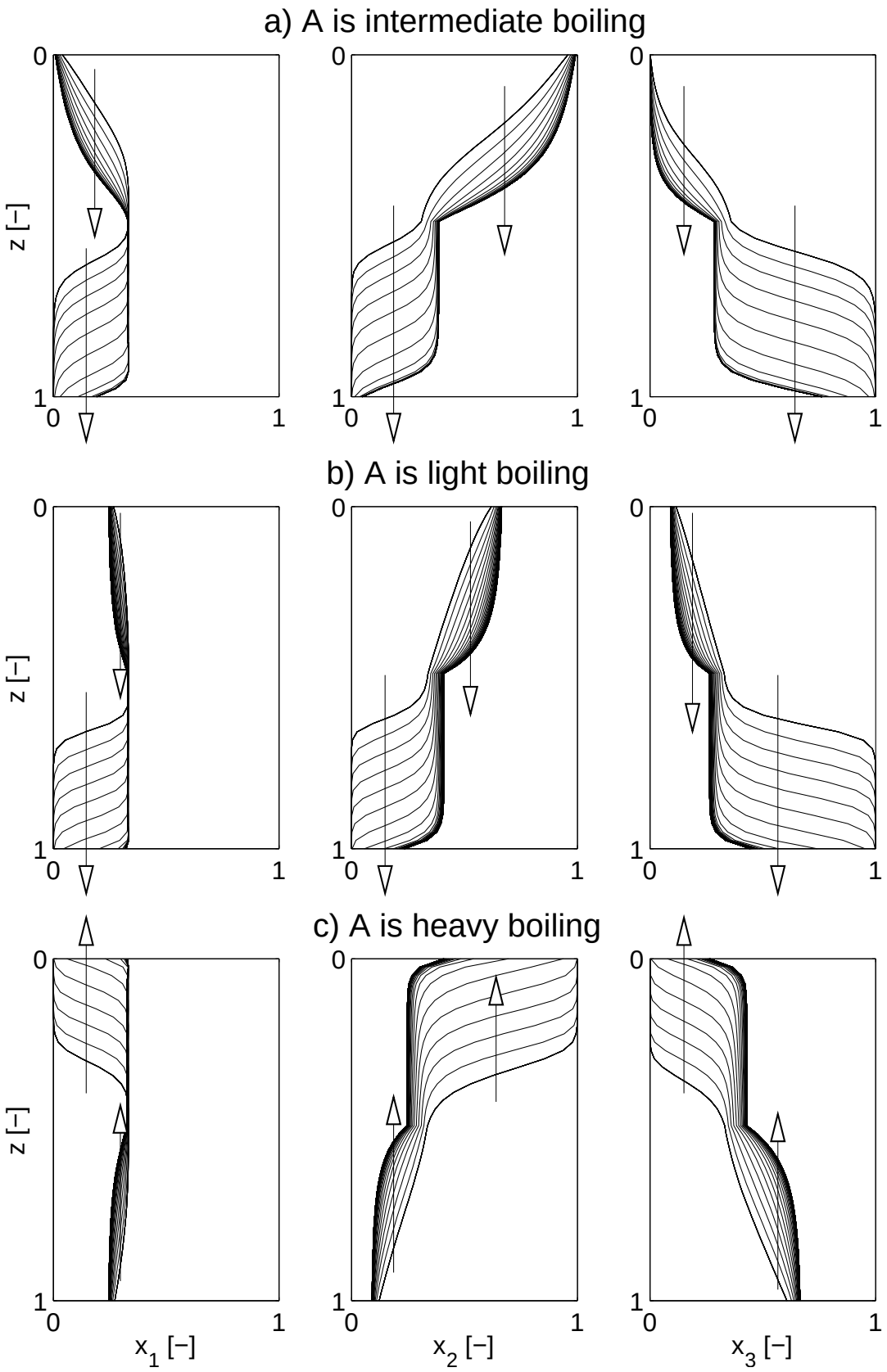

Figure 3.3: Wave patterns in physical concentrations variables corresponding to the three cases given in Fig. 3.2.

Parameter	a) A has intermediate volatility	b) A has highest volatility	c) A has lowest volatility
α_1	3.0	5.0	1.0
α_2	5.0	3.0	5.0
α_3	1.0	1.0	3.0
K		1.0	
x_{feed}		$x_1 = 1.0,\ x_2 = 0.0,\ x_3 = 0.0$	
Number of stages		40	
Feed stage		20	
Feed flow rate		2.0	
Reflux/distillate	1.25	$1.5981 \rightarrow 1.4$	$3.5 \rightarrow 3.9$
Vapor flow rate	$2.25 \rightarrow 2.3$	$3.2942 \rightarrow 3.1925$	$3.2942 \rightarrow 3.2$

Table 3.1: Parameters for the reactive distillation examples shown in Figs. 3.2 - 3.4. The last two rows show the step changes of the operating parameters for obtaining the transients shown in the figures

the feed point to the points of tangency differ only little from the equilibrium function and thus the sharpening tendency of the corresponding shocks is weakly pronounced. Since this results in flat shock profiles as seen in the top and bottom sections for cases 2 and 3, respectively, the expansive part of the combined waves is hardly visible in Figs. 3.2 and 3.3. Towards the end of the transients shown the waves are pushed against the boundaries and thus steep up. The physical parameters for the simulations are given in table 3.1. To investigate the influence of the reaction equilibrium constant K Fig. 3.4 shows the combined phase and reaction equilibrium function for different values of K for all three cases. The arrows point in direction of increasing K. Fig. 3.4 a) shows that, for the case the educt is intermediate boiling, no reactive azeotrope exist but the equilibrium function is bulged and finally touches the bisection line in the limit $K \rightarrow 0$. This may give rise to combined waves for low values of K while for higher values of K only constant pattern waves exist since then the equilibrium function becomes convex . In the two other cases, i.e. the educt is either light or heavy boiling, there is always a reactive azeotrope. This property was already rigorously proofed by [7]. For the educt as light boiling component

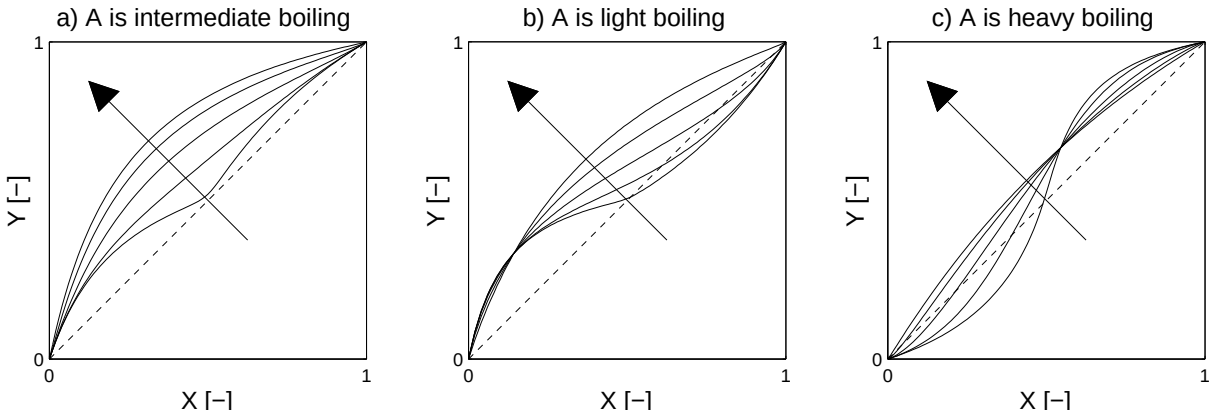

Figure 3.4: Influence of the chemical equilibrium constant K on the combined phase and reaction equilibrium function for the three cases given in Fig. 3.2. $K = 10^{-3},\ 10^{-1},\ 10^{0},\ 10^{1},\ 10^{3}$. The arrows point in the direction of increasing K.

there is always a minimum azeotrope. This azeotrope moves from pure educt A, i.e. $X = 0.5$ to pure product B, i.e. $X = 1$ as K is increased. In the third case with heavy boiling educt a maximum azeotrope moves from pure educt A to pure product C, i.e. $X = 0$ as the reaction equilibrium constant K is increased.

This first look at monovariant systems has shown that reaction and the resulting combined phase and reaction equilibrium can introduce inflection points as well as reactive azeotropes to ideal nonreactive systems. Further more it was shown that this can have sever consequences for the dynamics as well as the steady state behavior of the system.

In the next section bivariant systems as the simplest form of multivariant systems will be considered. This is done with an example from chromatography but as was previously shown the procedure is the same as for distillation processes since both only differ in the boundary systems. This will be exploited to point out some parallels to the considered monovariant example from distillation.

3.1.2 Bivariant Systems

Bivariant systems are the standard case for chromatographic separations such as chromatographic moving bed processes. As examples for bivariant systems at first the familiar two solute Langmuir chromatography is considered and then a three component reactive system. For the second system it is again the reaction equilibrium that takes away one degree of freedom and thus the system is bivariant. Due to the two degrees of freedom

bivariant systems are preferably analyzed by investigating their corresponding path grid. To get further information about e.g. wave types and propagation speed the characteristic speeds along the paths have to be tracked. Since it is not possible to give a detailed graphical representation of the propagation speeds the graphs have to represent this information a condensed form. A good understanding of the changes in propagation speed is obtained by sketching the lines of inflection into the graphs and put arrows along the paths that indicate the direction of increasing eigenvalues and thus propagation speed. This allows to determine the initial wave types and gives hints on the presence of combined or more complex waves.

Two Solute Langmuir Chromatography

As focus in many previous books and papers on nonlinear waves in chromatography, as e.g. [18] or [40], is on Langmuir systems the phase or sorption equilibrium of this first example is chosen to be of that type. The competitive Langmuir isotherm is given as

$$q_i = \frac{a_i c_i}{1 + \sum_{k=1}^{N_s} b_k c_k}, \forall i = 1(1)N_s. \tag{3.17}$$

In the middle of Fig. 3.5 typical profiles resulting from a step increase of the inlet concentrations to an initially unloaded column are shown. Since the competitive Langmuir isotherm Eq. 3.17 is convex there are no combined waves and the step change is resolved into two sock waves. Typical for Langmuir systems is the enrichment of the fluid phase with the less strongly adsorbed component in the plateau being well beyond the initial concentration. Starting from an initially saturated column after reducing the inlet concentration to zero this step change again is resolved into two waves which are now of expansive nature as shown at the bottom of Fig. 3.5. Again a plateau is formed but now with a concentration well below the initial concentration. The corresponding pathgrid is shown at the top of Fig. 3.5 with the two wave patterns shown in bold. If the path is followed in direction of the arrows this wave is an expansive wave and other wise a shock wave. Since the paths of the $\Gamma^{(k)}$ are straight lines and the $\Sigma^{(k)}$ are always tangent to them at their starting point both coincide and hence, in contrast to the general case, do not depend on the operating conditions. The construction of the wave patterns is now easily made by connecting the inlet concentration with the initial concentration, following

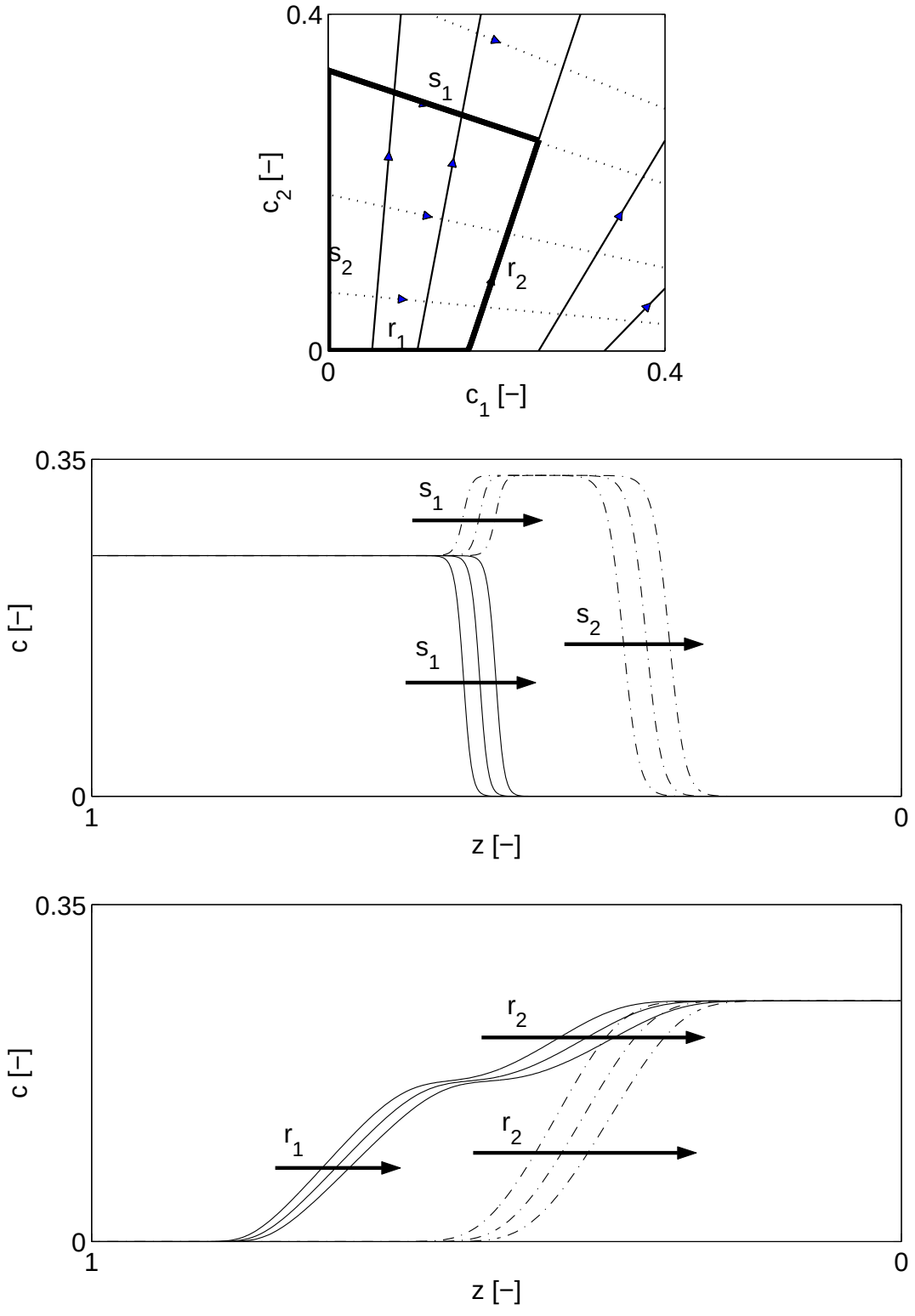

Figure 3.5: Step changes in the inlet composition for a binary Langmuir system. Top: wave patterns in the hodograph space; middle: wave pattern evolving from feeding mixture to an initially unloaded column; bottom: wave pattern evolving from feeding pure solvent to an initially saturated column.

at first a (1) wave and then a (2) wave. Since for both step changes one of the two waves is along an axis this wave and the preceding plateau are free of one component and thus both components of the mixture can be completely separated. A pulse injected to an

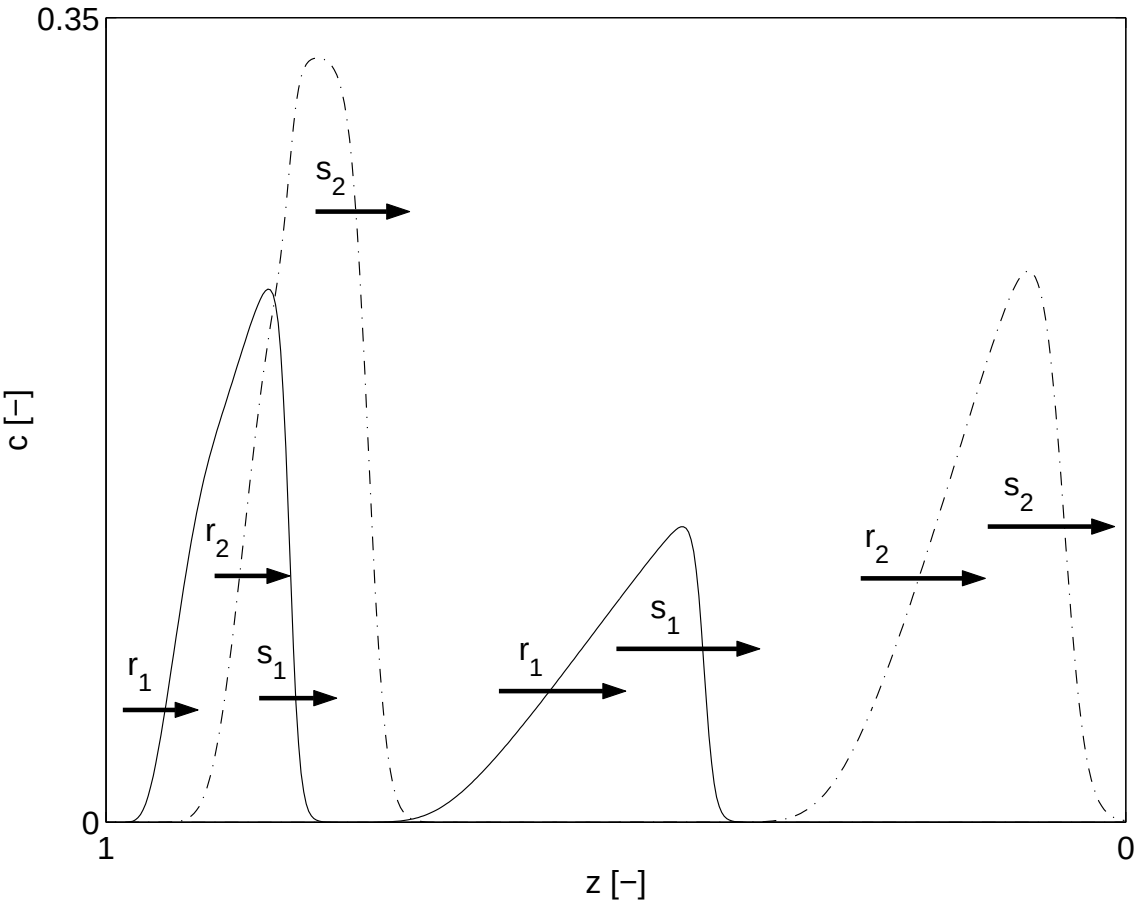

Figure 3.6: Snapshots of column profiles. Left part: profiles right after injection of the pulse. Leading and tailing step change have resolved into separate waves but no interaction has taken place so far. Right part: after some time the fast rarefaction wave has transmitted through the slow shock wave resulting in two pure component pulses.

initially unloaded column can be interpreted as a sequence of two such step changes in the inlet concentration. A short time after the injection the leading step change has resolved into two shock waves while the tailing step change has resolved into two expansive waves. In the following the waves interact and according to the elementary rules of wave interaction [20], [19], [21] and [18] the $\Gamma^{(2)}$ passes through the $\Sigma^{(1)}$ and the pattern finally resolves into two separated pure component pulses. This is shown in Fig. 3.6.

Reactive Chromatography

After considering the nonreactive two solute Langmuir chromatography in the previous section as a representative example for a bivariant system this section now deals with a simple bivariant example from reactive chromatography. The phase or sorption equilibrium is again described by the competitive Langmuir isotherm Eq. 3.17 and in the liquid phase a reaction of type $2A \rightleftharpoons B + C$ occurs. The finite rate model Eq. 2.11 and Eq. 2.12 of such a system reads

$$\frac{\partial c_1}{\partial t} - \frac{\partial c_1}{\partial z} = -\tilde{j}_1(\boldsymbol{c}, \boldsymbol{q}) - 2\tilde{r}'(\boldsymbol{c}) \tag{3.18}$$

$$\frac{\partial c_2}{\partial t} - \frac{\partial c_2}{\partial z} = -\tilde{j}_2(\boldsymbol{c}, \boldsymbol{q}) + \tilde{r}'(\boldsymbol{c}) \tag{3.19}$$

$$\frac{\partial c_3}{\partial t} - \frac{\partial c_3}{\partial z} = -\tilde{j}_3(\boldsymbol{c}, \boldsymbol{q}) + \tilde{r}'(\boldsymbol{c}) \tag{3.20}$$

for the liquid phase and

$$\nu\frac{\partial q_1}{\partial t} + \mu\frac{\partial q_1}{\partial z} = \tilde{j}_1(\boldsymbol{c}, \boldsymbol{q}) \tag{3.21}$$

$$\nu\frac{\partial q_2}{\partial t} + \mu\frac{\partial q_2}{\partial z} = \tilde{j}_2(\boldsymbol{c}, \boldsymbol{q}) \tag{3.22}$$

$$\nu\frac{\partial q_3}{\partial t} + \mu\frac{\partial q_3}{\partial z} = \tilde{j}_3(\boldsymbol{c}, \boldsymbol{q}) \tag{3.23}$$

for the adsorbed phase. Component A has index '1', component B has index '2' and component C has index '3'. This gives $\boldsymbol{\nu} = [-2 \;\; 1 \;\; 1]^T$ as the stoichiometric matrix and the transformation matrix is

$$\boldsymbol{L} = \begin{bmatrix} \frac{1}{2} & 1 & 0 \\ \frac{1}{2} & 0 & 1 \end{bmatrix} \tag{3.24}$$

yielding

$$C_1 = \frac{c_1}{2} + c_2, \tag{3.25}$$

$$C_2 = \frac{c_1}{2} + c_3, \tag{3.26}$$

$$Q_1 = \frac{q_1}{2} + q_2, \tag{3.27}$$

$$Q_2 = \frac{q_1}{2} + q_3. \tag{3.28}$$

Applying the transformation and further assuming phase equilibrium the model equations become

$$\frac{\partial \boldsymbol{C}}{\partial t} + \left(\nu\frac{\partial \boldsymbol{Q}}{\partial \boldsymbol{C}} + \boldsymbol{I}\right)^{-1}\left(\mu\frac{\partial \boldsymbol{Q}}{\partial \boldsymbol{C}} - \boldsymbol{I}\right)\frac{\partial \boldsymbol{C}}{\partial z} = 0. \tag{3.29}$$

The variables were ordered in such a way that now $C_1 = 0$ corresponds to pure product C while $C_2 = 0$ corresponds to pure product B. The educt A is characterized by $C_1 = C_2$ i.e. the bisection line in a C_2 over C_1 plot. For the further analysis the combined phase and reaction equilibrium function has to be computed by solving

$$\boldsymbol{C} = \boldsymbol{L}\boldsymbol{c} \tag{3.30}$$

$$K = \frac{c_2 c_3}{c_1^2} \tag{3.31}$$

for $\boldsymbol{c}(\boldsymbol{C})$ and substituting this into

$$\boldsymbol{Q}(\boldsymbol{C}) = \boldsymbol{L}\boldsymbol{q}(\boldsymbol{c}) \tag{3.32}$$

with $\boldsymbol{q}(\boldsymbol{c})$ according to Eq. 3.17. As for the reactive distillation example there are three different cases for the ordering of the adsorptivities of the components. Each of these cases is shown in a column of Fig. 3.7. In the left column A has intermediate adsorptivity, in the middle highest and in the right column lowest adsorptivity. In the first case, just as for the reactive distillation example, the reactive process is almost completely equivalent to an ideal system here represented by the nonreactive Langmuir system shown in Fig. 3.5 and Fig. 3.6. The only difference is the existence of inflection lines indicated by the dash-dotted lines in the hodograph plots in Fig. 3.7 and thus the possible existence of combined waves. In the other two cases the differences are much stronger and more obvious. In the second case there is always a line of reactive selectivity reversal below the feed line while in the third case such a line is always present above the feed line. A detailed mathematical analysis of this and an extension to reactions in the adsorbed phase can be found in [14].

These reactive selectivity reversals impose similar product limitations as reactive azeotropes in distillation. The resulting unreachable compositions are indicated by the shaded regions in the hodograph plots in Fig. 3.7. This can be further illustrated by pulse injection experiments for a chromatographic reactor. Fig. 3.8 shows the pulse patterns after an injection of pure educt A. In all three cases the final pattern consists of two pulses just as in the nonreactive example. Total conversion and pure products B and C however are only obtained in the first case with the educt A as intermediate component. In the second case, i.e. if A has highest adsorptivity only component C can be obtained pure in a leading pulse and is followed by a second pulse that is always azeotropic . In the third

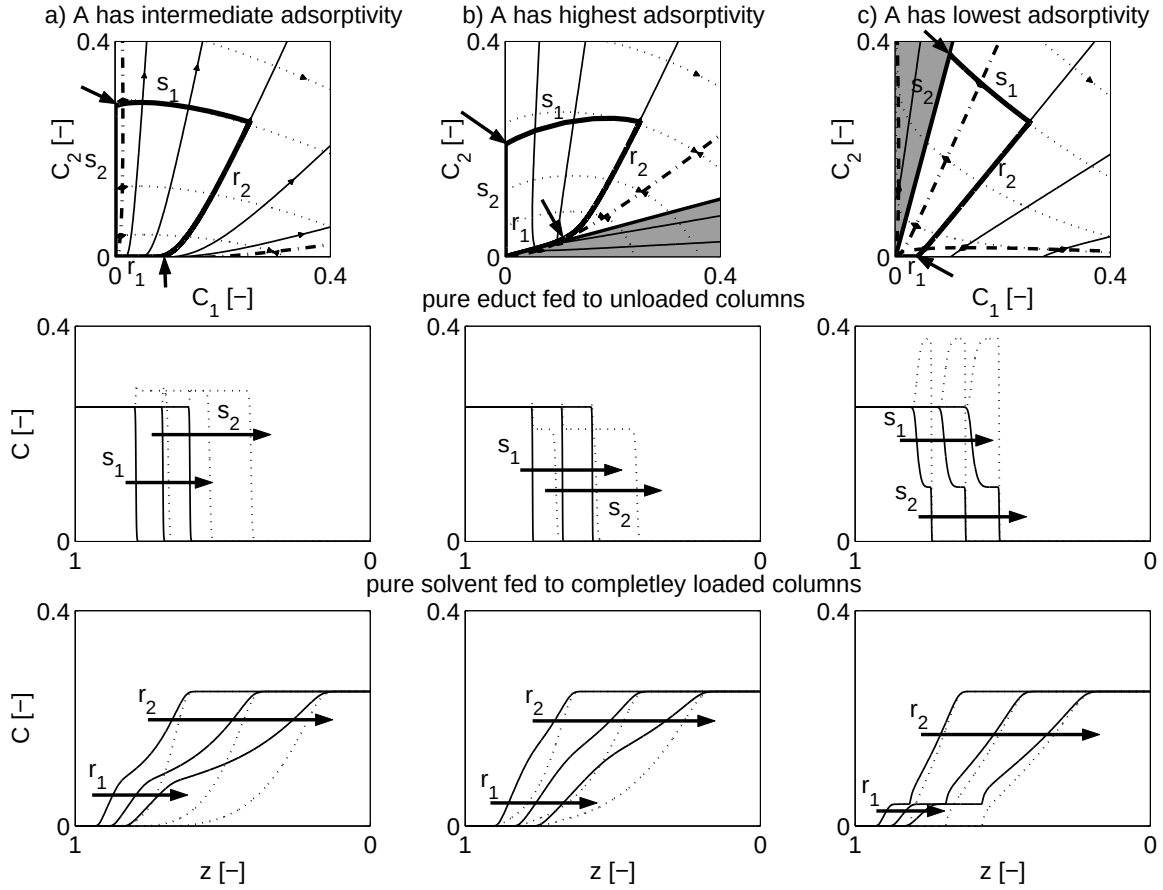

Figure 3.7: Step changes in the inlet composition for reactive chromatography of a ternary mixture with Langmuir isotherm and a reaction according to $2A \rightleftharpoons B + C$. From left to right adsorptivity of the educt has been changed to be a) intermediate, b) highest and c) lowest. Top: wave patterns in the hodograph space, arrows indicate potential product compositions; middle: wave pattern evolving from feeding mixture to an initially unloaded column; bottom: wave pattern evolving from feeding pure solvent to an initially saturated column.

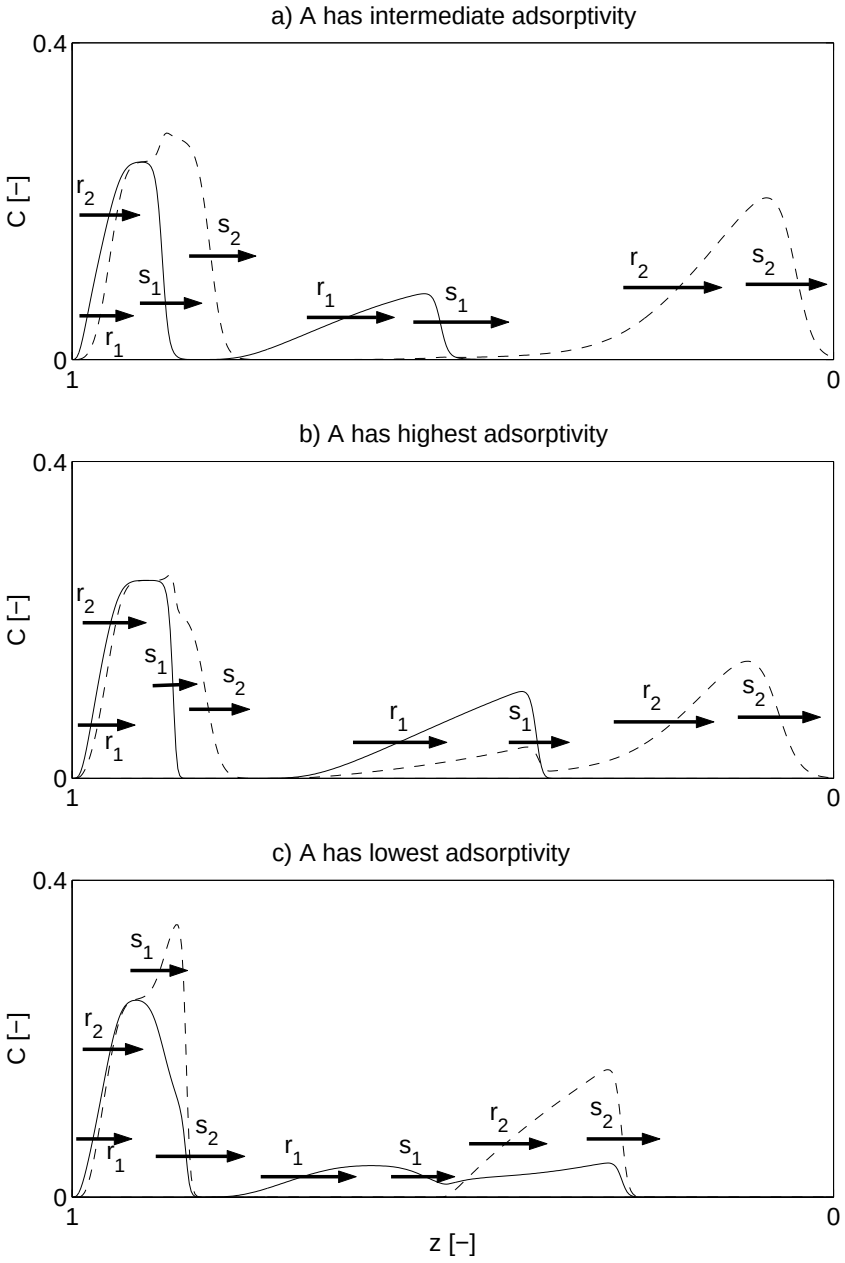

Figure 3.8: Snapshots of column profiles in transformed composition variables. From top to bottom adsorptivity of the educt has been changed to be a) intermediate, b) highest and c) lowest. Left part: profiles right after injection of the pulse. Leading and tailing step change have resolved into separate waves but no interaction has taken place so far. Right part: after some time the fast rarefaction wave has transmitted through the slow shock wave. However this results only in case a) in two pure component pulses while in the other cases only one pulse is pure.

Parameter	a) A has intermediate adsorptivity	b) A has highest adsorptivity	c) A has lowest adsorptivity
$a_1 = b_1$	3.0	5.0	1.0
$a_2 = b_2$	5.0	3.0	5.0
$a_3 = b_3$	1.0	1.0	3.0
K	1.0		
c_{feed}	$c_1 = 0.5,\ c_2 = 0.0,\ c_3 = 0.0$		
Number of stages	2000		
Bed length	80.0 length units		
Pulse length	20.0 time units		

Table 3.2: Parameters for the chromatographic reactor examples shown in Figs. 3.7-3.9.

case, i.e. if A has lowest adsorptivity the leading pulse is azeotropic while B is obtained pure in the second pulse. Finally Fig. 3.9 shows the same profiles as Fig. 3.8 but in physical variables. The parameters used for Figs. 3.7, 3.8 and 3.9 are shown in Tab. 3.2. Note, that due to the inflection lines the wave patterns may comprise combined waves, e.g. for case c) such a combined wave is slightly visible in the expansive wave denoted r_2 which, at its lower end is a shock wave.

From the plots of the wave solutions in the hodographs it becomes clear, that in all three cases counter current moving bed chromatographic reactors can be designed. The candidate product compositions are marked by arrows in the hodograph plots in Fig. 3.7 while Fig. 3.10 illustrates those processes by means of the stationary plant profiles. With the educt A having intermediate adsorptivity the products of the true moving bed reactor (TMBR) are the pure components. Since pure educt A was fed to the column this shows that the TMBR achieves total conversion. The corresponding stationary profiles are shown in Fig. 3.10 a). In Fig. 3.10 b) the educt has highest adsorptivity and just as in the pulse experiments there is a fraction that can only be withdrawn as azeotropic mixture. From the pulse experiments it is already known that this is the slower fraction and thus it is withdrawn at the extract port. This can be predicted without looking at pulse experiments since in the pathgrid it is the slow expansive wave that lies along

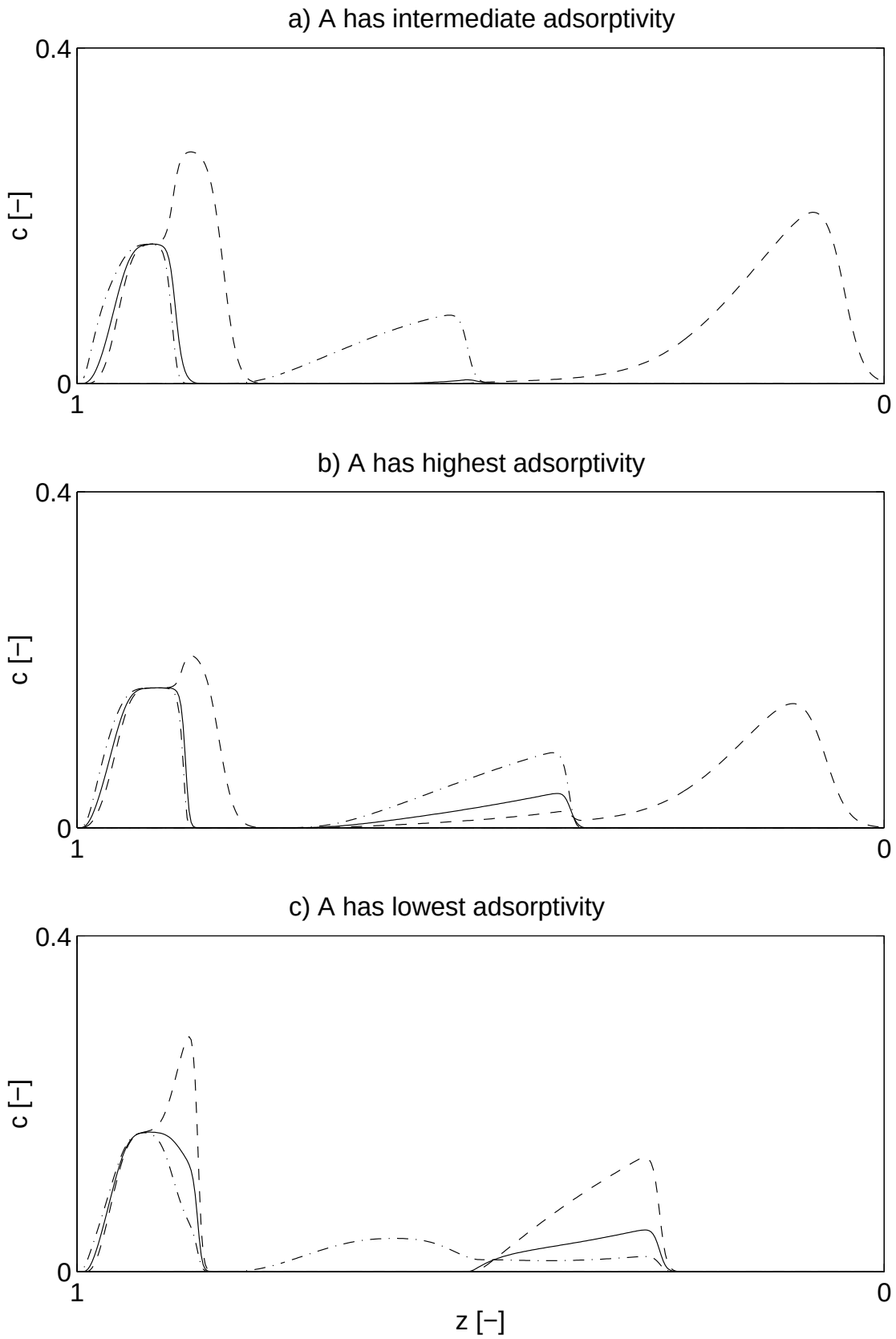

Figure 3.9: These plots show the same profiles as the preceding figure 3.8, but now in physical variables.

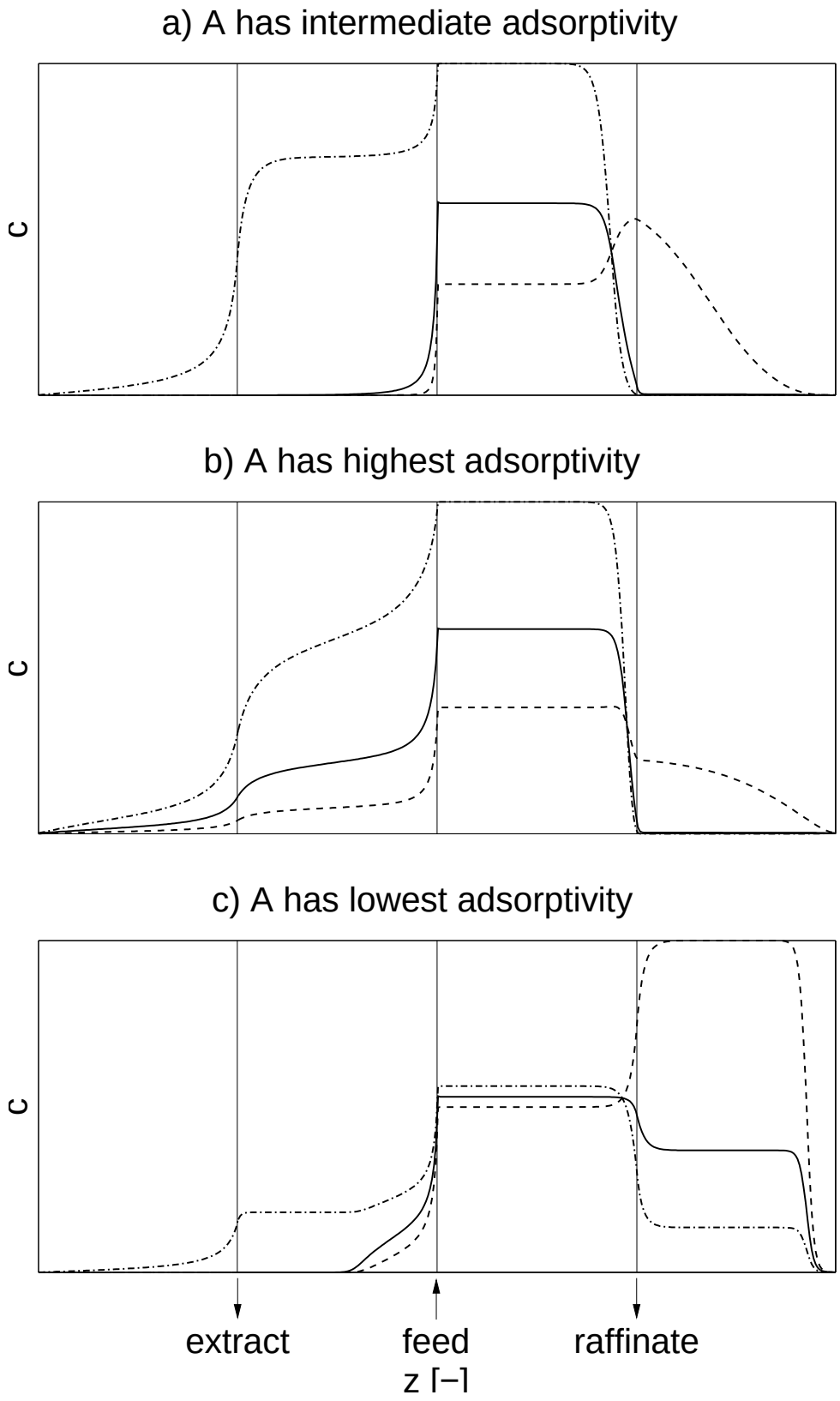

Figure 3.10: Stationary profiles in TMBR-plant. Feed is pure educt and adsorptivity is varied as in Fig. 3.7. Operating parameters are given in Tab. 3.3 and were found by a direct optimization based approach.

Parameter	a) A has intermediate adsorptivity	b) A has highest adsorptivity	c) A has lowest adsorptivity
v_{zone1}	5.0	3.2	5.0
v_{feed}	0.375	0.15	1.055
$v_{raffinate}$	1.825	1.25	1.2425
$v_{extract}$	2.6	1.1	3.4

Table 3.3: Parameters for the moving bed chromatographic reactor examples shown in Fig. 3.10. All other reaction and phase-equilibrium data as in Tab. 3.2.

the reactive selectivity reversal. For the third case, shown in Fig. 3.10 c), with the educt having the lowest adsorptivity again one fraction has to be withdrawn as azeotropic mixture but now it is the faster fraction which is consequently withdrawn at raffinate port. Again this information can be found in the pathgrid since now it is the fast, leading shock wave that lies along the reactive selectivity reversal. Note, that again in this case a combined wave is present since just above the extract composition, indicated by the arrow, the wave crosses an inflection line and since it has been an expansive wave up to that point it must turn into a shock wave beyond that point. The operating parameters are given in Tab. 3.3.

Note, that the behavior of the chromatographic reactor and the reactive distillation process are close to perfect analogues. For the educt being the intermediate one of the three components both processes behave comparable to ideal processes, while in the two other cases both processes behave like nonreactive processes having azeotropes or selectivity reversals.

3.1.3 Multireaction Systems

The previous sections on monovariant and bivariant systems considered rather simple systems with just a single reaction. However, typical systems of industrial relevance are multireaction systems. E.g. the wanted reaction is accompained by unwanted side reactions or the process comprises a whole cascade of reactions.

In the following first a multireaction system with three reactions and five components from chromatography is studied followed by an example process from reactive distillation with two reactions and five components. Hence both processes can be reduced to bivariant systems that can be studied by their two dimensional pathgrids.

Chromatographic Processes

Recently [2] among others studied the separation of the enantiomers of binaphthol by achiral chromatography in combination with reactions. Their observations will be reviewed in the following using the developed theory of nonlinear wave propagation for combined reaction/separation systems.

They made the following experimental observations. Upon injecting a pulse with racemic composition, i.e. with a equimolar mixture of both enantiomers, to the column no separation occurred. But in all cases of injecting a non-racemic mixture to the column the pulse split into two pulses, the first of them with pure excess enantiomer and the second with almost racemic mixture.

Following the notation of [2] the enantiomers are denoted by S and R and they can build three different dimers according to

$$R + R \rightleftharpoons RR, \tag{3.33}$$

$$S + S \rightleftharpoons SS, \tag{3.34}$$

$$R + S \rightleftharpoons RS. \tag{3.35}$$

The dimers RR and SS are called homochiral dimers and the mixed dimer RS is called heterochiral dimer. An enantiomeric pure fraction may contain both, the enantiomer itself and the matching homochiral dimer but it does not contain the heterodimer. [46] showed that the separation of a non-racemic feed mixture results from the combination of two effects. Namely the difference in reaction equilibrium constants of the homo- and heterochiral dimerization reaction as well as the difference in adsorptivity of the homo- and heterodimers.

This system shall now be further investigated by means of nonlinear wave propagation theory. The basis for these investigation is the model that was proposed and experimentally validated in [2]. While in that paper the system was investigated by direct numerical

simulation for some boundary and initial conditions the following study will use the path-grid to do this for any set of piecewise constant initial and boundary conditions. The model is based on two crucial assumptions.

(i) Solid and fluid phase are in phase equilibrium. The phase equilibrium is modeled by the competitive Bi-Langmuir isotherm which reads

$$q_i = \frac{h_i c_i}{G} + \frac{a_i c_i}{B}, \quad i = R,\ S,\ RR,\ SS,\ RS, \tag{3.36}$$

with

$$\begin{aligned} G &= 1 + g_1(c_R + c_S) + g_2(c_{RR} + c_{SS}) + g_3 c_{RS}, \\ B &= 1 + b_1(c_R + c_S) + b_2(c_{RR} + c_{SS}) + b_3 c_{RS}. \end{aligned}$$

The selectivity between all monomers and homochiral dimers is equal respectively, i.e. it is an achiral solid phase while a large difference in adsorptivity between homo- and heterochiral dimers exists.

(ii) The dimerization takes place in the fluid phase only. It is sufficiently fast to justify the assumption of reaction equilibrium. The equilibrium constants of the homo- and heterochiral dimerization are related to each other according to

$$K_{\text{hetero}} = 2K_{\text{homo}}. \tag{3.37}$$

By these assumptions the degrees of freedom of the system are reduced from 5 for phase equilibrium only to 2 in the combined phase and reaction equilibrium. The stoichiometric matrix may be written as

$$\boldsymbol{\nu} = \left[\begin{array}{ccc} -2 & 0 & -1 \\ 0 & -2 & -1 \\ \hline 1 & 0 & 0 \\ 0 & 1 & 0 \\ 0 & 0 & 1 \end{array}\right] \tag{3.38}$$

implying the vector of concentrations to be ordered as

$$\boldsymbol{c}^T = [c_R,\ c_S,\ c_{RR},\ c_{SS},\ c_{RS}].$$

The stoichiometric matrix of the reference components $\boldsymbol{\nu}_R$ is the lower 3×3 submatrix and $\boldsymbol{\nu}_T$ is the upper 2×3 submatrix of $\boldsymbol{\nu}$ as indicated by the horizontal line. The transformation matrix is then

$$\boldsymbol{L} = \left[\begin{array}{ccccc} 1 & 0 & 2 & 0 & 1 \\ 0 & 1 & 0 & 2 & 1 \end{array}\right] \tag{3.39}$$

and the transformed concentration variables read

$$C_R = c_R + 2c_{RR} + c_{RS}, \tag{3.40}$$

$$C_S = c_S + 2c_{SS} + c_{RS}. \tag{3.41}$$

Note that $C_R = 0$ implies that S is present enantiomeric pure and vice versa allowing to think in the transformed variables in a very natural way. The resulting set of variables is the very same as given by [2].

As the system has reduced to a bivariant system the analysis is done with the help of the pathgrid which is shown in Fig. 3.11 in the top row. All three pathgrids are identical but the three columns of Fig. 3.11 represent wave solutions for different feed compositions. The wave solutions are plotted in the pathgrids and the waves are labeled with 's' for a shock wave and 'r' for expansive waves while the numbers indicate the wave family which, in a bivariant system is either '1' or '2'. The pathgrid and the wave solutions are now discussed in some more detail and aspects regarding process feasibility are worked out.

The first remarkable difference of the binaphthol system to the previously discussed non-reactive Langmuir system concerns topology. This becomes most obvious for the solid lines, corresponding to fast waves, which all intersect at the origin. Further more at the origin the characteristic velocities of the fast and the slow waves coincide, i.e. the system is non-strictly hyperbolic at this point. Such singularities were introduced in section 2.2. Another interesting feature of the pathgrid is its symmetry to the bisection line and the fact that the slow waves change their orientation along that line. This feature is clearly due to the enantiomeric symmetry of the binaphthol system.

For a non-racemic feed, the wave solution for an initially unloaded column always consists of two shocks. The leading shock is along the axis of the enantiomer that is fed in excess and thus this enantiomer is obtained pure at the column end. This is illustrated in the center row of Fig. 3.11 (left column) and 3.11 (right column). For any racemic feed

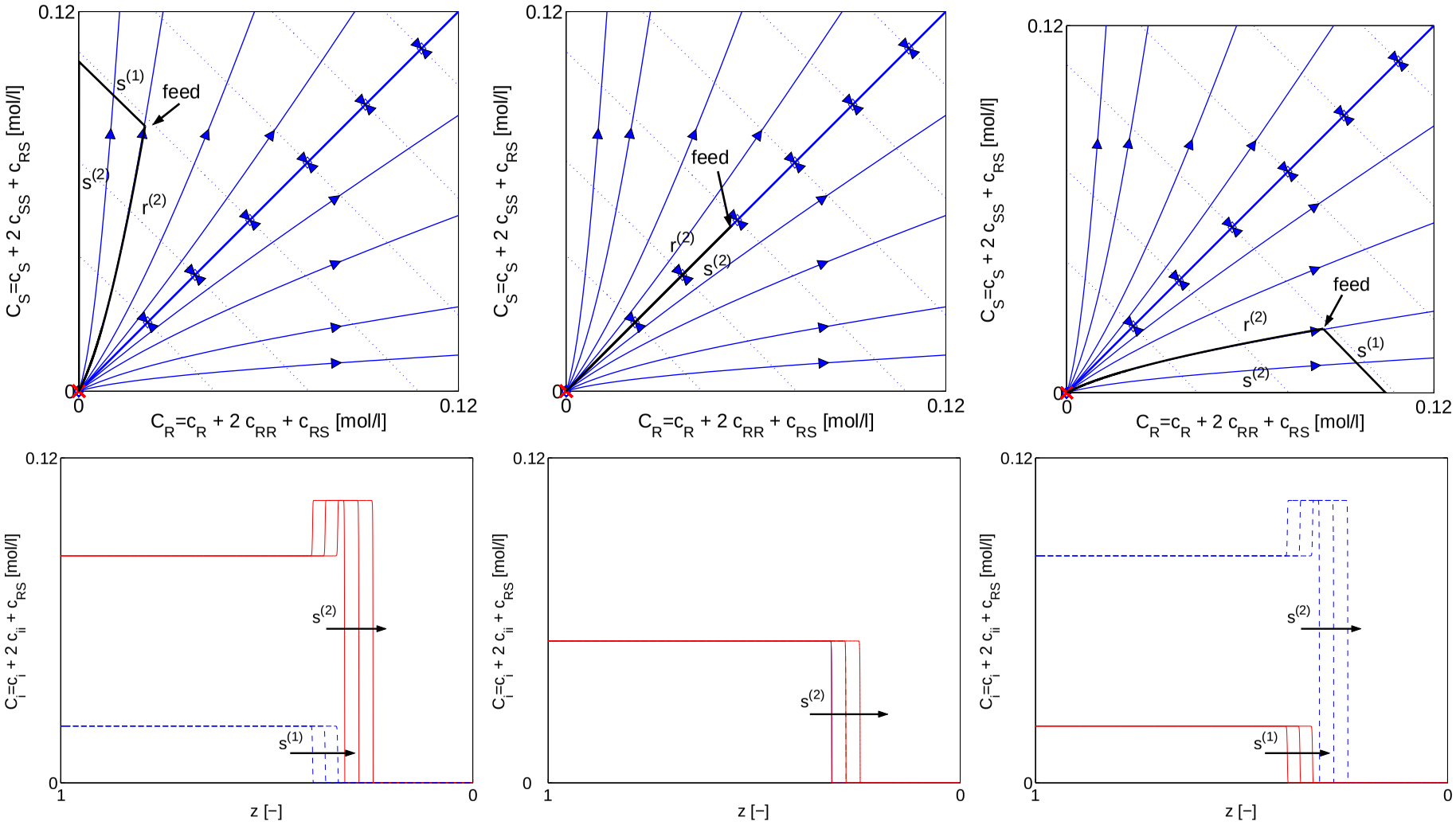
0.12
0
0.12
$C_S=c_S + 2\,c_{SS} + c_{RS}$ [mol/l]
$C_R=c_R + 2\,c_{RR} + c_{RS}$ [mol/l]
$s^{(1)}$
feed
$s^{(2)}$
$r^{(2)}$
$C_i=c_i + 2\,c_{ii} + c_{RS}$ [mol/l]
z [−]
1

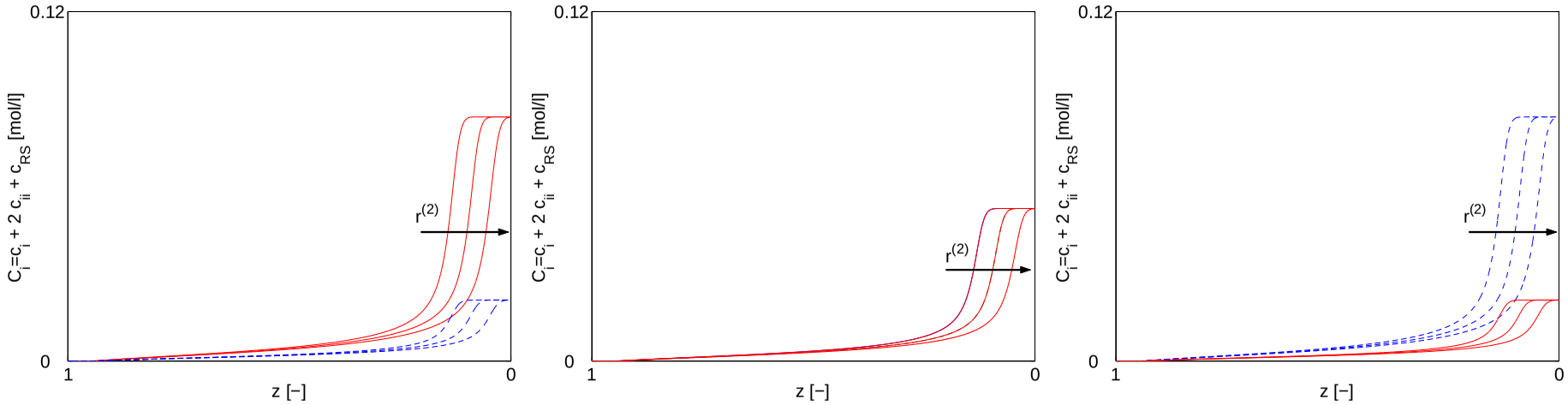

Figure 3.11: Wave solutions for the binaphthol system in transformed concentration variables. Step changes of the inlet concentration. Top row: wave solutions in the hodograph space. Center row: concentration profiles for the loading of an initially empty bed. Bottom row: purge of a completely saturated bed with pure solvent. Solid line: C_R, dashed line: C_S. Left column: non-racemic feed with excess of the S enantiomer, center column: racemic feed, right column: non-racemic feed with excess of the R enantiomer

mixture the bisection line itself is a wave solution and thus, respecting the orientation of the eigenvalues along that line, the solution is a single racemic shock as shown in 3.11 (center column).

A completely different situation is found for purging an initially loaded column with pure solvent represented by the origin in the path gird. Any initial composition, no matter if it is racemic or non-racemic can be directly connected to the origin by a single wave. As shown in the bottom row of Fig. 3.11 the solution is a single expansive wave comprising both enantiomers and thus no separation can be achieved. The strange shape of the expansive waves, resembling a combined wave is due to a strong variation of the characteristic velocity close to origin and a small variation in the rest of the composition space.

From these considerations it becomes clear that a pulse injection can again be considered as the sequential combination of a positive and a negative step change in the inlet composition. Examples of a positive step change are shown in the second row of 3.11 while the matching negative step changes are shown in the bottom column of 3.11. Eventually the patterns due to the step changes interact and final patterns as shown in Fig. 3.12 are obtained.

These pulse patterns exhibit properties that cannot be found in e.g. non reactive langmuir systems but can be predicted upon taking the pathgrid into account. For a racemic mixture the pattern consists of a single pulse with the same shape and velocity for both components. Hence no separation is possible. For a non-racemic mixture the final pattern is obtained by partial transmission of the expansive wave r_2 through the shock s_1. A partial transmission happens due to the fact that the r_2 extends to the umbilic point and there the compositions travel as if they were part of an r_1 wave that cannot overtake the s_1 shock. This in turn means that no separate pulses can be found, no matter how long the column is chosen. The expansive r_2 wave remains for ever in the state of being transmitted through the s_1 shock.

Regarding the question of process feasibility it is evident by the analysis of the pathgrid that it is never possible to obtain both enantiomeric fractions pure. On the other hand the analysis showed that it is always possible to get the enantiomer that is fed to the column in excess as a enantiomeric pure fraction.

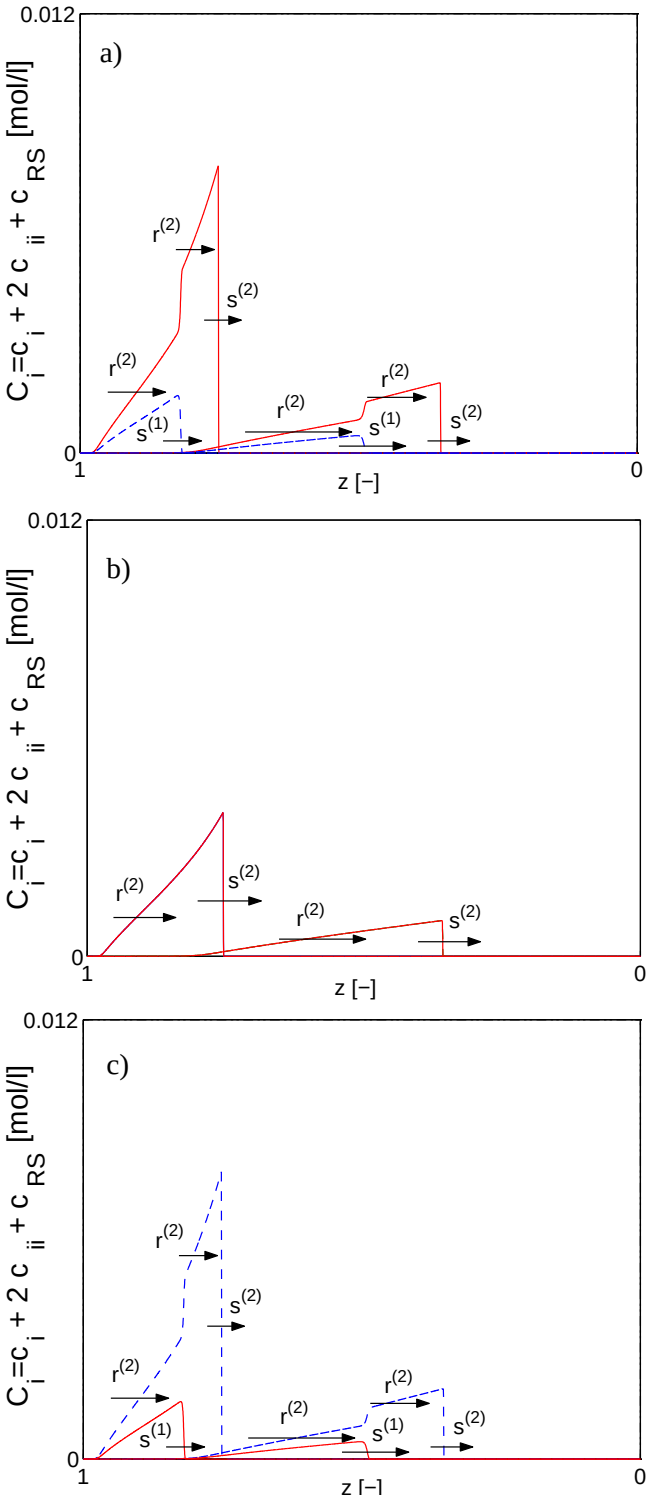

Figure 3.12: Initial and final wave patterns for pulse injections made up of the step changes considered in Fig. 3.11. Solid line: C_R, dashed line: C_S. a) non-racemic feed with excess of the S enantiomer, b) racemic feed, c) non-racemic feed with excess of the R enantiomer

From the analysis of the path grid an interesting question comes to mind. What is the influence of the enantiomeric excess in the feed on the width of the preceding pure fraction. From the previous considerations it is clear that in the extreme case of no enantiomeric excess in the feed no separation at all happens while for the rather large enantiomeric excess used in the previous simulations, cf. Fig. 3.11 and Fig. 3.12, a nice purification is possible. Moreover the structure of the wave solution for those two cases is completely different and the question arises how this change happens. The answer to this question can be found by considering the propagation speeds of the two leading shock fronts for non-racemic feed. Since this cannot be visualized directly in the pathgrid it is done by the simulation studies shown in Fig. 3.13. For the cases a) to c) the enantiomeric fraction

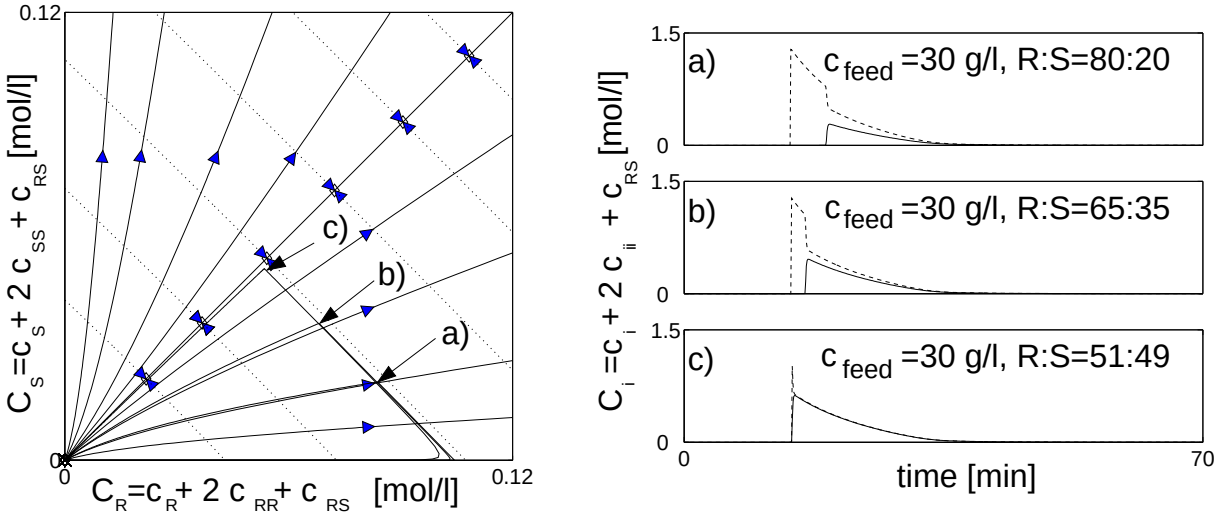

Figure 3.13: Structure of the wave solution and breakthrough curves for the binaphthol system in a fixed bed reactor in transformed concentration variables for feed mixtures of different enantiomeric excess: a) R:S = 80:20, b) R:S = 65:35, c) R:S = 51:49. Solid line: C_S, dashed line: C_R.

in the feed was decreased from 80:20 over 65:35 down to 51:49 which is an almost racemic mixture. From the breakthrough plot in the right column it can be directly seen that the difference in propagation speed for the two shocks decreases as the enantiomeric excess in the feed pulse is decreased. A detailed analysis shows that the difference in shock speeds tends to zero as the enantiomeric excess in the feed tends to zero. Thus regarding the structure of the wave solution there is a sudden change but in terms of the profiles there is a continuous change.

Distillation Processes

While chromatographic reactors are just about to find their way to industrial application reactive distillation is a serious alternative to the traditional sequential use of reactors and possibly complex separator networks. Hence as example for this section an industrial process is considered. However this implies the need to mask the real process and therefore no physical data will be given here and all variables are arbitrarily normalized. Despite these modification the results of the following discussion could be easily transfered to the real process.

In Fig. 3.14 a sketch of the column, which was studied together with Bayer AG [15] is given. The column is fully reactive and the single liquid feed composed of B and C enters on tray 25. Inside the column the two equilibrium reactions

$$B + C \rightleftharpoons A + D \text{ and} \tag{3.42}$$

$$B + D \rightleftharpoons A + E \tag{3.43}$$

take place in the liquid phase and the column was found to be operated close to chemical equilibrium. At the top the product stream consisting of component A with impurity B is withdrawn while the bottom product stream consists of E and again B as impurity. This highly nonideal mixture of $N_c = 5$ components has, considering the nonreactive phase equilibrium 1 binary azeotrope with a temperature minimum and 4 binary azeotropes with a temperature maximum. In this section the nonlinear wave propagation phenomena which were already reported in [15] will be analyzed in some more detail. While in [15] this was done solely by simulations the investigations in this section are based on the underlying pathgrid.

To start with the analysis the combined phase and reaction equilibrium function needs to be determined. Since in distillation the summation condition holds for fractions of the composition either on mole or weight basis the assumption of reaction equilibrium results in $N_c - 1 - N_r$ degrees of freedom which yields in this case 2 degrees of freedom. Ordering

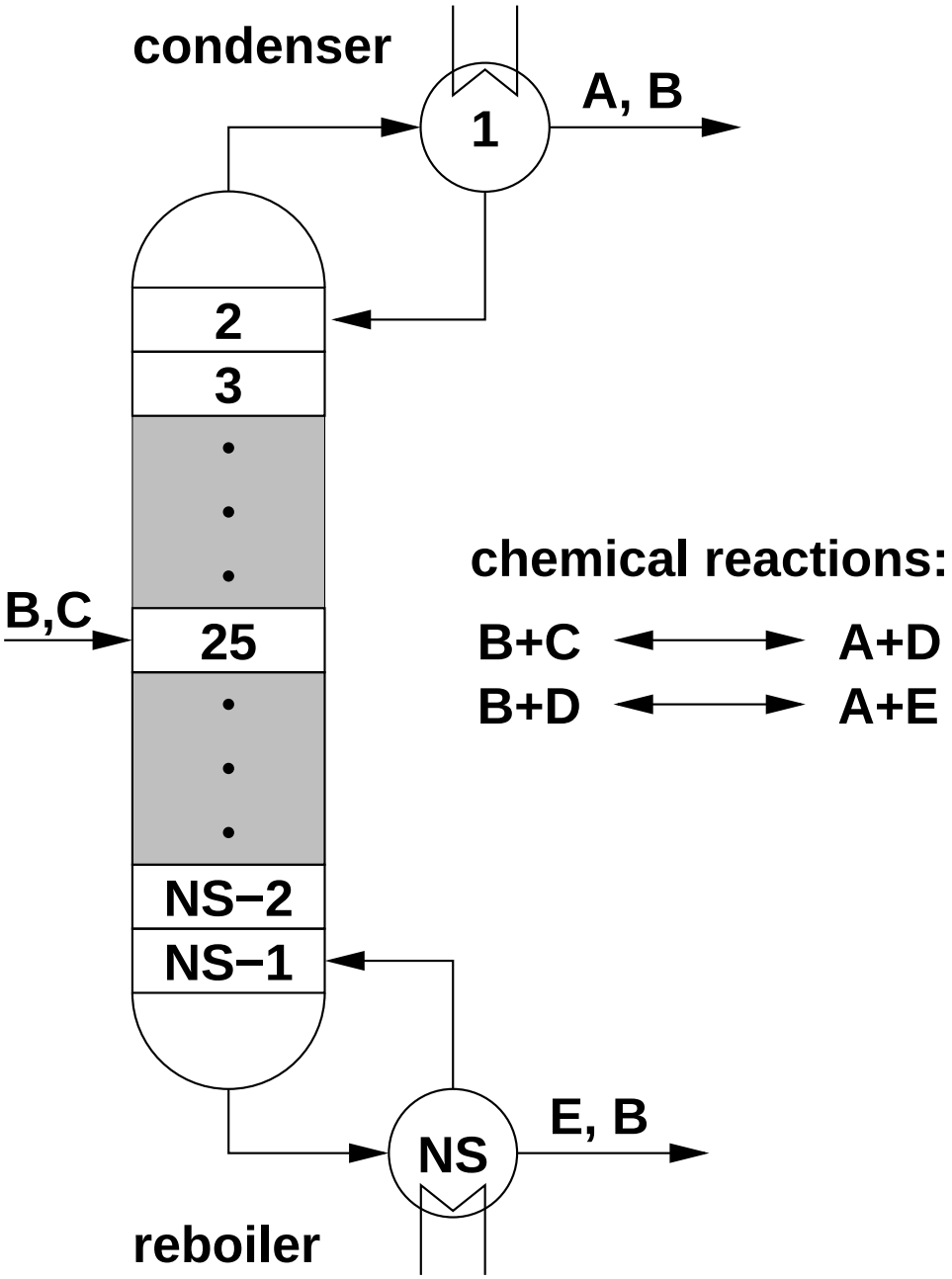

Figure 3.14: An industrial reactive distillation column

the components as $\boldsymbol{x}^T = [A\ E\ B\ C]$ the stoichiometric matrix is

$$\boldsymbol{\nu} = \left[\begin{array}{cc} 1 & 1 \\ 0 & 1 \\ \hline -1 & -1 \\ -1 & 0 \end{array}\right]. \tag{3.44}$$

The upper quadratic matrix is the matrix $\boldsymbol{\nu}_T$ of the components to be transformed while the lower quadratic matrix is the matrix $\boldsymbol{\nu}_R$ of the stoichiometric coefficients of the reference components. The transformation matrix reads thus

$$\boldsymbol{L} = \left[\begin{array}{cccc} 1 & 0 & 1 & 0 \\ 0 & 1 & 1 & -1 \end{array}\right] \tag{3.45}$$

and the transformed variables in the liquid phase are

$$X_1 = x_A + x_B, \quad X_2 = x_B - x_C + x_E. \tag{3.46}$$

By this choice of variables it follows that $X_1 = 1, X_2 = 0$ corresponds to pure top product A and $X_1 = 0, X_2 = 1$ corresponds to pure bottom product E. This again allows for a quick determination of the product purities from the transformed variables. Note that the transformed concentration phase space now is a pentagon. A similar situation occurs for the reactive xylen separation problem investigated by [67]. In order to see possible top and bottom products the reactive residue curve map shown in Fig. 3.15 has to be considered and the azeotropes have to identified. In the chosen coordinate system the corners and the origin correspond to pure components as annotated in the figure. As in the nonreactive case the two binary pairs A/B and C/D behave as nonreactive azeotrope while the other nonreactive azeotrope mentioned occur for potentially reactive mixtures and vanish. Instead due to the chemical reaction new reactive azeotropes emerge. There is a binary reactive azeotrope on the B/E edge and a ternary reactive saddle azeotrope close to this. From the complex geometry of the residue curve map five distillation regions can be identified (labeled as I to V in Fig. 3.15), to every feed in that region one unique set of possible top and bottom products for a fully reactive distillation column can be assigned. The products correspond to the starting and end point of the trajectories in this area respectively. The column under consideration is operated in region II and thus at

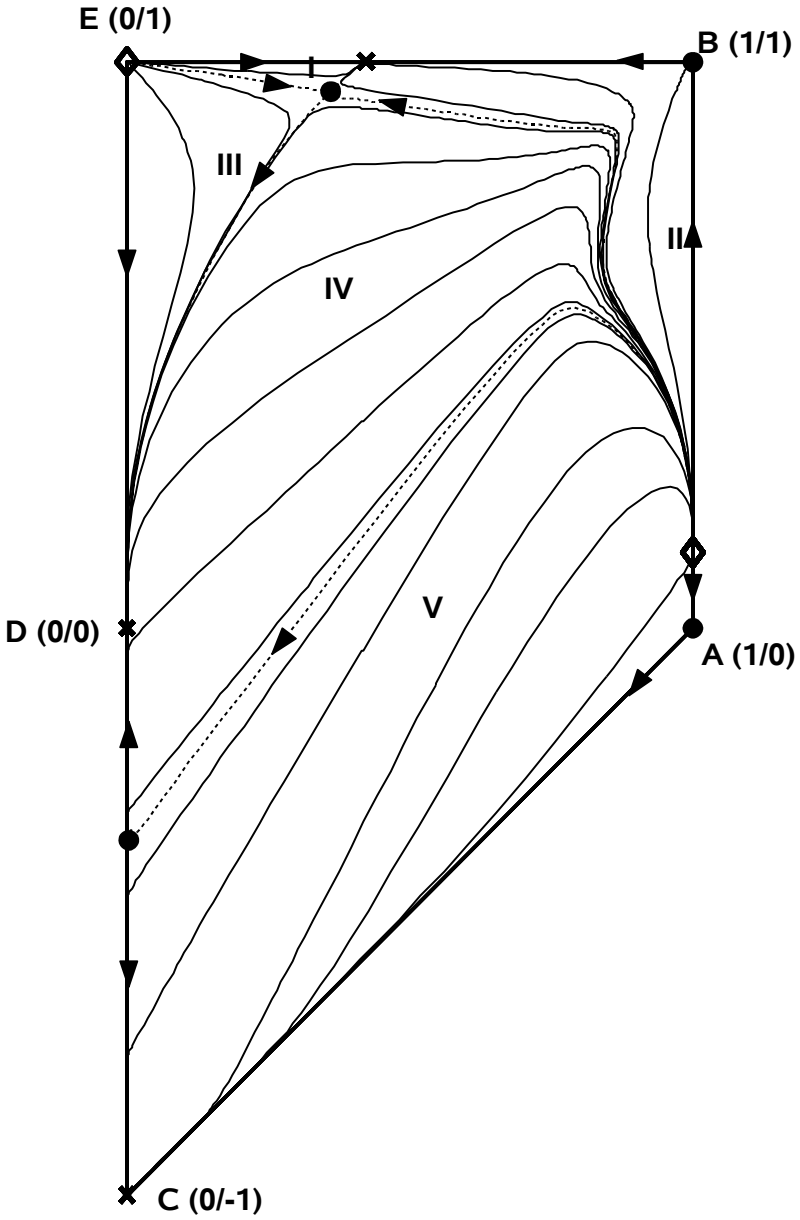

Figure 3.15: Residue curve map of the column in Fig. 3.14 given in transformed variables. Arrows indicate the orientation of the residue curves (solid lines). Distillation regions marked by I to V, dotted lines mark the boundaries of the distillation regions. Diamonds: unstable nodes, crosses: stable nodes, dots: saddles.

steady state the top product is close to the nonreactive A/B azeotrope while the bottom product lies close to the B/E edge.

By the help of the (reactive) residue curve map it is possible to find top and bottom products for a (reactive) distillation process. Together with a global material balance it is further possible to determine the external flow rates at steady state. Beyond this no further information can be deduced from the (reactive) residue curve map. At this point nonlinear wave propagation theory gives further insight relevant for the practical operation of the column.

The first point concerns the profile shape along the column. Think of the case that the feed and the product point, as deduced from the residue curve map are connected by an expansive wave. The expansive wave will eventually cover the whole column section length and hence one would rate the column performance as poor and feel the need to make the column longer. However if the feed and product point were connected by a shock wave a sharp transition would be observed along the column section length and the performance would be considered as good. Note that this rating of the column performance not only depends on the profile shape but also on the fact that a shock wave can be made stationary or balanced as whole, while in an expansive wave this is only possible for a single composition out of the whole wave. All other compositions will either move up or down the column. This directs focus to the second point aiming at the propagation speeds inside the column.

Wave propagation speeds are related to the internal flow rates. Think of the simplified situation that a single constant pattern wave connects the feed point and the product composition. The external flow rates may be chosen such that the global material balances are respected but the wave may still be propagating to the column boundary and the product will be spoilt. To overcome such problems it is essential to know the wave type and its propagation speed in order to balance the wave by proper selection of the internal flow rate ratios in each column section. Since the internal flow rate ratios in a distillation column are limited due to the boundary systems configuration this may also affect feasibility as was shown for the illustrative examples in conjunction with azeotropic points. However the necessary information can be deduced from the pathgrid and nonlinear wave propagation theory.

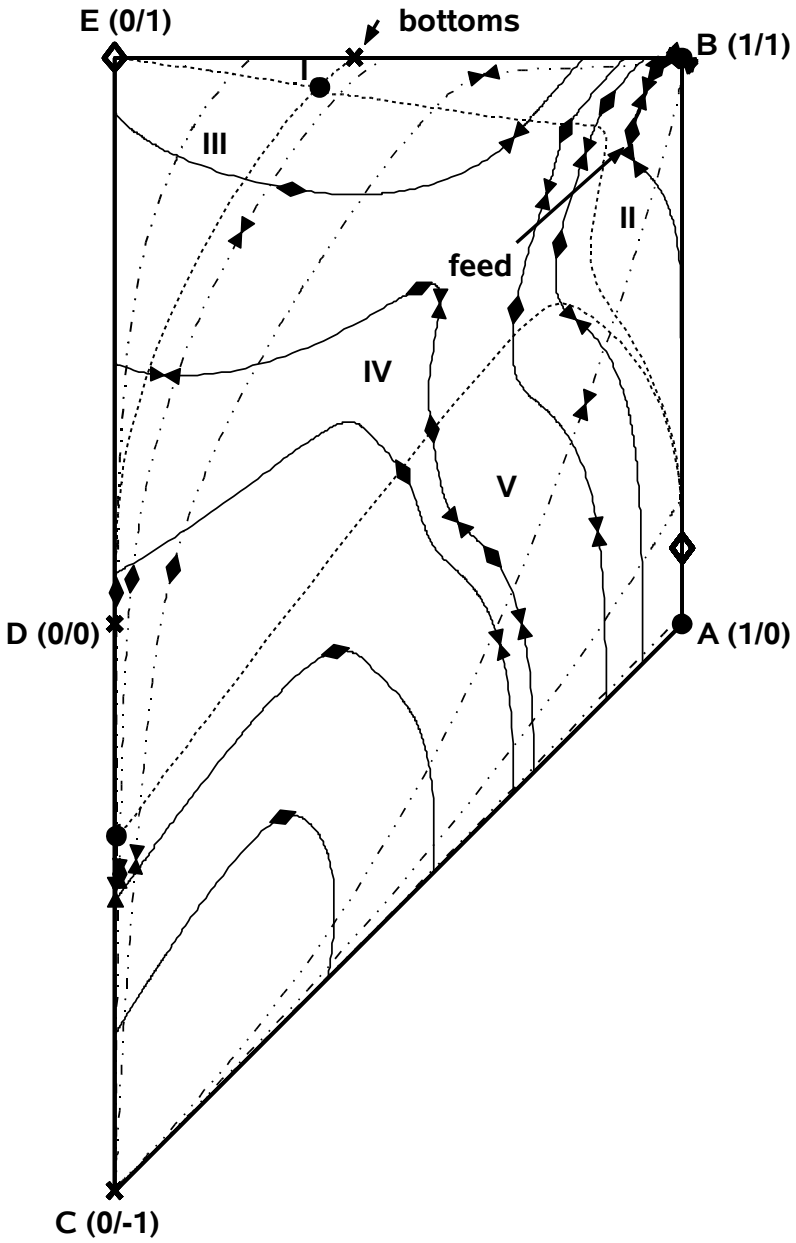

Figure 3.16: Pathgrid for the system used in the process shown in Fig. 3.14. Solid lines: fast waves, dashed dotted lines: slow waves. Arrows point in direction of increasing characteristic velocity. Dotted lines: boundaries of the distillation regions, symbols as in Fig. 3.15.

In order to address especially those two points as a first step in such a nonlinear wave propagation based analysis the pathgrid for the combined phase and reaction equilibrium function is computed. Due to the highly complicated thermodynamics of the system at hand this is done numerically as described in Appendix A and the resulting pathgrid is shown in Fig. 3.16. On basis of this pathgrid any wave solution for a given feed and product can be constructed. Again in the pathgrid solid lines mark fast waves while dashed dotted lines correspond to slow waves. The arrows point in direction of increasing characteristic velocity. Note that especially in the upper right corner the gradient of the characteristic velocity changes its sign quite often and thus complicated combined waves are expected. In the pathgrid the feed to a pure stripping column and the resulting product composition is marked by arrows and labeled accordingly. The feed is the same as for the industrial column. The resulting wave pattern consists of two parts. The first part from the feed to the E/B edge and the second part from there along the E/B edge to the E/B azeotrope. Along the first part the gradient of the characteristic velocity changes its sign several times and a detailed analysis shows that this wave consists of two shock waves connected by an expansive wave. In contrast to this the second wave is just a single shock wave. These predictions are confirmed by dynamic simulations as shown in Fig. 3.17.

The example shows that the original process design yields a shock wave close to the column end. This was achieved without knowing about nonlinear wave propagation and the favorable properties of constant pattern waves.

On basis of this example the theoretically motivated discussion can even be further extended. In hyperbolic systems there exists a fixed ordering of the waves. Consequently there is a wave that makes the final product quality. Now if this wave, which will be called from now on key wave is a shock wave it can be balanced inside the column no matter what type the other waves are and thus product quality is ensured. This concept will be further elaborated in the following section on process control.

3.1.4 Concluding Remarks

This section started with simple example processes used to illustrate the developed combined phase and reaction equilibrium theory. It was shown that reactive processes can

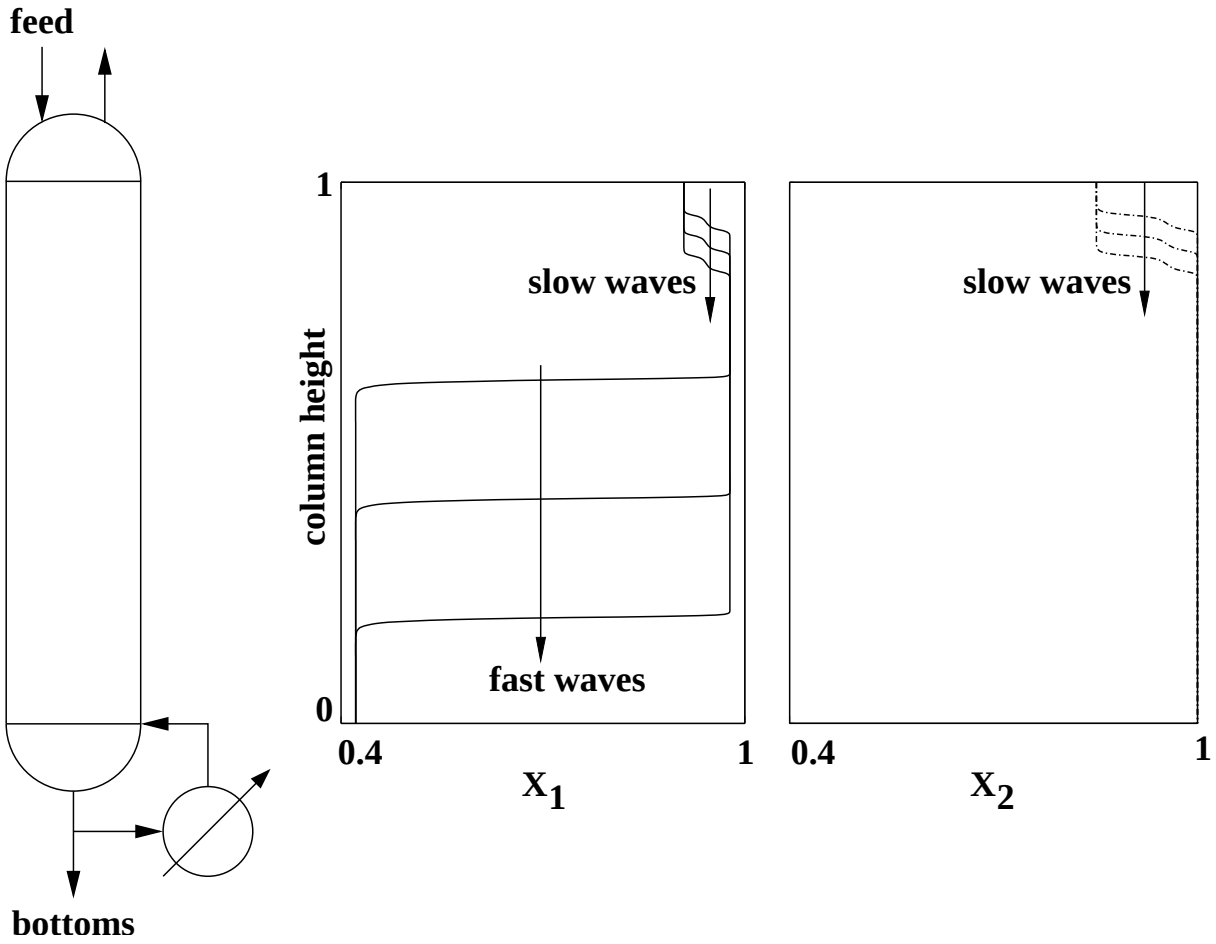

Figure 3.17: Dynamic simulation for the system used in the process shown in Fig. 3.14. Feed to the column is as marked in Fig. 3.15.

behave similar to nonreactive processes but also exhibit some new phenomena like reactive azeotropy or reactive selectivity reversals. For these simple example processes many of the results could have been found with a good deal of process understanding but the nonlinear wave propagation theory provides formal mathematical and graphical tools to do this. These formal tools were then used to discuss rather complicated processes with multiple reactions and complicated phase equilibria.

The next section is focused on the use of the developed theory in process control. Applications range from the development of a simple wave based control scheme for chromatographic processes over nonlinear wave based observer design for reactive distillation columns to wave based nonlinear model predictive control of distillation columns.

3.2 Process Control

Once the basic design of a process is made it is necessary to design a suitable control system. For chemical plants at least two hierarchy levels of control can be distinguished. Those of low level controllers that are in charge of controlling basic parameters e.g. levels, pressures or flow rates and those of high level controllers that are in charge of ensuring the specified product qualities. The discrimination between those two classes of control objectives is sometimes vague and, regarding plantwide control, sometimes not appropriate.

The control aspects dealt with in this section belong to the second class and hence the low level control of e.g. the demanded flow rates is not to be discussed here. Instead focus is on the application of nonlinear wave propagation theory in order to design a composition control system.

The first two examples are only sketched in the work at hand since they are worked out by others up to the level of application to pilot plant in the first case [58] and a full scale plant in the second case [54]. However the basic concepts were developed together with these authors in the context of the work at hand [16], [57].

The third and fourth examples are genuine outcome of the thesis at hand and will be discussed in more detail. First focus is on general aspects of nonlinear observer design for distillation columns on basis of nonlinear wave propagation phenomena. These considerations are then used in the next section by application to the fairly complex Bayer Process (see section 3.1.3) together with results of closed loop performance with a nonlinear controller.

3.2.1 Wave Based Process Control of Distillation Processes

In the past numerous studies on the control of distillation columns have been published and a review of the work until the early 90s is given by [61]. Although some studies on nonlinear control of distillation columns exist, e.g. [13], most of those studies consider the control of high purity binary distillation columns. A good review of these approaches together with a study is given in [3].

In previous studies tray temperatures instead of the product compositions are used as controlled variables, e.g. [33], [34], [71]. These concepts are called inferential control

concepts. In order to be able to respect the product specifications in the presence of disturbances the temperature measurements are placed some distance from the column ends i.e. the points of product removal. Those concepts rely on the good correlation between temperature and composition that is given in binary distillation. For multicomponent mixtures the correlation may become poor and the product compositions may be violated even if the controlled temperatures are kept at their setpoints [43]. These problems may be overcome by the use of composition estimators [31], [41], [42], [48], [4], [10].

In the last decade the results of nonlinear wave propagation theory have been exploited to deduce models of immensely reduced order [37] which were restricted to binary or quasi binary systems. Recently this class of models was extended to multicomponent systems and augmented by proper profile shapes for distillation processes described by constant relative volatilities [27]. Such reduced wave models provide precise insight into the dynamics of the processes as they directly describe the dynamics of the column profiles in terms of a few variables such as wave positions and boundary compositions. Concentrating on the key front (see 3.1.3) it becomes clear that not a temperature but the location of this key front is to be controlled.

In [60] a nonlinear profile observer together with a profile position control was presented. However this work was done for a binary distillation column and relied on the fact that temperature and product composition are well correlated. As noted before such a correlation may be poor for multicomponent distillations. For binary distillation processes [52] recently demonstrated the capabilities of wave position observers, i.e. an observer that does not estimate the profile but only the position of the waves the profile is made up.

In the area of nonlinear control the concept of model predictive control has considerably matured in recent time and now provides an efficient control technique able to deal with the multi-variable nature of distillation processes while at the same time it is capable to explicitly respect process constraints [1].

Wave based control of binary distillation columns is discussed in e.g. [17], [3] but the concepts used are restricted to the binary case and hence examples of wave based control of multicomponent distillation columns are still missing.

The wave based process control concept for multicomponent distillation columns developed here is sketched in Fig. 3.18. It combines the power of both, the wave models and

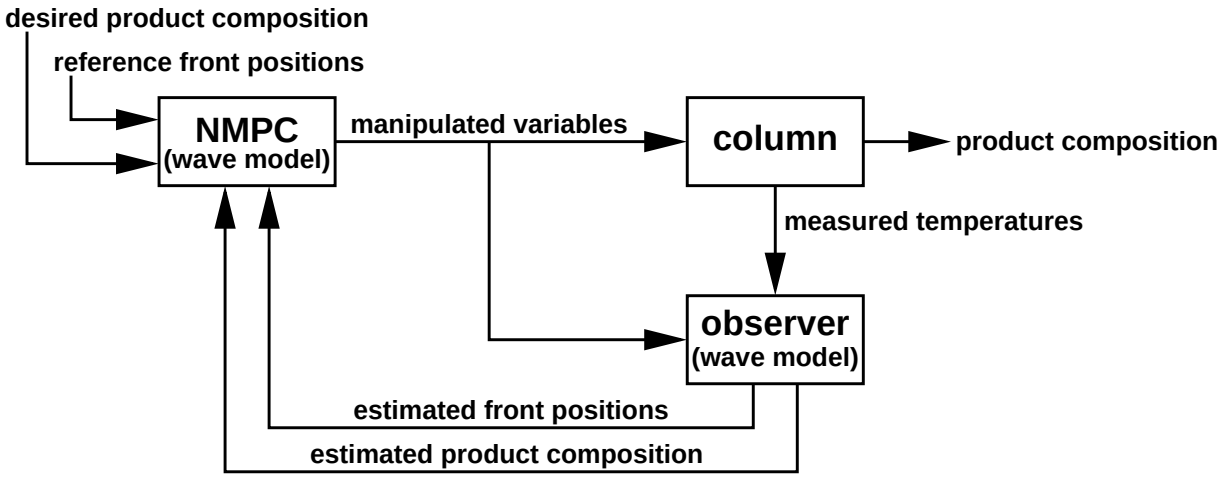

Figure 3.18: Control setup for the wave based composition control concept.

nonlinear model predictive control in the following way. Instead of controlling temperatures on individual trays the nonlinear model predictive control is formulated in such a way, that the deviation of the positions of the key waves from their setpoints are minimized while at the same time the product specifications are enforced as constraints. An observer based on the wave model of the process is used to estimate the necessary process parameters, i.e. key wave positions and product compositions which in turn are states of the wave model. As the nonlinear model predictive controller is also based on the wave model these process parameters can be directly used in the controller.

The advantages of this control concept become obvious even for binary distillation as in Fig. 3.19. Note that for binary problems there is only one wave per column section. Hence this wave is also the key wave. With the disturbance at about time t=100 seconds the light component in the feed increases considerably. As the controller pushes the key wave in each section back to their nominal positions the product compositions become violated. To compensate for this violation the controller allows the waves to move away from their setpoints and thus manages to fulfill the constraints. Looking at the established temperatures at around t=1250 seconds one realizes that they are now about 2 Kelvin away from the original setpoint values and it becomes clear that with some inferential control the product specifications would have been violated. Once the disturbance is removed, i.e. after t=1500 the controller brings the system back to its original state.

Further details on the control concept, especially the nonlinear model predictive control aspects can be found in [16] and [58].

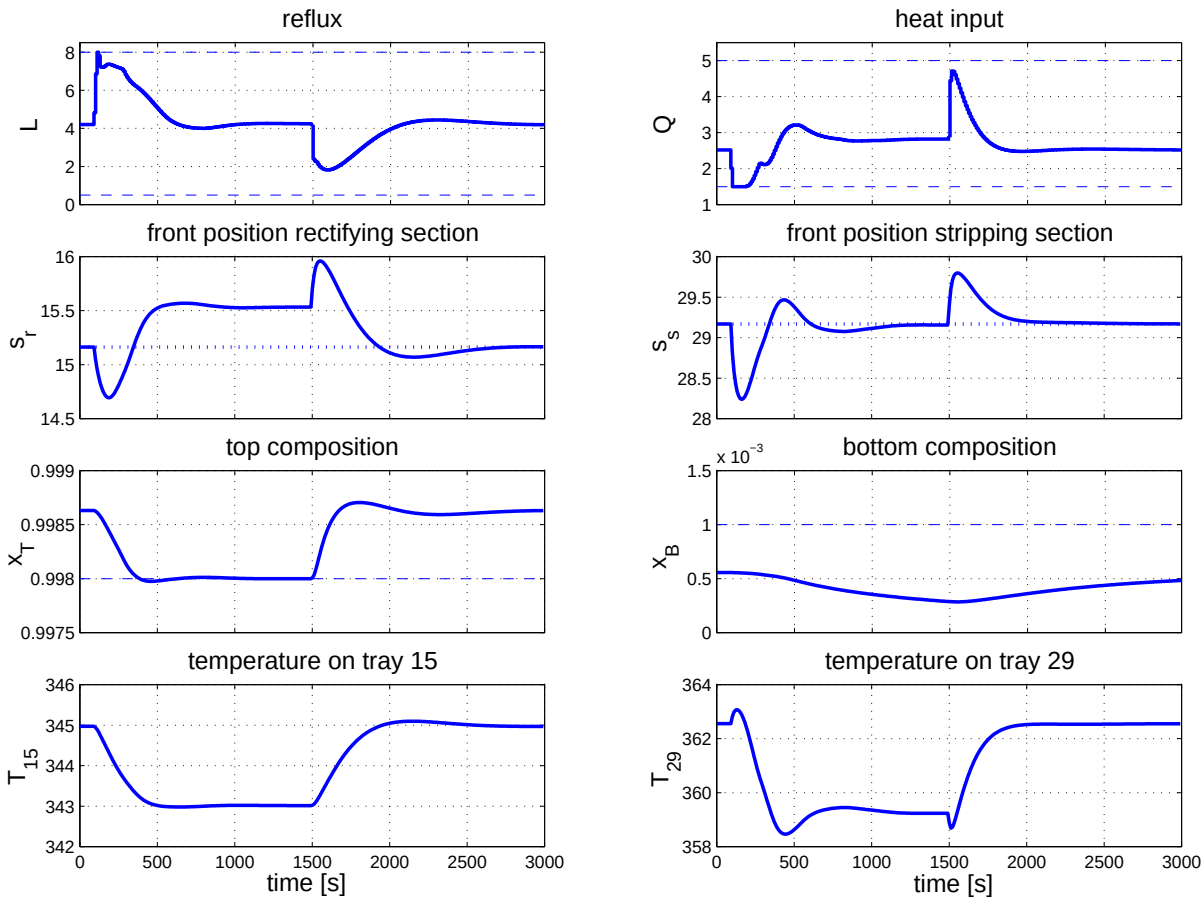

Figure 3.19: Closed loop simulation experiment after 50% increase and decreasing to the original value of the light component in the feed. Dashed lines: boundaries, dotted lines: setpoints.

3.2.2 Control of Moving Bed Chromatographic Processes

In the design stage of moving bed chromatographic processes it is possible to find optimal operating conditions by numerical optimization of a detailed process model. For Langmuir systems and similar systems the triangle theory [64] provides a simple method to obtain suitable operating parameters. Furthermore it follows from the triangle theory that the optimal operating point is located at the out most boundary of operating parameters that fulfill the specifications, i.e. complete separation of both products [57].

Since moving bed processes are highly sensitive to disturbances they are operated with safety margins and the economic optimum is not realized. In order to operate them at the optimal operating point closed loop control of the process has to be established. However since the control concepts developed in the past, e.g. [8], [28], [29], [38] ,[44], are very

complex closed loop operation of moving bed chromatographic processes is far from being common industrial practice.

In contrast to this the wave based control concepts presented in the following are far more simple but still allow a robust operation of the process at the economic optimum. While their application is demonstrated in the following for binary Langmuir systems the theoretical background developed in the previous chapter clearly shows that the wave based approaches can be directly extend to more complex systems including reactive processes.

Model Free Control Concept

The first and more simple control concept for moving bed chromatographic processes is transferred from distillation column control and is known there as inferential control [34]. This concepts is called inferential control since the variables the specifications are given for are not directly controlled. Instead some other variables are controlled and the variables the specifications are given for are interfered from them. In distillation column control the controlled variables are typically easily measurable temperatures while the specifications are given in terms of product compositions. In chromatographic processes the role of temperatures is taken by the sum of the concentrations that is easily measurable by UV-detectors while specifications are given in terms of product purities. Fig. 3.20 shows a schematic of the concept.

In a typical moving bed chromatographic process the profile is composed of four distinct waves, each located in a different zone of the plant. The conceptual idea is to stabilize each wave in its zone, i.e. to prevent it from protruding into the next or previous zone and thus spoil the products. Since the individual waves are visible in the UV-detector signals keeping these signals at predefined setpoints stabilizes the waves as required. As the flow rate ratio in each section is chosen as manipulating variable the use of simple single input single output PI-controllers is possible. The flow rate ratio in one section does hardly influence the wave in other sections, i.e. cross coupling will be neglectable small. Note that this control concept is model free, especially it does not require any knowledge of equilibrium function parameters. Fig. 3.21 demonstrates the nice performance of the control concept for disturbances in the flow rates. The shown disturbances due to a

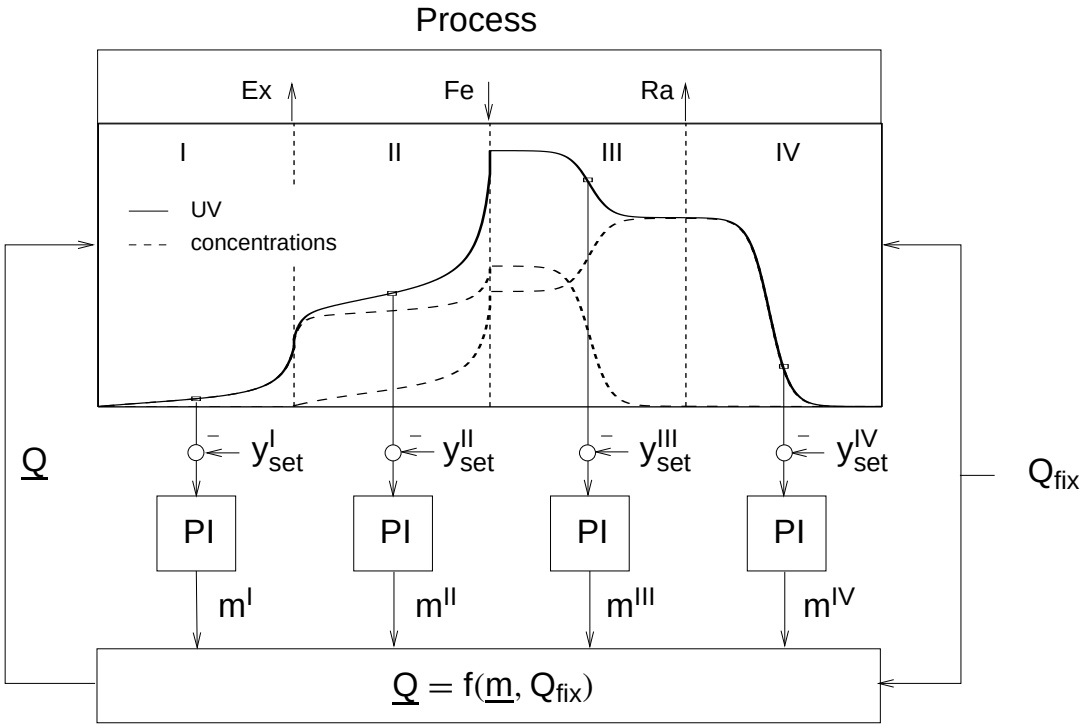

Figure 3.20: Schematic block diagram of the inferential control scheme for moving bed processes

stepchange in the solid flow rate are quickly eliminated and the set points of the controlled variables are reestablished. This leads back to the desired product compositions. Further details are given in [56], [55].

For a disturbance in concentrations e.g. feed concentration the performance of the control concept decreases considerably and the major drawback of the concept becomes apparent. There is no direct control of the product purities. However in order to account for such disturbances a far more advanced control concept needs to be developed as shown in the following. Further details on the control concept up to the level of application to a production scale plant can be found in [56], [55], [57].

Model Based Control Concept

In order to overcome the drawback of the presented model free control concept a more advanced control strategy is needed. This control concept is model based but still remains fairly simple, especially compared to the model based control concepts presented in the literature, e.g. [8], [28], [29], [38], [44]. Its simplicity is due to the exploitation of the typi-

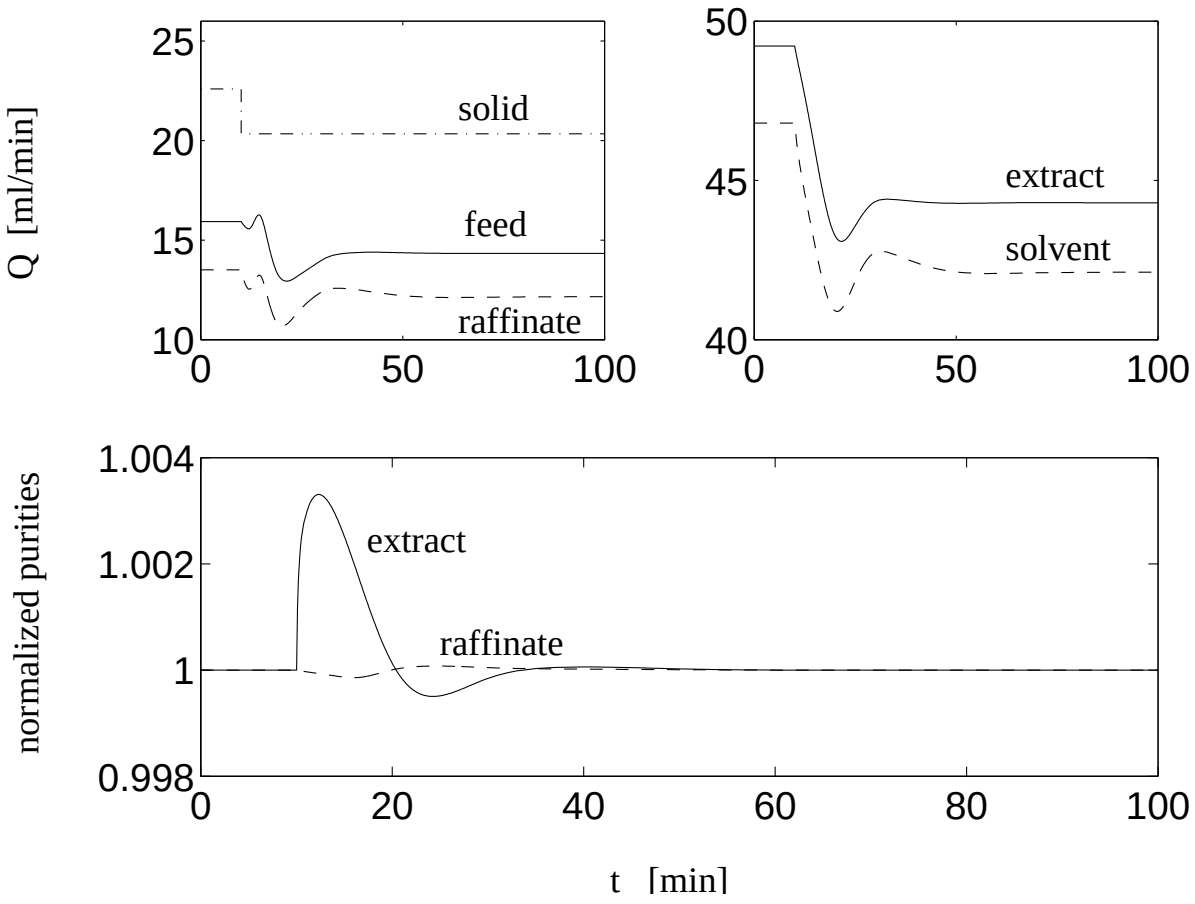

Figure 3.21: Inferential Control: Manipulated flows (top) and controlled purities for a step disturbance in the solid flow (after 10 minutes). The purities are normalized with the initial purities. TMB unit.

cal nonlinear wave propagation phenomena associated with moving bed chromatographic processes and is briefly sketched in the following.

The conceptual idea of the model based control concept is as for the model free control concept based on the fact that chromatographic moving bed processes show distinct wave patterns, i.e. if complete separation is achieved there is only a single wave in each zone. Both, the in the field of chromatography well established theory of coherence of Helfferich [21] based on physical insight, as well as nonlinear wave propagation theory based on purely mathematical considerations allow to compute the propagation speed of the individual waves. The computations are based on the compositions at the section boundaries, the equilibrium function between liquid and solid phase and the operating conditions, i.e. flow rates in the solid and the liquid phase. The control scheme now aims at adjusting

the wave propagation speeds in each zone suitably. Since complete regeneration of the solid phase is required in the two outer zones it follows that the propagation speed w^I according to Eq. 2.39 in the zone I between solvent and extract port is required to hold $w^I \geq 0$ while w^{IV} according to Eq. 2.42 in the zone IV between raffinate and solvent port is required to hold $w^{IV} \leq 0$. If further complete separation is required the wave propagation speeds w^{II} according to Eq. 2.39 in the zone between extract and feed port as well as w^{III} according to Eq. 2.42 in the zone between feed and raffinate port are required to hold $w^{II} \geq 0$ and $w^{III} \leq 0$.

Note that for moving bed chromatographic plants optimal operating points at complete separation are typically characterized by minimal solvent consumption and maximum feed throughput. Minimal solvent consumption is achieved if the difference between the fluid flow rate between zones IV and I is minimal while maximum feed throughput is achieved if the difference between the fluid flow rate between zones II and III is maximal. This is achieved by setting $w^I = w^{II} = w^{III} = w^{IV} = 0$.

In typical applications the complete regeneration of the solid phase in zones I and IV is a basic requirement, while the requirement of complete separation may often be substituted by high but finite purities of e.g 99%. In order to fulfill such requirements the control structure of the model based control concept is build up as shown in Fig. 3.22. The wave propagation speeds in zones I and IV are fixed at $w^I = w^{IV} = 0$ while the propagation speeds w^{II} and w^{III} are adjusted by simple SISO PI-controllers. The input to the PI-controllers is the difference of the actual product purity g_i^{port} and the corresponding desired purity $g_{i,\text{des}}^{\text{port}}$ and the output of the PI-controllers is the required propagation speed of the waves. The rectangular block following the PI-controllers converts the required wave propagation speeds to actual flow rates on basis of the before mentioned boundary compositions and a fixed flow rate Q_{fix}. Since a direct measurement of the required boundary compositions is not possible they need to be obtained from UV-measurement by a suitably designed estimator. In order to give an impression of the capabilities of this fairly simple model based control concept Fig. 3.23 shows the performance of the control concept in presence of a, for the control system unknown, step change of 10% in the feed composition of one component. This simulation study shows the direct application of the control scheme to a simulated moving bed process by the use of sample-and-hold elements

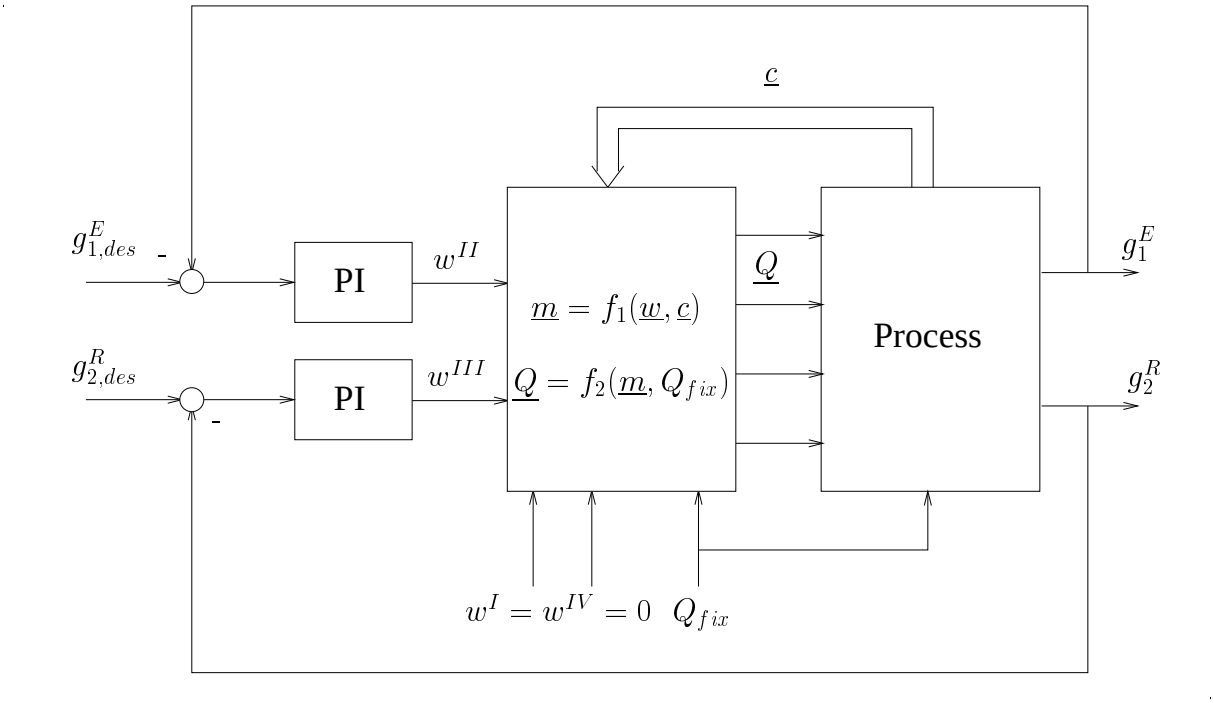

Figure 3.22: Schematic block diagram of the model based control scheme for moving bed processes

and an identity observer. Further more the simulation study demonstrates the capability of the control concept to get arbitrary product purities. In the simulation study the set-point for both product purities is 99% and is quickly reestablished in the presence of the disturbance.

Further details on both control concepts, including experimental result on a full scale production simulated moving bed plant can be found in [56], [55], [57].

3.2.3 Nonlinear Observer Design Concept for Distillation Columns

As noted in the section on wave based distillation column control 3.2.1 there exists a considerable amount of literature on nonlinear observer design based on temperature measurements, e.g. [60], [31], [41], [42], [48], [4], [10], [52]. However those concepts are either restricted to binary distillation columns and their direct correspondence of temperature and composition or they are highly complicated and as a result no details regarding their robustness to modeling and parameter errors can be given. However

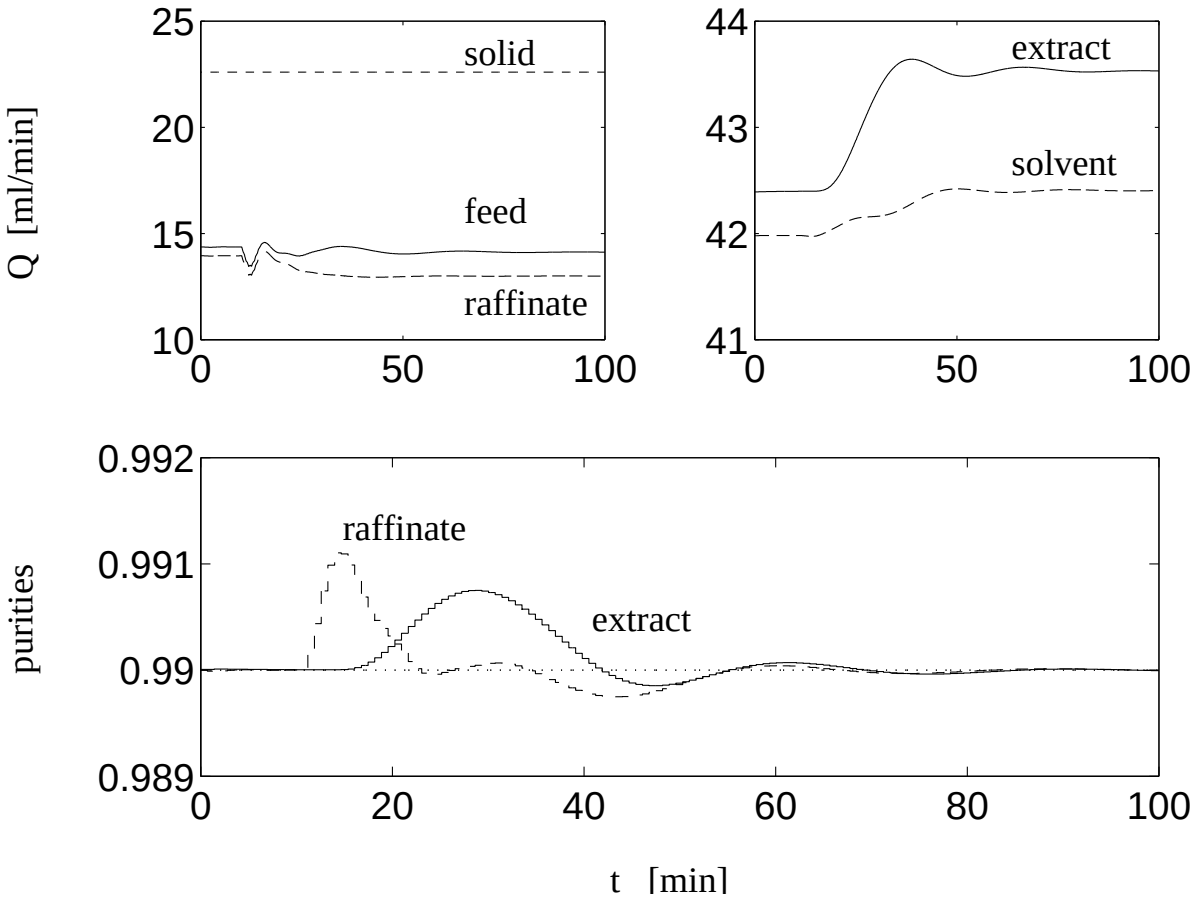

Figure 3.23: Simulation result for a 10% increase in the more strongly adsorbed component with model based control concept. Setpoint for both purities is 99%.

robustness of the observer design is essential for its use in connection with nonlinear controllers and application to real plants.

Distillation columns can be interpreted as systems with distributed parameters yielding model equations 2.1 and 2.2. Hence, following the ideas of [72], the observer design can be decomposed into two basic tasks. The first task is the selection of the measured quantities. For distributed parameter systems this step extends to the choice of suitable positions for the sensors along the spatial coordinate and in general turns out to be a challenging task. Note that a poor choice in this step may result in bad observer performance or even instability. The second task is the design of the error injection. For nonlinear distributed parameter systems the analytic design methods are complicated and often not feasible for large scale systems. However these problems can often be overcome by designing the error injection on basis of detailed process understanding. In [72] this concept has been

worked out and formalized to some extend. It addresses both the sensor placement and the design of the error injection. Successful application of the concept can be found in [31] for a distillation column and [35] for an adsorption process. However these applications are specific to the used process model since they rely on certain aspects of the model structure thus preventing their general applicability.

The concept presented in the following overcomes these problems. It gives direct rules to number and placement of sensors as well as to the design of the error injection. Yet the concept remains simple and its robustness to errors in the model structure as well as parameters is intuitively given.

Starting point of the concept is the existence of what was introduced in section 3.2.1 as the key wave. If such key waves exist in both sections of a, possibly reactive, distillation column the prerequisites of the concept are given. The key wave is always a balanced wave and hence this wave is sensitive to changes in boundary compositions or flow rates including the feed. Further more changes in the key wave position result in changes of the product compositions that may lead to violations of the product specifications, while changes in the positions of other waves do not since they cannot overtake the key wave. From these considerations it follows that it is not necessary to reconstruct the complete state of the column but focus has to be set on the key wave. Since the column temperature is a unique function of the composition a single temperature measurement at the nominal location of the key wave is sufficient to detect its movements. Hence for a distillation column composed of two sections the observer will work with only two temperature measurements positioned within the corresponding key wave. These considerations give a constructive solution to the first task in the observer design, i.e. sensor placement.

The next step is the design of the error injection itself. Instead of giving a solution to this design step in terms of formulas the underlying design philosophy will be given. Despite being rather abstract at first glance it is straight forward applicable to a variety of distillation column models as will be shown by a simple illustrative example. As worked out in the considerations regarding the sensor placement the position of the key wave is crucial and the observer should aim at matching its key wave position to that of the real process. The wave solution shows how the individual components vary along the key wave and from this it can be concluded that the amount of some components has to be

increased to make the wave move in one direction while at the same time the amount of other components has to be decreased or may remain unchanged. The direction of the necessary movement can be determined from the observation error, i.e. the difference of measured and estimated temperature. In order to achieve the required movement of the key wave in the observer model an error injection in the component material balances is made proportional to the estimation error and the direction of the gain vector is chosen according to the change of components along that wave. The elements of this vector are not restricted to result in point wise error injection at the position of the key wave but may be spatial functions accounting for the finite width of the key wave. In summary this results in a simple error injection with only two tuning parameters namely the length of the gain vectors and possibly the shape of the corresponding spatial weighting functions. While as a guideline for the shaping of the weighting functions the width of the key waves should be taken into account the tuning of the gain vectors must be done in open- and closed-loop simulation studies. This is possible since the effect of the gain is intuitively clear, larger gain values result in faster convergence and smaller steady state offsets at the price of stronger attenuation of noise. Further to tuning by the help of simulation studies online tuning at the real plant is possible.

Note that the concept assumes the key waves to remain within the reach of the sensors. This does not limit the applicability of the concept since observers are usually used in conjunction with stable closed-loop control systems which in turn keep the waves close to their nominal positions and thus within the reach of the sensors.

In order to give an impression of the performance of observers designed with these rules Fig. 3.24 shows simulation results for a disturbance in the feed composition of 10% for an ideal ternary mixture. The distillation column is modeled in this study by a tray to tray constant molar over flow model using saturation pressures to describe the vapor-liquid equilibrium while the observer model is a wave model according to [27], i.e. is based on constant relative volatilities. Hence both models differ considerably in number of states and with respect to the underlying thermodynamic relations. The error injection is made in the global component material balances of the wave model and the temperature measurements were chosen on tray 11 and tray 32.

In Fig. 3.24 the bold lines correspond to the nominal operating point without any dis-

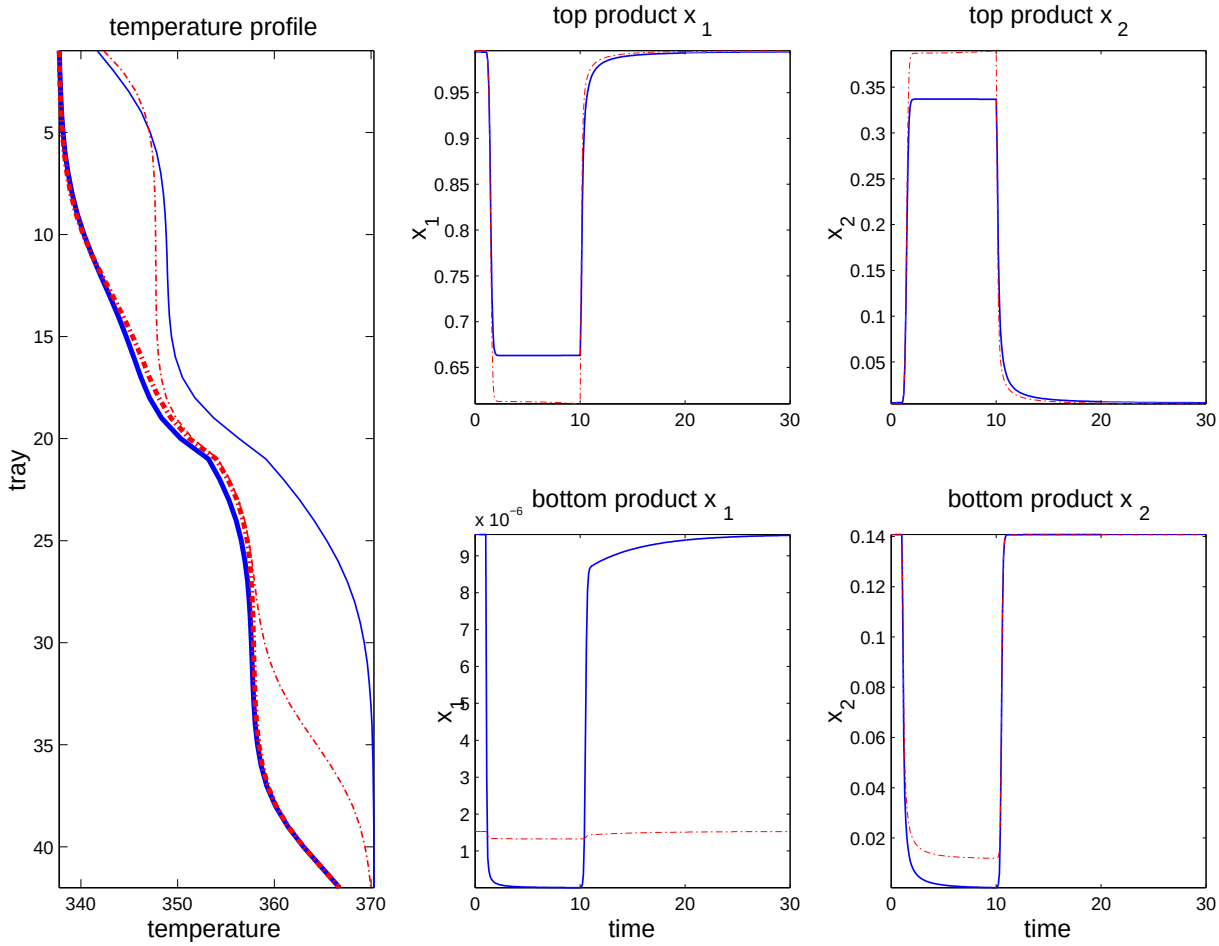

Figure 3.24: Simulation study of detailed column model and wave model based observer. After a short time the feed composition is disturbed by 10%. At time=10 the disturbance is removed. Bold lines: nominal operating point, thin lines: disturbed stationary profiles. Solid lines: plant, dashed-dotted lines: observer.

turbance, i.e. both plant and observer get the nominal feed conditions. The differences of the models become obvious upon noting that even at the nominal operating point the temperature profiles differ. However in the region of the key waves the deviations are neglectable due to the error injection. After the disturbance to the feed conditions is introduced the process moves away from its nominal position and the observer, still assuming nominal feed conditions, follows the process quite well due to the error injection. The observer captures the dynamics of the process due to the unknown disturbance in a nice way as can be seen from the time plots of the product compositions Fig. 3.24. At the same time some deviations in the actual and the predicted product compositions are apparent. Looking again at the stationary temperature profiles in the disturbed state the

reason for the deviations is clearly due to the fact that the key waves have moved far away from their nominal positions. This would not have happened in stable closed loop operation.

In summary the observer shows good and robust performance while at the same time its design was straight forward according to the presented rules. In the following section the observer design procedure is applied to the fairly complex reactive Bayer process already introduced in section 3.1.3.

3.2.4 Wave Based Observer Design for Nonlinear Control of an Industrial Reactive Distillation Column

While in the previous examples only nonreactive processes were considered and the applicability to combined reaction separation processes was concluded on basis of the developed theory this example now considers the observer design for a combined reaction separation process, the Bayer process as introduced in section 3.1.3. The example is worked out beyond the stage of the observer design and a complete closed loop controller with observer is designed. The controller design is based on asymptotically exact input/output linearization which essentially relies on the robustness of the underlying observer design [13], [12]. Hence it is worthwhile to discuss the observer design in some more detail while the actual controller design can be found in [15].

The first step in the proposed observer design procedure is the identification of the key wave. This can be done by the pathgrid as shown in Fig. 3.16. A shortcut to this method is the analysis of the responses of the column profiles in simulation studies to disturbances in the flow rate ratios. However this shortcut only gives information for the considered disturbances while other, possibly only slightly different disturbances may yield unexpected results, especially in conjunction with combined waves. Once the key waves have been identified their positions at the nominal operating point can be determined on basis of steady state column profiles as shown in Fig. 3.25. Here the trays number 4 and number 60 are chosen. Note that the sensor locations can be chosen from the profiles in physical coordinates since the transformed coordinates are simply linear combinations of them.

The next step is the design of the error injection. Following the proposed procedure the

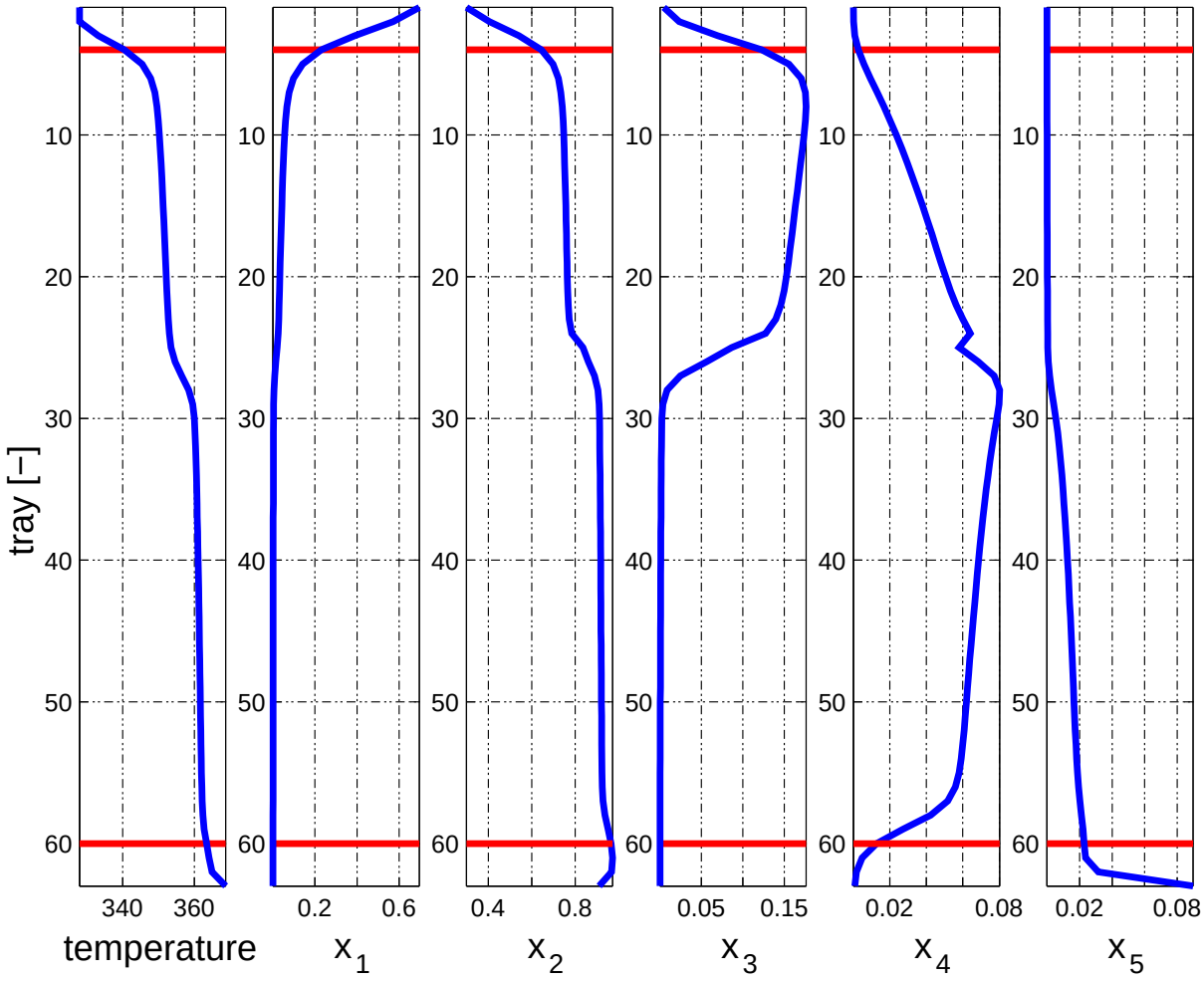

Figure 3.25: Steady state column profiles. The horizontal lines mark tray 4 and tray 60, the positions of the key waves at the nominal operating point.

error injection is designed to be proportional to the error in the estimated temperatures. The direction of the gain vector is determined from the change of compositions along the key waves. For instance for tray 4 the direction is found to be $\boldsymbol{g}_4 = [1,\ -1,\ 0,\ 0]$ and for tray 60 $\boldsymbol{g}_{60} = [0,\ 0,\ 0,\ -1]$. As a simplification it was assumed that all elements in the direction vectors can be set equal to ± 1. The spatial weighting was done by a dirac delta function, i.e. the error was only injected into the component material balances at the sensor locations.

The gain was set to the same constant value of 4 for both measurements. This gain value was found from simulation studies starting the observer from a disturbed state while the uncontrolled column was at steady state. This gain value is a compromise between steady state offset, speed of convergence and noise attenuation. For values above 4 no

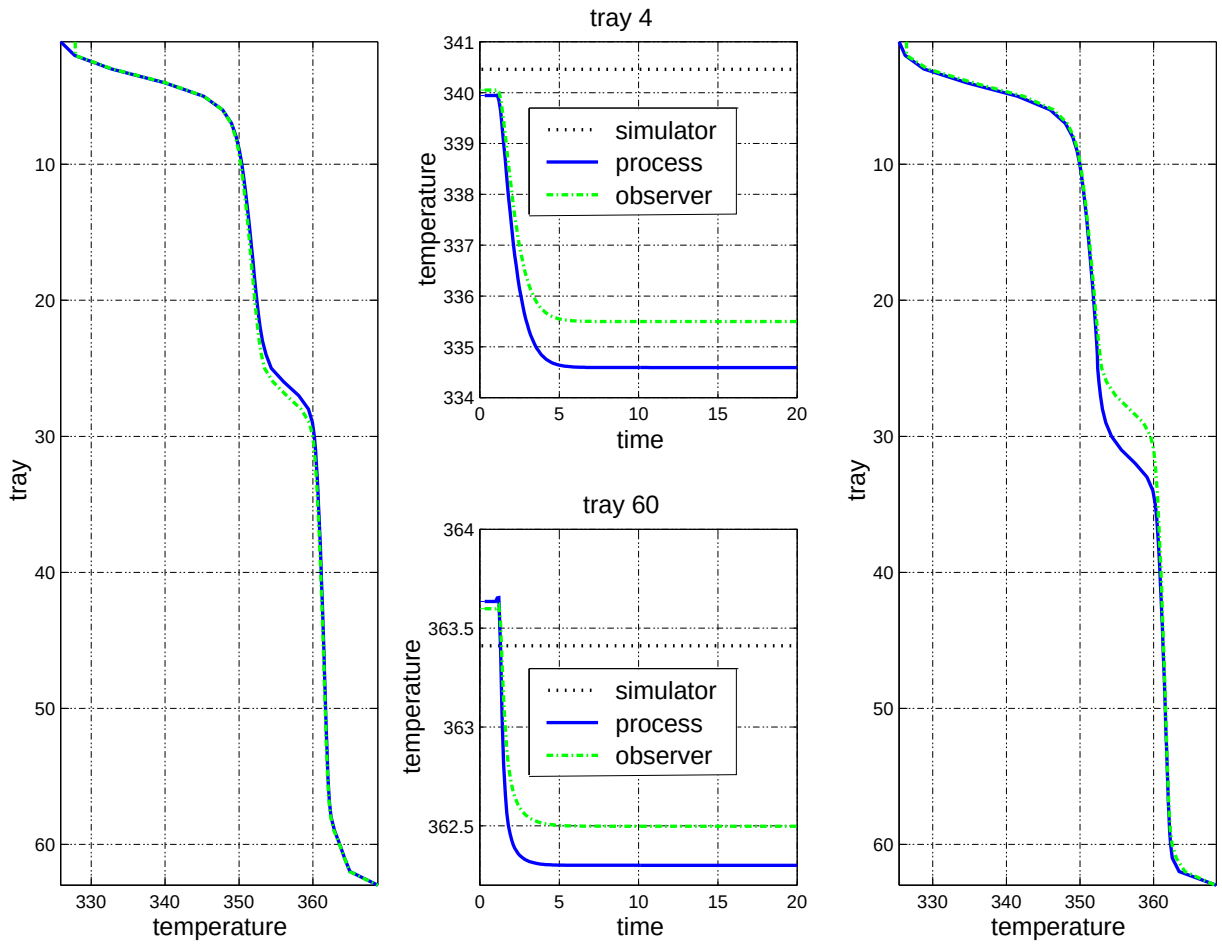

Figure 3.26: Observer performance. Left column: nominal operating point, right column: disturbed steady state, center column: transients of the measured temperatures from nominal operating point to disturbed steady state.

substantial increase in the speed of convergence is found while the steady state offset is within tolerable margins. Thus further increase of the gain will yield only a small increase in performance which may be spoilt by attenuation of measurement noise.

Fig. 3.26 demonstrates the performance of the observer in an open loop simulation study. Note that the plant is simulated by a detailed model including dynamic mass- and energy balances and liquid dynamics and pressure drop as functions of the vapor flow rate while the observer is based on a simplified model that is also used in the controller design. Further details on this aspect as well as the differences of the models can be found in [15]. The left column of Fig. 3.26 shows the plant and observer temperature profiles at the nominal operating point. The profiles are almost indistinguishable near the key waves, while at the feed point some deviations are clearly visible. The right column shows

the profiles after some disturbance in the operating variables of the plant while those for the observer are kept at their nominal values. Clearly the error injection accomplishes to match the key fronts of the observer to those of the plant while the deviation around the feed point is considerably increased. The time plots in the middle column of the figure show the transients of the measured and estimated temperatures together with the constant temperature the observer model would yield without the error injection. For up to time 1 the nominal operating conditions are applied and clearly it is seen that the error injection considerably reduces the steady state offset. Once the disturbance is active the estimated temperatures nicely follow the process. However the new steady state offset is increased in comparison to the nominal operating point since the error injection is similar to a proportional controller for the observation error. Including an integral action to overcome this problem seems at first promising. Taking into account the possibility that the error injection is not able to achieve zero observation error this can result in further problems, especially in dynamic situations.

As for nonlinear systems the separation principle is not valid the closed loop stability and performance of the observer can not be deduced from open loop considerations. To show closed loop stability and performance the closed loop system has to be considered. Fig. 3.27 shows the closed loop response of the nonlinear control system [15] in comparision to a modern multi input multi output linear controller [11]. This clearly demonstrates the superior performance of the nonlinear controller and hence the capabilities of the designed observer.

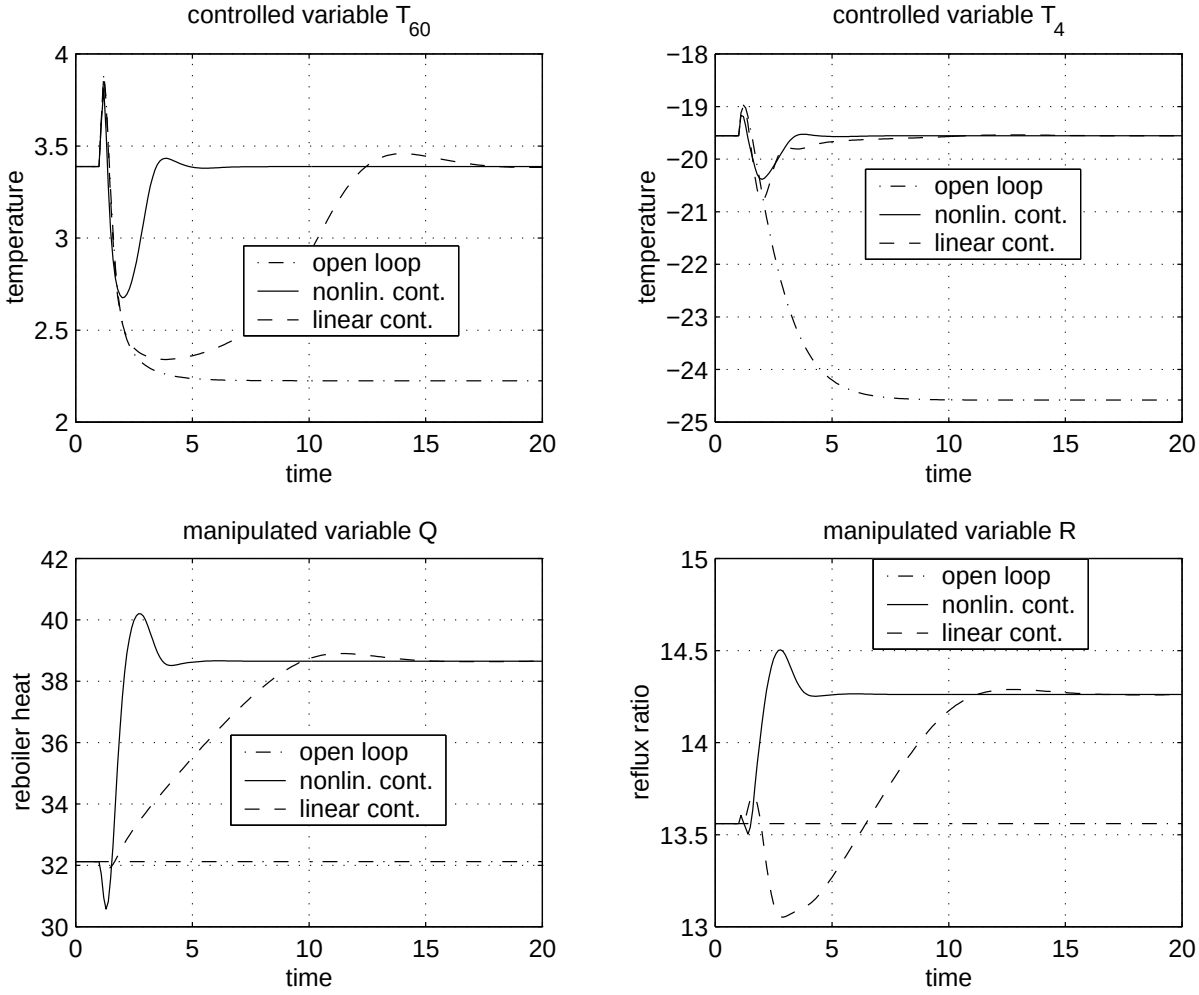

Figure 3.27: Closed loop performance of the nonliner control system in comparison to an advanced linear multi input multi output controller.

3.3 Conclusions

This section, devoted to the application of the theory of nonlinear wave propagation in combined reaction/separation processes, was split into two parts.

The first part illustrated the use of the developed theory to gain insight into the dynamics of combined reaction separation processes. It was shown, that some combined reaction/separation processes behave like ideal separation processes while others show significat differences. Especially it was shown that by allowing for simultaneous chemical reaction and separation an ideal separation process can turn into a strongly non ideal combined reaction/separation process.

No matter if a distillation or chromatographic process was considered the pathgrid proved to be a useful tool in predicting such behaviors. Towards the end of the first part complicated multireaction systems were considered. There the developed theory proved to be useful in explaining and predicting experimental results. For the considered industrial distillation process the chosen operating point was justified on basis of the pathgrid while due to the global insight provided by the pathgrid an extremely rich and complex behavior of the process was uncovered.

The second part eventually pointed out new concepts for control system design for separation as well as combined reaction/separation processes. The concept of inferential control, well established for distillation columns, was justified for multicomponent processes by introduction of key waves. Once provided with a sound theoretical background the concept was transfered to moving bed chromatographic processes. Further more the concept of key waves allows for a straight forward selection of measurement positions for observer design in counter current processes. The pathgrid then provides a useful tool in the design of the error injection.

Chapter 4

Conclusion

Starting point of this thesis was the need to easily predict and exploit the dynamics of combined reaction/separation processes. For ordinary separation processes, in general modeled by 1st order quasilinear homogeneous partial differential equations, this was already possible using nonlinear wave propagation theory in the past. However combined reaction/separation processes are characterized by reaction terms and thus lead to 1st order quasilinear inhomogeneous partial differential equations and nonlinear wave propagation theory is not directly applicable.

Extending the concept of reaction invariant compositions for stationary systems of [5] to dynamic systems the inhomogeneous equations of combined reaction/separation systems can be transformed to equivalent homogeneous equations, i.e. equivalent ordinary separation processes, and thus analysis with nonlinear wave propagation theory is possible. Though the theoretical basis of this transformation is the assumption of simultaneous phase and reaction equilibrium it is shown that this assumption may be relaxed and the results are applicable to systems that are sufficiently close to simultaneous phase and reaction equilibrium.

The potential of the new theory in predicting and exploiting the dynamics of combined reaction/separation processes is uncovered by applying it to several example problems.

Even for simple model systems with convex phase equilibrium function and a single reversible reaction in one phase it is shown that combined reaction/separation processes can in some cases behave like ordinary separation processes while in other cases they show highly nonideal behavior. Further to this the analysis underlines the similarity of

chromatographic and distillation processes since for both the requirements for ideal or nonideal behavior are the very same.

In the analysis of the illustrating example processes the issue of process feasibility was touched on. There the developed theory of combined reaction/separation processes proves to be a useful tool. It is not restricted to assess feasibility for a specific set of boundary conditions but gives a global understanding of the potential process dynamics and thus enables the process designer to quickly scan for alternative process variants.

Since the developed theory of combined reaction/separation processes takes process dynamics directly into account it is a valuable tool in the design of control systems for such processes. Nonlinear wave propagation theory gives rise to a new interpretation of inferential control as a control scheme aiming at stabilizing key waves at their nominal positions. Consequently a direct outcome of the common theory for chromatographic and distillation processes is the transfer of this control concepts from distillation to chromatographic processes. In addition the concept of stabilizing key waves was further elaborated to take e.g. the product specifications into account explicitly. Crucial part in many modern control concepts is a robust observer. Based on nonlinear wave propagation theory an efficient concept for sensor placement as well as design of the error injection it self is developed. The concept leads to a intuitively robust observer which is e.g. successfully used in a nonlinear control for a reactive distillation column.

Appendix A

Computation of Pathgrids for Implicit Equilibrium Functions

The pathgrid belonging to any equilibrium function $\Xi(\Phi)$ can be obtained by integrating along the eigenvectors of the corresponding jacobian $\partial\Xi(\Phi)/\partial\Phi$. For most systems the computation of this jacobian is not directly possible since the combined equilibrium function $\Xi(\Phi)$ can not be obtained as an explicit expression. In the following it is shown how to compute the required jacobian in terms of known expressions.

In the context of chromatographic reactors dependence on temperature T is often neglected by using reaction parameters at a suitable reference temperature. This is not the case for reactive distillation since boiling temperature is a function $T(\boldsymbol{\phi})$ of composition $\boldsymbol{\phi}$. Hence the following presentation is done for the more complex case arising in reactive distillation and the simplifications for the other case are straight forward.

The combined equilibrium function is thus defined by the following system of equations:

$$\boldsymbol{\Xi} = \boldsymbol{\nu}_T \boldsymbol{\xi}(\boldsymbol{\phi}(\boldsymbol{\Phi}), T(\boldsymbol{\phi}(\boldsymbol{\Phi}))) \tag{A.1}$$

$$\mathbf{0} = \boldsymbol{\Phi} - \boldsymbol{\nu}_T \boldsymbol{\phi} \tag{A.2}$$

$$\mathbf{0} = \boldsymbol{\rho}(\boldsymbol{\phi}(\boldsymbol{\Phi}), T(\boldsymbol{\phi}(\boldsymbol{\Phi}))) \tag{A.3}$$

$$\mathbf{0} = \sum \xi_i(\boldsymbol{\phi}(\boldsymbol{\Phi}), T(\boldsymbol{\phi}(\boldsymbol{\Phi}))) - 1 \tag{A.4}$$

Equation (A.3)describes the reaction equilibrium. Direct differentiation of (A.1) respecting the chain rule yields

$$\frac{\partial \boldsymbol{\Xi}}{\partial \boldsymbol{\Phi}} = \boldsymbol{\nu}_T \left(\frac{\partial \boldsymbol{\xi}}{\partial \boldsymbol{\phi}} + \frac{\partial \boldsymbol{\xi}}{\partial \boldsymbol{T}} \frac{\partial \boldsymbol{T}}{\partial \boldsymbol{\phi}} \right) \frac{\partial \boldsymbol{\phi}}{\partial \boldsymbol{\Phi}}. \tag{A.5}$$

While the partial derivatives in the braces are standard and straight forward to compute the computation of $\partial\boldsymbol{\phi}/\partial\boldsymbol{\Phi}$ shall be presented in some more detail. The equations (A.2) and (A.3) can be regarded as a single vector equation of the form

$$\mathbf{0} = \boldsymbol{F}\left(\boldsymbol{\Phi}, \boldsymbol{\phi}(\boldsymbol{\Phi}), T(\boldsymbol{\phi}(\boldsymbol{\Phi}))\right) \tag{A.6}$$

and implicit differentiation yields

$$\mathbf{0} = \frac{\partial \boldsymbol{F}}{\partial \boldsymbol{\Phi}} + \left(\frac{\partial \boldsymbol{F}}{\partial \boldsymbol{\phi}} + \frac{\partial \boldsymbol{F}}{\partial T}\frac{\partial T}{\partial \boldsymbol{\phi}}\right)\frac{\partial \boldsymbol{\phi}}{\partial \boldsymbol{\Phi}} \tag{A.7}$$

and can be solved for the desired $\partial\boldsymbol{\phi}/\partial\boldsymbol{\Phi}$ as

$$\frac{\partial \boldsymbol{\phi}}{\partial \boldsymbol{\Phi}} = -\left(\frac{\partial \boldsymbol{F}}{\partial \boldsymbol{\phi}} + \frac{\partial \boldsymbol{F}}{\partial T}\frac{\partial T}{\partial \boldsymbol{\phi}}\right)^{-1}\frac{\partial \boldsymbol{F}}{\partial \boldsymbol{\Phi}}. \tag{A.8}$$

Note that the inversion of the braced matrix expression must always be possible for suitably chosen reference components since otherwise the transformation form $\boldsymbol{\Phi}$ back to $\boldsymbol{\phi}$ would not be possible.

The pathgrid is now computed by integrating along the eigenvectors of the matrix

$$\frac{\partial \boldsymbol{\Xi}}{\partial \boldsymbol{\Phi}} = -\boldsymbol{\nu}_T\left(\frac{\partial \boldsymbol{\xi}}{\partial \boldsymbol{\phi}} + \frac{\partial \boldsymbol{\xi}}{\partial \boldsymbol{T}}\frac{\partial \boldsymbol{T}}{\partial \boldsymbol{\phi}}\right)\left(\frac{\partial \boldsymbol{F}}{\partial \boldsymbol{\phi}} + \frac{\partial \boldsymbol{F}}{\partial T}\frac{\partial T}{\partial \boldsymbol{\phi}}\right)^{-1}\frac{\partial \boldsymbol{F}}{\partial \boldsymbol{\Phi}}. \tag{A.9}$$

As initial conditions for this integration a point $\boldsymbol{\Phi}$ through which the pathgrid is to run is chosen. In order to compute (A.9) the knowledge of $\boldsymbol{\phi}$ is necessary and hence the system to be integrated is a DAE-system consisting of equations (A.2),(A.3) and (A.9). Before the integration can be started consistent initial conditions have to be computed, especially a $\boldsymbol{\phi}$ and T has to found that solves (A.2) and (A.3) for the given $\boldsymbol{\Phi}$. Care has to be taken to use physically sensible $\boldsymbol{\phi}$ and T. Since the independent variable in this DAE system has not the role of a time also backwards integration has to be performed to get the complete path through the chosen $\boldsymbol{\Phi}$.

Bibliography

[1] F. Allgöwer, T. Badgwell, J. Qin, and J. Rawlings. Nonlinear predictive control and moving horizon estimation - an introductory overview. In P. Frank, editor, *Advances in Control, Highlights of ECC'99*, pages 391–449. Springer, 1999.

[2] R. Baciocchi, G. Zenoni, M. Mazzotti, and M. Morbidelli. Separation of binaphthol enantiomers through achiral chromatography. *Journal of Chromatography A*, 944:225–240, 2002.

[3] L. Balasubramhanya and F. Doyle III. Nonlinear control of a high-purity distillation column using a traveling-wave model. *AIChE J.*, 43(3):703–714, 1997.

[4] R. Baratti, A. Bertucco, A. Da Rold, and M. Morbidelli. A composition estimator for multicomponent distillation columns - development and experimental test on ternary mixtures. *Chem. Eng. Sci.*, 53(20):3601–3612, 1998.

[5] D. Barbosa and M. Doherty. A new set of composition variables for the representation of reactive-phase diagrams. *Proc. R. Soc. Lond. A*, 413:459–464, 1987.

[6] D. Barbosa and M. Doherty. Theory of phase diagramsand azeotropic conditions for two-phase reactive systems. *Proceedings of the Royal Society of London*, A(413):443–458, 1987.

[7] D. Barbosa and M. Doherty. The influence of equilibrium chemical reactions on vapor-liquid phase diagrams. *Chem. Eng. Sci.*, 43(3):529–540, 1988.

[8] M. Benthabet, M. Bailly, and J. Corriou. Nonlinear control of a simulated moving bed. In *AIChE Annual Meeting, Sacramento*, 1997.

[9] G.-Q. Chen, C. Levermore, and T.-P. Liu. Hyperbolic conservation laws with stiff relaxation terms and entropy. *Comm. Pure. Appl. Math.*, 47:787–830, 1992.

[10] S. Dodds, G. Adams, W. Heath, and G. Goodwin. Application of an extended kalman filter to a binary distillation column model. In *6th IFAC Symp. on Dynamics and Control of Process Systems*, pages 497–501, Jejudo Island, Korea, June 4-6 2001.

[11] G. Fernholz, M. Friedrich, S. Grüner, K.-D. Mohl, A. Kienle, and E. Gilles. Control structure selection and linear multiple-input-multiple-output controller desig for an industrial reactive distillation column. In *6th IFAC Symp. on Dynamics and Control of Process Systems*, pages 137–142, Jejudo Island, Korea, June 4-6 2001.

[12] M. Groebel. *Asymptotisch exakte Ein-/Ausgangs-Linearisierung von Destillationskolonnen.* PhD thesis, Institiut für Systemdynamik und Regelungstechnik, Universität Stuttgart, 1996.

[13] M. Groebel, F. Allgöwer, M. Storz, and E. D. Gilles. Asymptotically exact I/O-linearization of an industrial distillation column. In *Proc. ACC' 95*, pages 2648–2652, 1995.

[14] S. Grüner and A. Kienle. Equilibrium theory and nonlinear waves for reactive distillation columns and chromatographic reactors. *Chem. Eng. Sci.*, 59:901–918, 2004.

[15] S. Grüner, K. Mohl, A. Kienle, G. Fernholz, and M. Friedrich. Nonlinear control of a reactive distillation column. *Control Engineering Practive*, 11:915–925, 2003.

[16] S. Grüner, S. Schwarzkopf, I. Disli-Uslu, A. Kienle, and E. Gilles. Nonlinear model predictive control of distillation columns using wave models. In *Proc. 7th International Symposium on Advanced Control of Chemical Processes, ADECHEM, 11-14 January 2004, Hong Kong (Hrsg.: Allgower, F. und Furong Gao), Hong Kong University of Science and Technology, Clear Water Bay. 2004, Pages 231-236*, 2004.

[17] M. Han and S. Park. Control of high-purity distillation column using a nonlinear wave theory. *AIChE J.*, 39(5):787–796, 1993.

[18] F. Helfferich. Review – Non-linear waves in chromatography – III. Multicomponent Langmuir and Langmuir-like systems. *J. Chromatogr. A*, 768:169–205, 1997.

[19] F. Helfferich and P. Carr. Review – Non-linear waves in chromatography – I. Waves, shocks, and shapes. *J. Chromatogr.*, 629:97–122, 1993.

[20] F. Helfferich and G. Klein. *Multicomponent Chromatography. Theory of Interference.* Marcel Dekker, New York, 1970. pp 298-397.

[21] F. Helfferich and R. Whitley. Review – Non-linear waves in chromatography – II. Wave interference and coherence in multicomponent systems. *J. Chromatogr. A*, 734:7–47, 1996.

[22] J. Hurley and B. Plohr. Some effects of viscous terms on riemmann problem solutions. *Mat. Contemp.*, 8:203–224, 1993.

[23] Y.-L. Hwang. Wave Propagation in Mass-Transfer Processes: From Chromatography to Distillation. *Ind. Eng. Chem. Res.*, 34:2849–2864, 1995.

[24] E. Isaacson, D. Marchesin, and B. Plohr. Transitional waves for conservation laws. *SIAM J. Math. Anal.*, 21:837–866, 1989.

[25] K. Kaczmarski, M. Mazzotti, G. Stroti, and M. Morbidelli. Modeling fixed-bedadsorption columns through orthogonal collocations on moving finite elements. *Comput. Chem. Engng.*, 21(6):641–660, 1997.

[26] A. Kienle. *Nichtlineare Wellenphänomene und Stabilität stationärer Zustände in Destillationskolonnen.* VDI Fortschritt – Berichte Nr. 3/506. VDI Verlag, Düsseldorf, 1997.

[27] A. Kienle. Low-order dynamic models for ideal multicomponent distillation processes using nonlinear wave propagation theory. *Chem. Eng. Sci.*, 55:1817–1828, 2000.

[28] K.-U. Klatt, F. Hanisch, G. Dünnebier, and S. Engell. Model-based optimization and control of chromatographic processes. *Computers Chem. Engng.*, 24:1119–1126, 2000.

[29] E. Kloppenburg and E. Gilles. Automatic Control of the Simulated Moving Bed Process for C_8 Aromatics Separation using Asymptotically Exact Input/Output-Linearization. *J. Proc. Contr.*, 9(2):41–50, 1998.

[30] R. Köhler, K. Mohl, H. Schramm, M. Zeitz, A. Kienle, M. Mangold, E. Stein, and E. Gilles. *Adaptive Method of Lines*, chapter 13. Chapman Hall/CRC Press, New York, 2001.

[31] L. Lang and E. Gilles. Nonlinear observers for distillation columns. *Computers chem. Engng.*, 14(11):1297–1301, 1990.

[32] R. LeVeque. *Numerical Methods for Conservation Laws.* Lectures in mathematics. Birkhäuser, 1992.

[33] W. Luyben. Profile position control of distillation columns with sharp profiles. *AIChE J.*, 18(1):238–240, 1973.

[34] W. Luyben, B. Tyreus, and M. Luyben. *Plantwide Process Control.* McGraw-Hill, New York, 1999.

[35] M. Mangold, G. Lauschke, J. Schaffner, M. Zeitz, and E. Gilles. State and parameter estimation for adsorption columns by nonlinear distributed parameter state observers. *J. Proc. Cont.*, 4(3):163–172, 1994.

[36] W. Marquardt. *Nichtlineare Wellenausbreitung — ein Weg zu reduzierten Modellen von Stofftrennprozessen.* VDI Fortschritt – Berichte Nr. 8/161. VDI Verlag, Düsseldorf, 1988.

[37] W. Marquardt. Traveling waves in chemical process. *International Chemical Engineering*, 30:585–606, 1990.

[38] P. Marteau, G. Hotier, N. Zanier-Szydlowski, A. Aoufi, and F. Cansell. Advanced control of c_8 aromatics separation with real-time multipoint on-line raman spectroscopy. *Process Control and Quality*, 6:133–140, 1994.

[39] M. Mazzotti, B. Neri, D. Gelosa, A. Kruglov, and M. Morbidelli. Kinetics of liquid-phase esterification catalyzed by acidic resins. *Ind. Eng. Chem. Res.*, 36:3–10, 1997.

[40] M. Mazzotti, G. Storti, and M. Morbidelli. Shock Layer Analysis in Multicomponent Chromatography and Countercurrent Adsorption. *Chem. Eng. Sci.*, 49(9):1337–1355, 1993.

[41] T. Mejdell and S. Skogestad. Composition estimator in a pilot-plant distillation column using multiple temperatures. *Ind. Eng. Chem. Res.*, 30:2555–2564, 1991.

[42] T. Mejdell and S. Skogestad. Estimation of distillation composition from multiple temperature measurements using partial-least-square regression. *Ind. Eng. Chem. Res.*, 30:2543–2555, 1991.

[43] C. Moore. *Practical Distillation Control*, chapter 8. Selection of controlled and manipulated variables, pages 140–177. Van Nostrand Reinhold, 1992.

[44] S. Natarajan and J. Lee. Repetitive model predictive control applied to a simulated moving bed chromatography system. *Computers Chem. Engng.*, 24:1127–1133, 2000.

[45] B. Neri, M. Mazzotti, G. Strotti, and M. Morbidelli. Multicomponent distillation design through equilibrium theory. *Ind. Eng. Chem. Res.*, 37:2250–2270, 1998.

[46] R.-M. Nicoud, J.-N. Jauber, I. Rupprecht, and J. Kinkel. Enantiomeric enrichment of non-racemic mixtures of binaphthol with non chiral packings. *Chirality*, 8:234–243, 1996.

[47] T. Petroulas, R. Aris, and R. Carr Jr. Analysis and performance of a countercurrent moving-bed chromatographic reactor. *Chem. Eng. Sci.*, 40:2233–2240, 1985.

[48] E. Quintero-Marmol, W. Luyben, and C. Georgakis. Application of an extended luenberger observer to the control of multicomponent batch distillation. *Ind. Eng. Chem. Res.*, 30:1870–1880, 1991.

[49] C. Reder. Metabolic control theory: A structural approach. *J. theor. Biol.*, 135:175–201, 1988.

[50] H.-K. Rhee, A. Aris, and N. Amundson. *First-Order Partial Differential Equations: Vol. I — Theory and Applications of Single Equations.* Prentice Hall, Englewood Cliffs, NJ, 1986.

[51] H.-K. Rhee, A. Aris, and N. Amundson. *First-Order Partial Differential Equations: Vol. II — Theory and Applications of Hyperbolic Systems of Quasilinear Equations.* Prentice Hall, Englewood Cliffs, NJ, 1989.

[52] B. Roffel, B. H. Betlem, and de Blouw R.M. A comparision of the performance of profile position and composition estimators for quality control in binary distillation. *Comput. Chem. Engng.*, 2002.

[53] D. Schaeffer and M. Shearer. The classification of 2 x 2 systems of non-strictly hyperbolic conservation laws, with applications to oil recovery. *Comm. Pure. Appl. Math.*, XL:141–178, 1987.

[54] H. Schramm. *Neue Betriebsweisen und Prozessfhrungskonzepte fr chromatographische Prozesse mit simuliertem Gegenstrom*. PhD thesis, Otto von Guericke Universität Magdeburg, Aachen, 2005.

[55] H. Schramm, S. Grüner, and A. Kienle. Control of moving bed chromatographic processes. In *Proc. European Control Conference, ECC2001, September 4 - 7 , Porto, Portugal, 2001. Paper Th-A04-04*, 2001.

[56] H. Schramm, S. Grüner, and A. Kienle. New control strategies for moving bed chromatographic processes. paper 15-52. In *3rd European Congress of Chemical Engineering, ECCE, June 26 - 28, Nürnberg*, 2001.

[57] H. Schramm, S. Grüner, and A. Kienle. Optimal operation of simulated moving bed chromatographic processes by means of simple feedback control. *Journal of Chromatography A*, 1006:3–13, 2003.

[58] S. Schwarzkopf. *PhD Thesis, in preparation.* 2005.

[59] A. Seidel-Morgenstern, C. Blümel, and H. Kniep. *Fundamentals Of Adsorption 6*, chapter Efficient design of the SMB process based on a perturbation method to measure adsorption isotherms and on a rapid solution of the dispersion model, pages 449–454. ELSEVIER, Paris, Amsterdam, Lausanne, New York, Oxford, Shannon, Tokyo, 1998.

[60] J. Shin, H. Seo, M. Han, and S. Park. A nonlinear profile observer using tray temperatures for high-purity binary distillation column control. *Chem. Eng. Sci.*, 55:807–816, 2000.

[61] S. Skogestad. Dynamics and control of distillation columns – A tutorial introduction. In *Trans IChemE*, 75, Part A, Sept. 1997, pages 539–562, 1997.

[62] J. Smoller. *Shock Waves and Reaction-Diffusion Equations, 2nd Edition*. Springer, New York, 1994.

[63] A. Spieker, E. Kloppenburg, and E. Gilles. *Bioseparation and Bioprocessing*, chapter 8 Computer Modelling of Chromatographic Bioseparation, pages 329–362. Subramanian, G., Wiley-VCH, Weinheim, 1998.

[64] G. Storti, M. Mazzotti, M. Morbidelli, and S. Carrà. Robust Design of Binary Countercurrent Adsorption Separation Processes. *AIChE Journal*, 39(3):471–492, Mar. 1993.

[65] S. Sundaresan, J. Wong, and R. Jackson. Limitations of the Equilibrium Theory of Countercurrent Devices. *AICHE Journal*, 33(9):1466–1472, September 1987.

[66] R. Taylor and R. Krishna. Modelling reactive distillation. *Chem. Eng. Sci.*, 55:5183–5229, 2000.

[67] S. Ung and M. F. Doherty. Calculation of residue curve maps for mixtures with multiple equilibrium chemical reaction. *Ind. Eng. Chem. Res.*, 34:3195–3202, 1995.

[68] S. Ung and M. F. Doherty. Theory of phase equilibria in multireaction systems. *Chem. Eng. Sci.*, 50(20):3201–3216, 1995.

[69] S. Ung and M. F. Doherty. Vapor-liquid phase equilibrium in systems with multiple chemical reactions. *Chem. Eng. Sci.*, 50(1):23–48, 1995.

[70] G. Whitham. *Linear and Nonlinear Waves*. A Wiley-Interscience publication. Wiley, New York, 1974.

[71] C.-C. Yu and W. Luyben. Use of temperatures for the control of multicomponent distillation columns. *Ind. Eng. Chem. Process Des. Dev.*, 23:590–597, 1984.

[72] M. Zeitz. *Nichtlineare Beobachter für chemische Reaktoren*. VDI-Verlag, Düsseldorf 1977, 1977.